SSURADS

LEVEL II

UNCLASSIFIED
FS-77-144
REVISION 1
MARCH 1978

SHIPBOARD SURVEILLANCE RADAR SYSTEMS PROGRAM

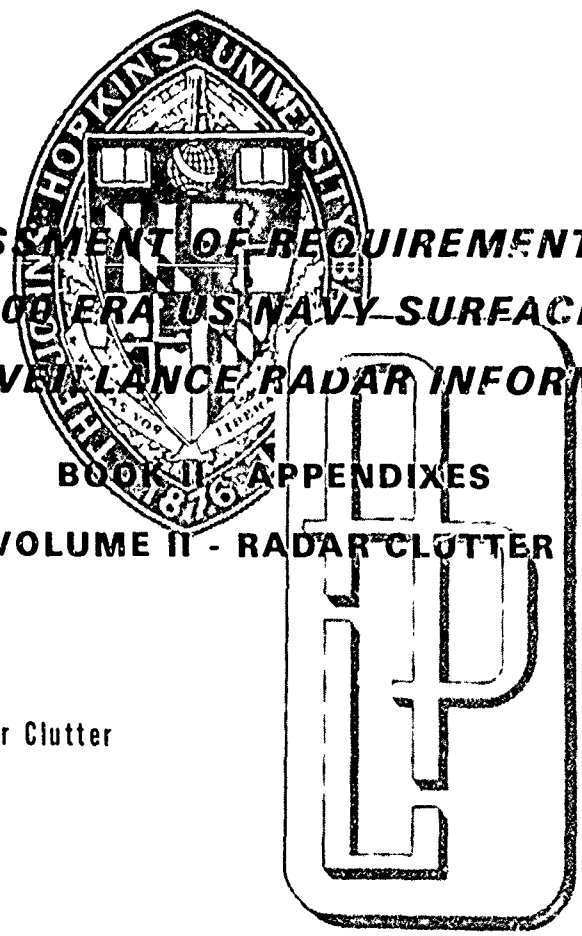

ASSESSMENT OF REQUIREMENTS OF 1985 - 2000 ERA U.S. NAVY SURFACE SHIPS FOR SURVEILLANCE RADAR INFORMATION

BOOK II - APPENDIXES

VOLUME II - RADAR CLUTTER

Appendix III Radar Clutter

FLEET SYSTEMS DEPARTMENT
THE JOHNS HOPKINS UNIVERSITY • APPLIED PHYSICS LABORATORY

UNCLASSIFIED

(14) APL/JHU/FS-77-144-REV-1

FS-77-144
REVISION 1

(11) MARCH 1978

(12) 151 p.

SSURADS

SHIPBOARD SURVEILLANCE RADAR SYSTEMS PROGRAM

(6)

ASSESSMENT OF REQUIREMENTS OF 1985 - 2000 ERA US NAVY SURFACE SHIPS FOR SURVEILLANCE RADAR INFORMATION.

BOOK II. APPENDIXES.

VOLUME II. RADAR CLUTTER.

Appendix III. Radar Clutter. Revised

(15) N0024-78-C-5324 (16) S0168

(17) AA

Prepared under the Sponsorship of

Naval Sea Systems Command NAVSEA 652

Shipboard Surveillance Radar Systems Program

FLEET SYSTEMS DEPARTMENT

THE JOHNS HOPKINS UNIVERSITY • APPLIED PHYSICS LABORATORY

JOHNS HOPKINS ROAD • LAUREL, MARYLAND • 20810

OPERATING UNDER CONTRACT N00017-72-C-4401 WITH THE DEPARTMENT OF THE NAVY

JCB

UNCLASSIFIED

INDEX
ASSESSMENT OF REQUIREMENTS OF
1985-2000 ERA US NAVY SURFACE SHIPS
FOR SURVEILLANCE RADAR INFORMATION (U)

APPENDIX III

RADAR CLUTTER

Author: W. K. Rivers

Note: This Appendix is based on Report TSC-W25-18 issued in March 1978 by the Technology Service Corporation.

TABLE OF CONTENTS

TABLE OF CONTENTS (Continued)

RADAR CLUTTER

1.0 INTRODUCTION

The models of shipboard surveillance radar clutter described in this appendix are intended to represent in a standardized way those features of the environment which are known to affect radar performance and, because of potential operational significance, are subjects for evaluation. Documentation of these models is motivated by a need to assure that all those operating in roles of radar specifiers, designers, or evaluators view the radar environment with a common perception in the context of a single radar program and that they communicate mutually with a common language. The models included reflect the best data available to date, but precision and level of detail are deliberately tempered to be consistent with the state of solid understanding of the external world as seen with radar, the natural variability of that world, and the sensitivity of radar performance to the details and parameter values.

The environment features modeled here are summarized in table 1-1. With that list are shown also the dependent and independent variables in terms of which the model is expressed, and the domains over which the models are usable. The domain values shown imply usability over that range, but it is not implied in all cases that the models fail outside those regions. Before model application outside the given domain is attempted, a further review of the model vis-a-vis the data base is advisable.

The models presented here are not requirements. That is, in every case at least one driving independent variable or model parameter has been left subject to choice by the user. In general, independent (input) quantities associate with operational descriptors or quantifiers of the environment, which when specified, condition system performance. The dependent (output) quantities are radar engineering in type (cross sections, loss factors, etc.). Thus, these models are merely transformers from an operational (requirements) space to a radar engineering space.

The selection of values of parameters in the models controls the interpretation of the meaning of the output. In these models, parameters have been chosen to represent most-probable, typical, or median, as appropriate, with a range provided to reflect variability of observations or uncertainty in estimates. These models are not

Table 1-1

Model Inputs and Outputs

AREA	INPUTS	OUTPUTS
Rain Backscatter	Rain Rate, Type, Frequency	Spatial Distribution of Reflectivity Spectrum Probability of Occurance
Chaff Backscatter	Amount and Type, Frequency, Dissemination Mode	Spatial & Temporal Distribution of Reflectivity Spectrum
Sea Backscatter	Sea State, Incidence Angle, Frequency, Polarization	Reflectivity (Average) Signal Distribution
Land Backscatter	Land Type, Incidence Angle Frequency	Distribution of Reflectivity Spectrum of Motions
Sea Reflection Multipath	Geometry, Frequency, Surface Roughness, Polarization	Coherent Propagation Loss Diffuse Scattering Intensity
Atmospheric Attenuation & Lens Refraction	Geometry, Frequency	Propagation Loss
Rain Attenuation	Rain Rate, Frequency, Polarization	Attenuation Rate
Jamming	Type	Signal Modulation Parameters

worst-case in type. Thus, their use should incorporate some exploration of system sensitivity to excursions about likely input (and parameter) values: to discover significant marginal limitations on performance, to prevent overlooking of acceptable or unacceptable operating regions, and to provide a basis for system trade-offs among options with different costs.

2.0 VOLUME SCATTERERS

The reflections from precipitation and chaff can constitute the major source of clutter on many radars. The reflections from a given radar cell appear noise-like on any given pulse, but have some correlation from pulse to pulse. This section is devoted to the statistics of these echoes.

The modeling or specification of this form of clutter is critical since few radars will see targets (especially aircraft) in the heaviest of storms, and there is as much difficulty in overspecification of the precipitation rate as there is in underspecification. The same holds true for chaff, and a specification of reflectivity has little meaning without specification of the size and dynamics of the chaff cloud.

While the phenomena are quite different, rain and chaff appear statistically similar to a radar. The short-term point amplitude distributions are Rayleigh whether there are 10 rain drops or 1,000 dipoles in the radar volume. They both are excellent tracers of the horizontal winds, and while the fall rate of rain is higher (up to 9 m/sec for large drops, but perhaps less than 0.1 m/sec for chaff), this only affects vertically pointing radars.

This chapter contains sections on the reflectivity of rain having various rates (see table 2-1), the dynamics of the atmosphere which are applicable both to rain and chaff, the frequency with which various rain rates are experienced, models for spatial distribution of rain of both continuous quasi-uniform type and storms. The reflectivity of various dipole and rope chaff types is given here. At the end of the chapter are collected data on cross section of clouds and birds.

2.1 Atmosphere Model

The ability of an MTI or pulse Doppler radar to suppress returns from chaff is highly dependent on the mean frequency and spectral width of the clutter. Since chaff dipoles are excellent tracers of the wind field, these quantities are highly dependent on the wind velocity, wind shear, and air turbulence effects. To produce meaningful calculations of radar performance in a chaff environment requires the use of a realistic model of atmospheric wind, shear, and turbulence effects. The model should be simple enough to be easily applied, but at the same time contain sufficient statistical information to give the radar user confidence in the results of calculations using the model. The atmospheric model

Table 2-1A

Reflectivity of Volume Scatterers - Summary

1. $\frac{\text{Average Cross Section}}{\text{Unit Cell Volume}} = \frac{\pi^5}{\lambda^4} |K|^2 Z$,

where λ = radar wavelength

$$K = \frac{\epsilon' - 1 - j\epsilon''}{\epsilon' + 2 - j\epsilon''}$$

$$\epsilon' = \frac{\epsilon_s - \epsilon_p}{1 + (\omega\tau_r)^2} + \epsilon_p$$

$$\epsilon'' = \frac{(\epsilon_s - \epsilon_p)\,\omega\tau_r}{1 + (\omega\tau_r)^2}$$

For Water: [2-5]

$\epsilon_p = 4.9$

τ_r	ϵ_s	Temp
1.87^{-11} sec	88	0° C
1.36^{-11} sec	84	10° C
1.01^{-11} sec	80	20° C

$|K|^2 \cong 0.93$

For Ice:

$\tau_r \cong 0$

$\epsilon' \cong 3.4$

$|K|^2 \cong 0.2$

2. $Z \cong k\,r^b$ in mm^6/m^3 ,

where r = rain rate in mm/hr.

(See Table 2-1B, 2-1C)

Table 2-1B

Values of Rain Backscatter Parameters k and b

#	TYPE/LOCATION	SOURCE & METHOD		k	b
1	Summer/Ottawa	Marshall-Palmer [2-1]	(1)	296	1.47
2	Summer/Ottawa	Marshall-Palmer [2-1]	(2)	220	1.60
3	General-Widespread	Marshall-Palmer [2-1]	(3)	200	1.6
4	Washington, D. C.	Laws and Parsons [2-28]	(2)	398	1.41
5	North Carolina	Mueller & Sims [2-29]	(4)	263	1.30
6	New Jersey	Mueller & Sims [2-30]	(4)	282	1.29
7	Virginia	Crane [2-31]	(4)	270	1.30
8	North Carolina [2-29]	Crane [2-32]	(4)	253	1.34
9	Convective Storms	Miller [2-3]	(2)	25	2.37
10	Thundershower	Joss [2-2]	(2)	500	1.50
11	Summer/Ottawa [2-1]	Wexler & Atlas [2-33]	(1)	See Table 2-1C	
12	Hail	Douglas [2-3]		3.1×10^4	1.30

Notes

(1) Computed from exponential-function representation of drop-size distribution and Mie scattering theory.

(2) Fit to (Z_i, r_i) observations.

(3) Approximation to case #2, used as "standard".

(4) Computed from measured drop-size distribution and Mie scattering theory.

(5) These parameters are used in figure 2-1 to intercompare their effort on Z as a function of rain rate.

Table 2-1C

Frequency and Rain-Rate Dependence of
Rain Backscatter Parameters, k and b [2-33]

FREQUENCY (GHz)	r (mm/hr)	k	b
3.0	0 - 100	295	1.45
5.45	0 - 100	280	1.45
6.42	0 - 100	280	1.45
9.35	0 - 100	275	1.55
16.0	0 - 20	330	1.54
	20 - 50	500	1.40
	50 - 100	750	1.30
24.2	0 - 5	356	1.50
	5 - 20	460	1.35
	20 - 100	820	1.15
34.9	0 - 5	350	1.32
	5 - 20	450	1.15
	20 - 100	780	0.95
48.4	0 - 5	240	1.10
	5 - 20	345	0.90
	20 - 100	540	0.75

Table 2-1D

Model Rain Reflectivities

BAND	NOMINAL FREQUENCY (GHz)	REFLECTIVITY (dBm^2/m^3)		
		4 mm/hr	8 mm/hr	16 mm/hr
UHF	0.5	-114	-109	-104
L	1.25	- 98	- 93	- 88
S	3.0	- 83	- 78	- 73
C	5.6	- 72	- 67	- 62
X	9.4	- 63	- 58	- 53
K_o	17	- 52	- 47	- 43
K_a	35	- 40	- 36	- 32

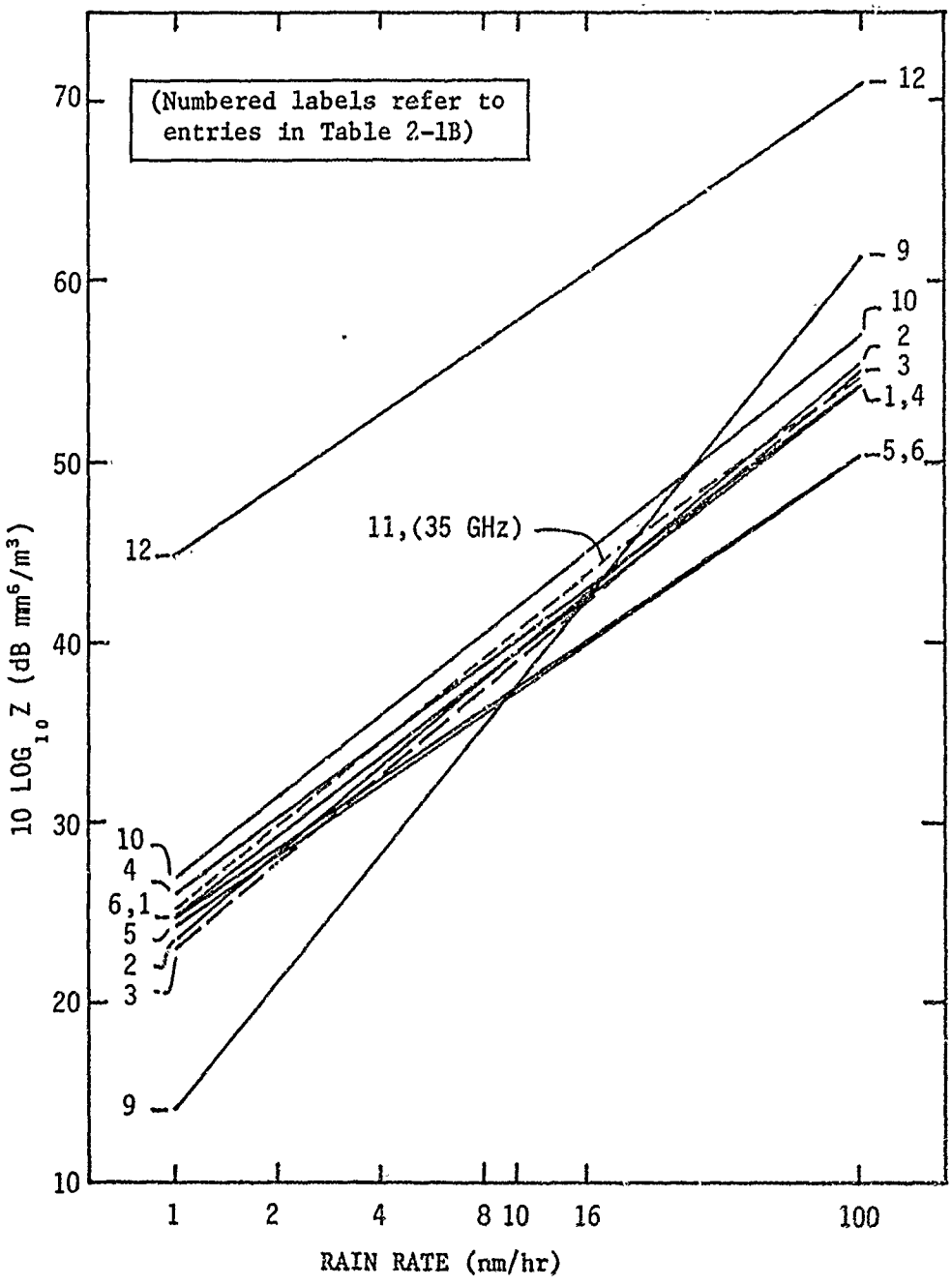

Figure 2-1

Variation Among Empirical and Theoretical Rain Reflectivity Laws

should describe the important atmospheric effects as a function of altitude and for various locations throughout the world.

It is convenient to describe the Doppler spectra of returns from rain and chaff by four mechanisms [2,4]:

1. Wind Shear - The change in wind speed with altitude results in a distribution of radial velocities over the vertical extent of the beam.

2. Beam Broadening - The finite width of the radar beam causes a spread of radial velocity components of the wind when the radar is looking crosswind.

3. Turbulence - Fluctuating currents of the wind cause a radial velocity distribution centered at the mean wind velocity.

4. Fall Velocity Distribution - A spread in fall velocities of the reflectors causes a spread of velocity components along the beam.

By assuming that above mechanisms are independent, then the variance of the velocity spectrum, σ_v^2, can be represented by the sum of the variances of each component.

$$\sigma_v^2 = \sigma^2_{shear} + \sigma^2_{beam} + \sigma^2_{turb.} + \sigma^2_{fall} \qquad (2\text{-}1)$$

For purposes of analysis, the spectrum shape may be taken to be Gaussian, with the following considerations applying:

- Regardless of assumptions about shape, Gaussian would be a good fit to observed data to a level at least 20 dB below the peak.

- In any cases where spectral envelopes are suspected to have tails, equivalent Gaussian width parameters can be computed so that about the same cancellation properties result for a specified filter.

2.1.1 Wind Speed Profiles

While there are many profiles of the change in wind speed versus altitude, it is necessary to make some simplifying assumptions and linearize the results to find the bounds on MTI performance. Figure 2-2 gives wind speeds for various winter conditions in the Eastern US. These are somewhat more severe than worldwide models.

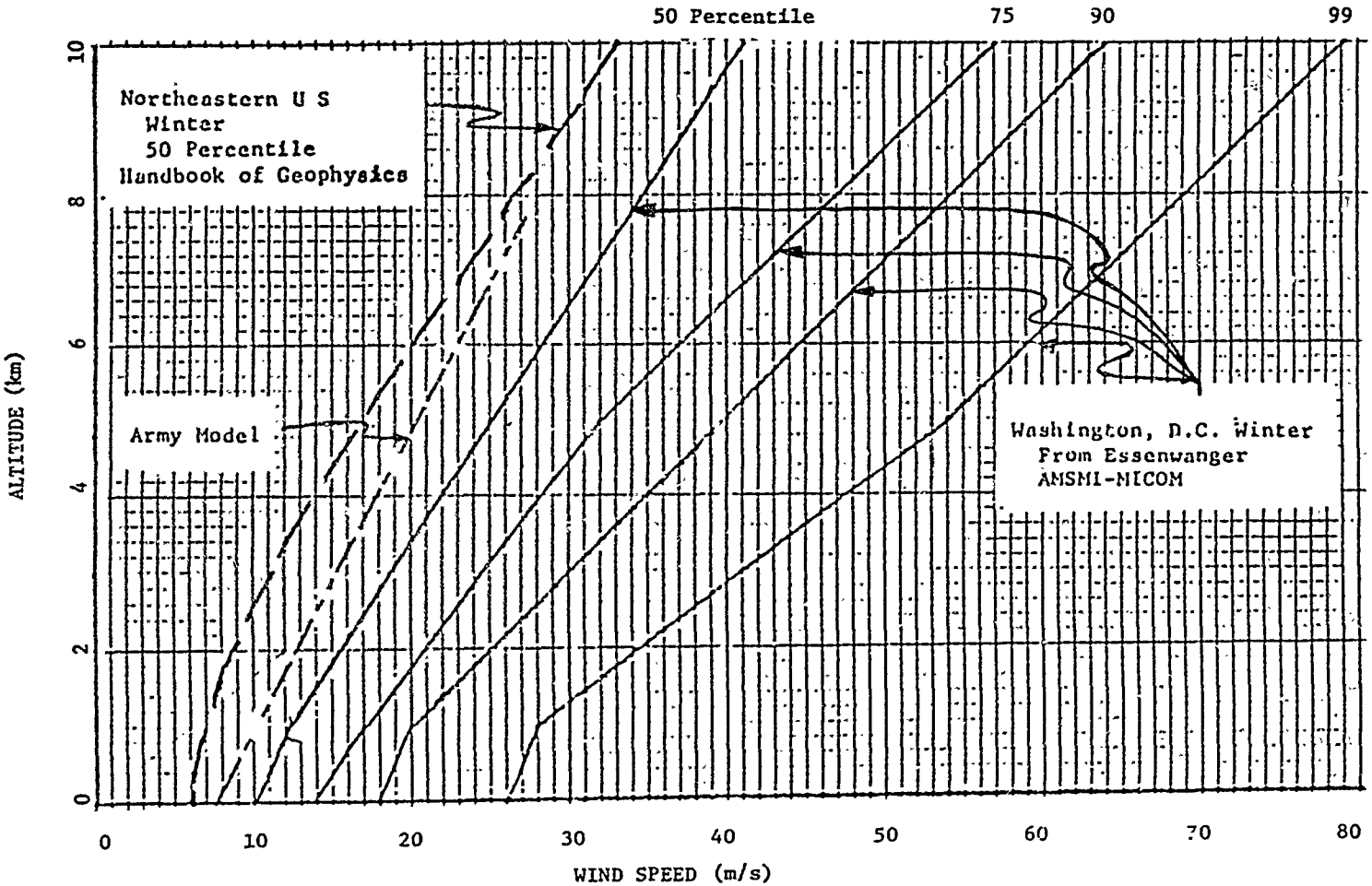

Figure 2-2

U S Wind Speeds in Winter

It shows that mean horizontal velocities go from 7.5 m/sec to 27 m/sec at altitudes where chaff is likely. This translates to Doppler frequencies between $\pm$ 270 Hz and $\pm$ 1000 Hz at C-band.

Reference 2-5 represents wind measurements made at the NASA Eastern Test Range, employing the FPS-16 Radar/Jimsphere method. The report gives 112 vector wind velocity profiles spanning the period November, 1964 to May, 1965. An example of a profile taken on 10 February 1975 is shown in figure 2-3, which shows rapidly changing wind speed versus altitude.

2.1.2 Wind Shear

Since the mean wind increases with altitude for virtually all altitudes where chaff and precipitation echoes are possible, the mean wind velocity at the top of a radar beam is generally higher than that at the bottom. This phenomenon is called "wind shear" and its effect is the dominant one in determining the Doppler distribution of chaff and precipitation echoes at ranges greater than 20 km.

The "slope" of the radial velocities with altitude is somewhat greater than the increase in mean velocity with altitude at any instant of time. The shear parameter, k, is usually expressed in meters per second per kilometer of altitude change. A suggested shear model based on an extensive search of the literature is shown in table 2-6.

2.1.3 Atmospheric Turburlence

In addition to wind speed and wind shear effects, the width of the chaff return spectrum is dependent on the random variation of air currents about the mean wind speed, commonly known as air turbulence.

Turbulence results from a variety of sources. In the lower portion of the atmosphere, extending to about 1,000 feet above the terrain, turbulence originates primarily from interaction between terrain roughness and the wind. Outside the earth boundary layer, turbulence has complex origins. Turbulence due to convection, usually identifiable with clouds, occurs at altitudes to 5,000 - 10,000 feet. With a further increase in altitude the overall probability of turbulence decreases and the mechanism becomes more closely related to wind shear effects. Clear air turbulence, or turbulence not in or in the vicinity of clouds, or precipitation, originates usually from the local shears of wind. As the jet stream is a source of large wind shears, clear air turbulence is most frequently found at high altitude in the vicinity of the jet stream.

THE JOHNS HOPKINS UNIVERSITY
APPLIED PHYSICS LABORATORY
LAUREL, MARYLAND

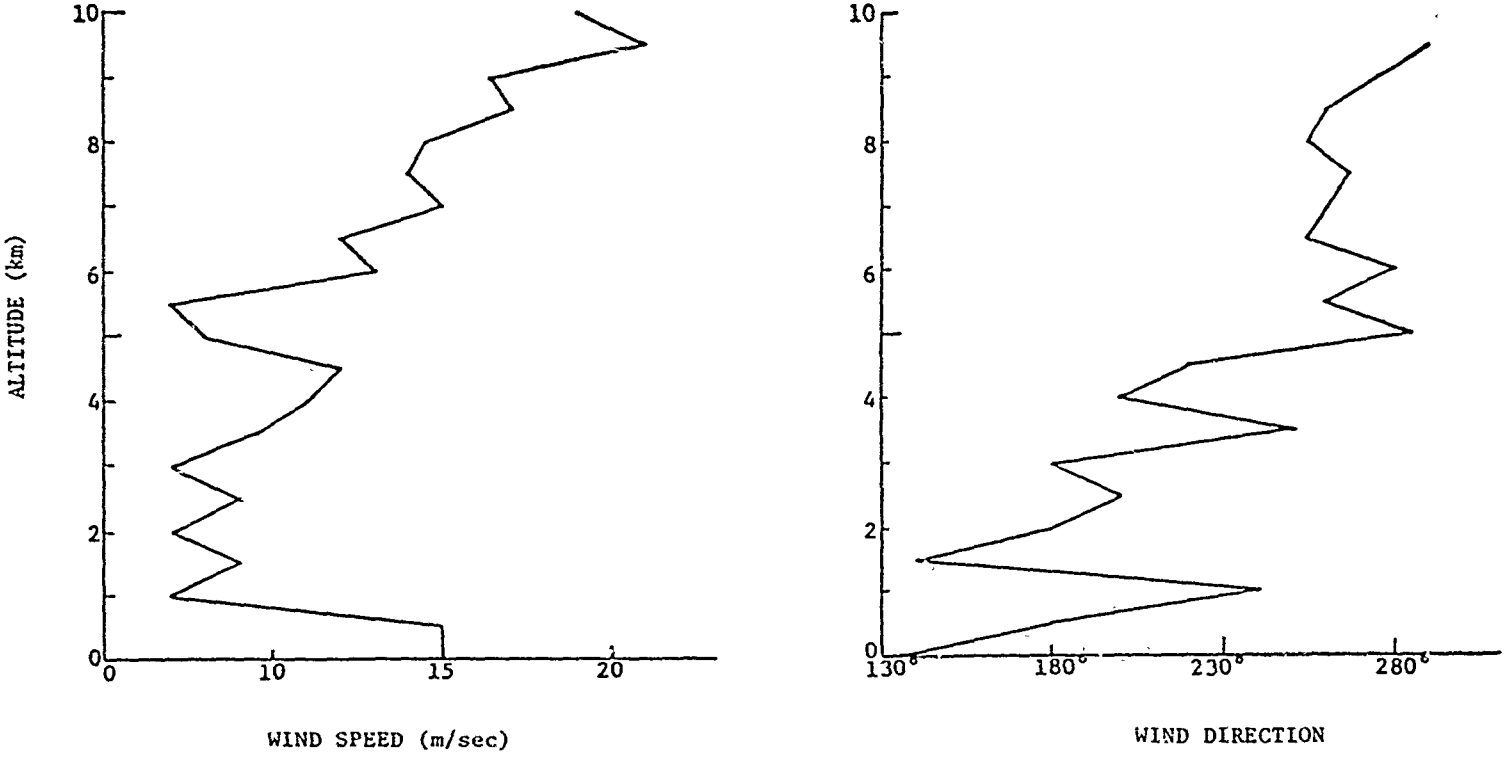

Figure 2-3

Wind Profile, February 10, 1965 2305Z ETR

Values of turbulence from a variety of sources and typical of conditions generally encountered worldwide are summarized in table 2-3.

2.1.4 Beam Broadening

The beam broadening effect is similar to the shear component and results in a standard deviation of

$$\sigma_{beam} = 0.42\ V_o\ \theta_2 \sin \beta$$

where θ_2 is the two-way, half-power azimuth beamwidth (radians), V_o is the wind velocity, and β is the azimuth angle relative to the wind direction. For most applications, the beam broadening component is quite small compared to turbulence and shear components.

2.1.5 Fall-Rate Broadening

Data [2-7,2-8] on the dispersion of fall rates of chaff lead to these model values:

Type	Dispersion (Std. Dev)
Glass Fiber	∿ 10% of fall rate
Aluminum Foil	∿ 50% of fall rate

Model fall rates are shown in figure 2-4 as a function of chaff type and altitude. Multifilament rope is a loose parallel twisted combination of some uncoated and some coated fibers (typically 10 coated out of 20). A multifilament resilient dipole is a rigidized parallel cluster of some uncoated and some coated fibers (typically 7 coated out of 20).

Fall rates of rain are much greater and vary from about 4 m/sec at a rain rate of 2 mm/hr to ∿ 9 m/sec for heavy rains. At all rain rates, the standard deviation of fall rate is about 1 m/sec, with a tail on the low-rate side caused by small drops. [2-4]

2.2 Point Frequency Distribution of Rain

Rainfall statistics accumulated and analyzed for purposes of characterizing the reliability of microwave communication links have been modeled in terms of the fraction of time that attenuation exceeds a given level. This distribution is accurately expressed by the log-normal distribution [2-9]. That is, if α is the attenuation

Table 2-2

Average Wind Shear (m/sec/Km) Vs
Altitude, Latitude, and Season

Altitude (Km)	Annual Ave. Shear	Winter			Summer		
		50°N	40°N	30°N	50°N	40°N	30°N
0-2	5	5.5	7.5	6.0	5.25	4.5	5.5
2-7	4	5.0	7.0	4.5	4.75	4.0	5.0
7-14	4	5.5	7.5	6.0	5.75	5.0	6.0
Typical Variations of Wind Shear Values		±3.75	±4.25	±4.25	±4.0	±3.0	±2.75

Table 2-3

Turbulence Vs Altitude

Altitude (Km)	Average σ_t (m/sec)	Typical Variations (m/sec)
0-1	1.2	±0.7
1-7	0.6	±0.3

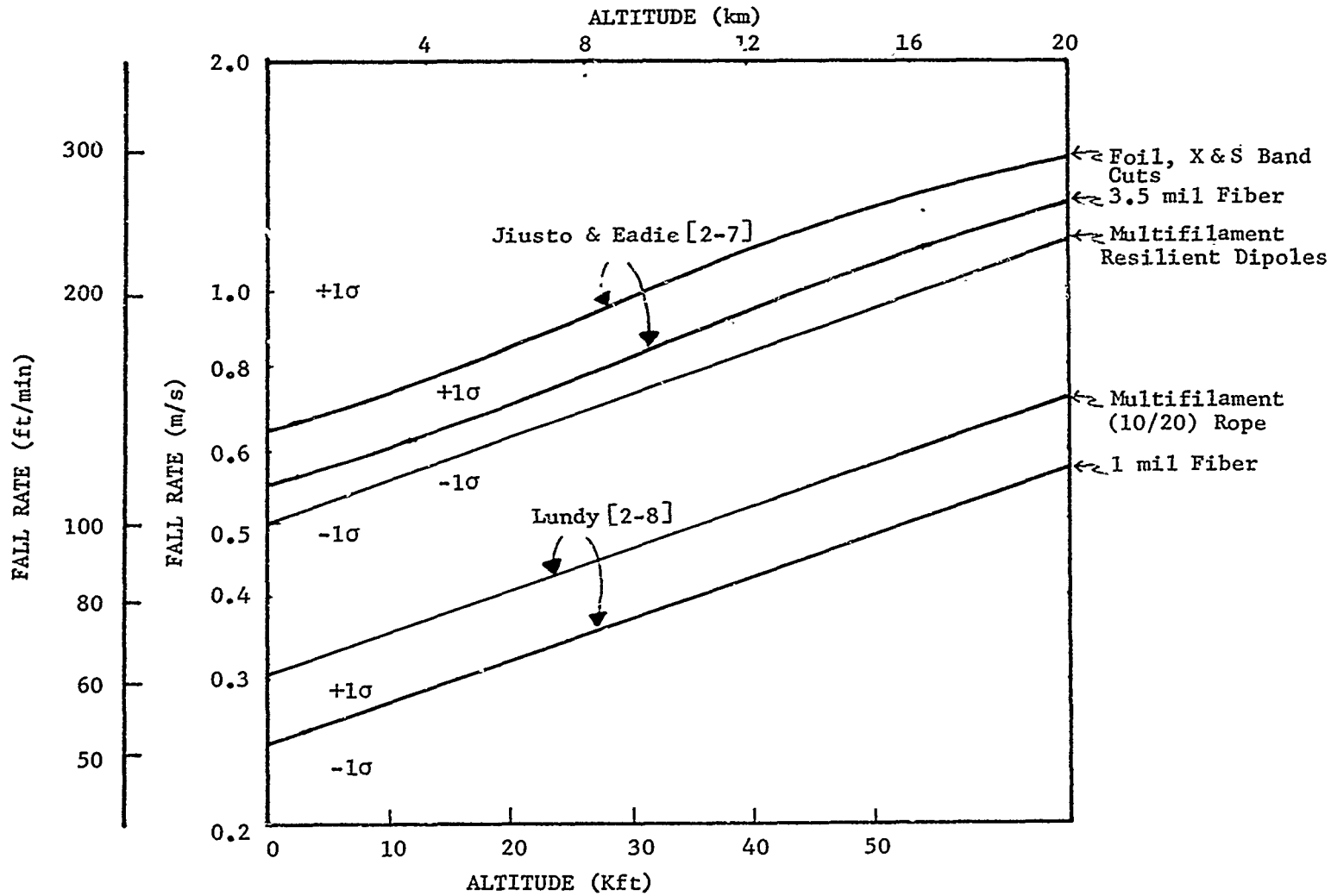

Figure 2-4

Fall Rates of Chaff

between two points, the quantity $y = \log_{10} \alpha$ is normally distributed, with mean μ_y and standard deviation σ_y, that are functions primarily of frequency and location, and partly of path length. This law for the distribution of rain attenuation is directly related to an observed distribution of rain rate which is also log normal. In that case, the parameters are principally associated with location.

Rain rate distributions are modeled in terms of three parameters, μ_y, σ_y, and P_o, as follows:

$$P(\beta)\, d\beta = \frac{1}{\sqrt{2\pi}} \exp\left\{-\beta^2/2\right\} d\beta$$

where $\beta = \dfrac{y-\mu_y}{\sigma_y}$,

$y = \log_{10} r$,

r = rain rate and

μ_y, σ_y = mean, standard deviation of y .

The fraction of time that rain rate exceeds r is:

$$P(\text{rate} \geq r) = P_o \cdot \frac{1}{2} \operatorname{erfc}\left\{\frac{\beta}{\sqrt{2}}\right\}$$

where* $\operatorname{erfc}(x) = 1 - \operatorname{erf}(x) = \dfrac{2}{\sqrt{\pi}} \displaystyle\int_x^\infty e^{-t^2}\, dt$.

P_o = Probability that it is raining at the point in question.
The above accurately fits observations of rain rate frequency to probability levels of 0.0001 [2-9].

---

* Note: $\frac{1}{2} \operatorname{erf} \left\{\frac{\beta}{\sqrt{2}}\right\}$ is the familiar one-sided probability integral:

$$\int_o^\beta \frac{1}{\sqrt{2\pi}} \exp\left\{-\frac{t^2}{2}\right\} dt.$$

essential parameters for application of this model, P_o, μ_z, & σ_z, can be extracted from the large body of rain observations that have been summarized in various places [e.g., 2-10, 2-11]. Table 2-4 lists typical year-round values of these parameters for various global locations and for the world as a whole. Typical point distributions are shown in figures 2-5, 2-6 and 2-7.

2.3 Spatial Distribution of Rain

Two types of rain states represent end points of what in nature is a continuum: quasi-uniform rain and storms. The former is widespread over a scale of mesoscale magnitude, such that a radar, all of its targets, and the space in between are immersed in rain having a single nominal descriptor. This presumption, however, need not be so unreal or restrictive as to deny variation in rain density from point to point. Storms are characterized by cells of rain, generally relatively dense at their core, and surrounded by areas of much lighter or no rain.

2.3.1 Quasi-Uniform Rain

This idealization of rain can be associated with the condition that the variation of rain rate from point to point (or time to time) over a region is smaller than the average over that region. It can be seen from figure 2-8 that this condition was seen in one two-year period about 60 percent of the time, but that the average rain rate never exceeded 8 mm/hr under those conditions [2-12]. Moreover, standard deviations of 30 percent or less in rain rate were seen only about 25 percent of the time and only for average rain rate less than about 4 mm/hr. In the limit of small fluctuation of rain, a Gaussian distribution about its median of the logarithm of rain rate is reasonable, with a typical standard deviation σ_y of $y = \ln r_{av}$ of

$$\sigma y = + 0.5 + 0.6 \ln r_{av}, \qquad 0.3 \geq r_{av} \geq 10 \text{ mm/hr}$$

where σ_y is in nepers (4.34 dB).

Note -- There is no table 2-5 and no figure 2-9.

2.3.2 Storms

There are three features of storms for which model data are available: the horizontal distribution of rain rate in a storm cell; the height of cells; and cell separation. In addition, much data exist to predict the frequency of occurrence of rain of given intensities (see Section 2.2).

Table 2-4

Parameters of Rain Frequency Distributions [2-11]

LOCATION	μ_y	σ_y	P_o
Whole World	-0.53	0.88	0.06
Thailand	+0.15	0.65	0.049
South Viet Nam	+0.20	0.66	0.042
Singapore	+0.44	0.61	0.035
Guam	-0.13	0.63	0.14
Atlantic - 40 - 60 N	-0.27	0.74	0.054
Atlantic - 60 - 65 N	+0.17	0.31	0.064
Denmark	-0.06	0.49	0.022
Turkey	+0.36	0.26	0.011

Definitions:

r = rain rate in mm/hr

y = $\log_{10} r$

μ_y = mean of y when $r > 0$

σ_y = standard deviation of y when $r > 0$

P_o = fraction of time $r > 0$

Prob (rain rate > r) =

$$P_o \cdot \int_y^{\infty} \frac{1}{\sqrt{2\pi}\sigma_y} \exp\left\{-\frac{(y-\mu_y)^2}{2\sigma_y^2}\right\} dy$$

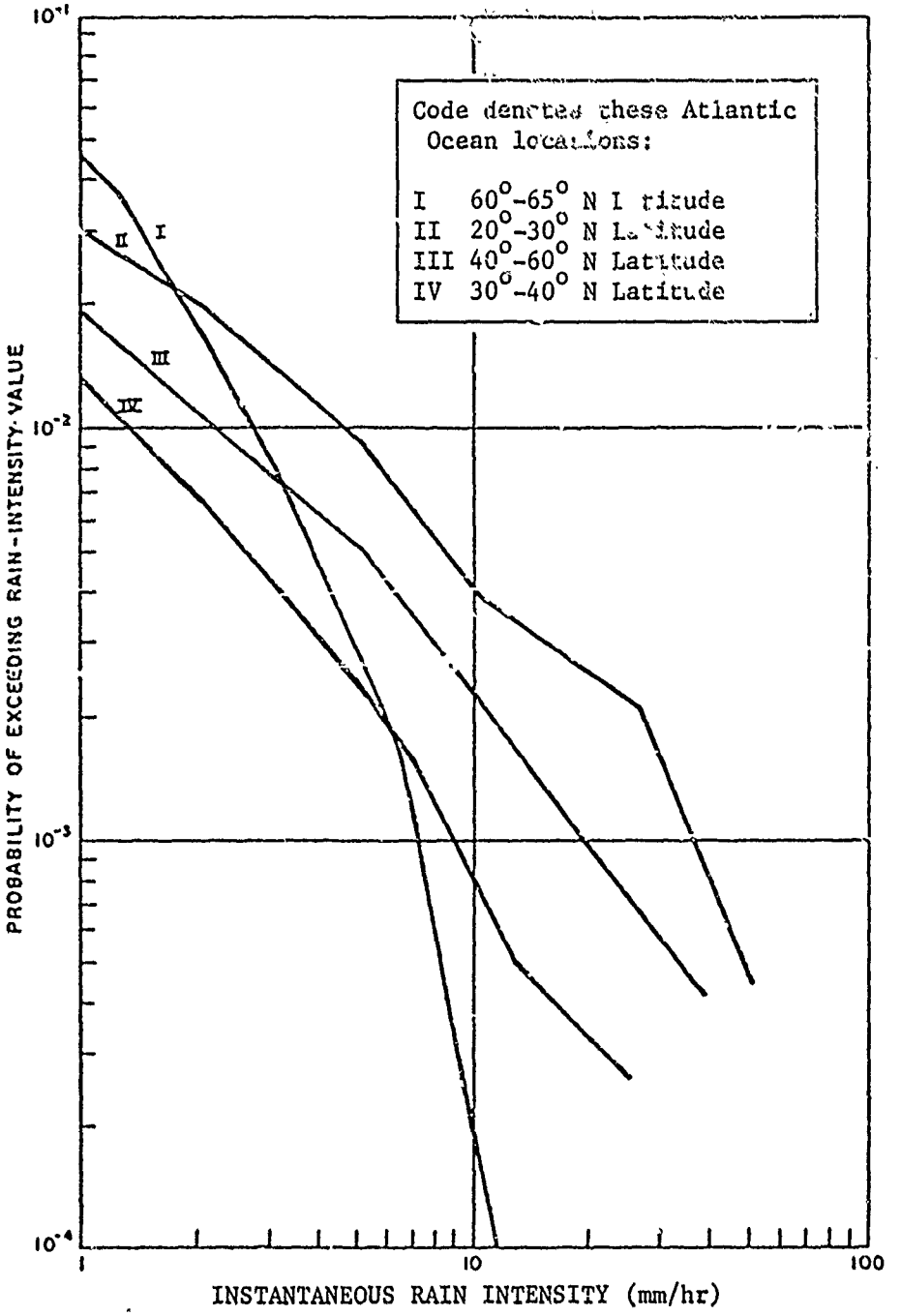

Figure 2-5

Probability That Rain Intensity Exceeds Specified Value for Atlantic Ocean Locations

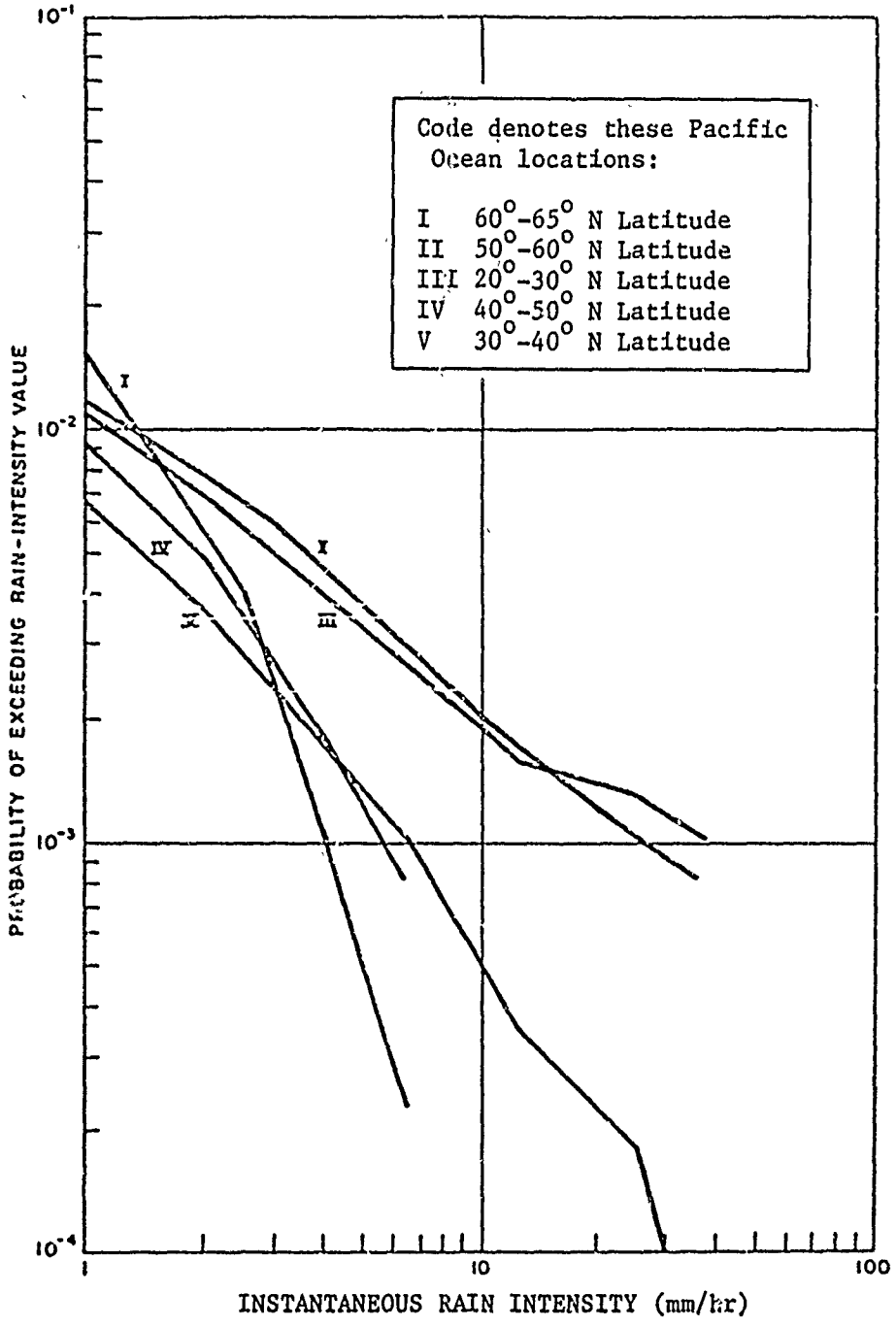

Figure 2-6

Probability That Rain Intensity Exceeds Specified Value for Pacific Ocean Locations

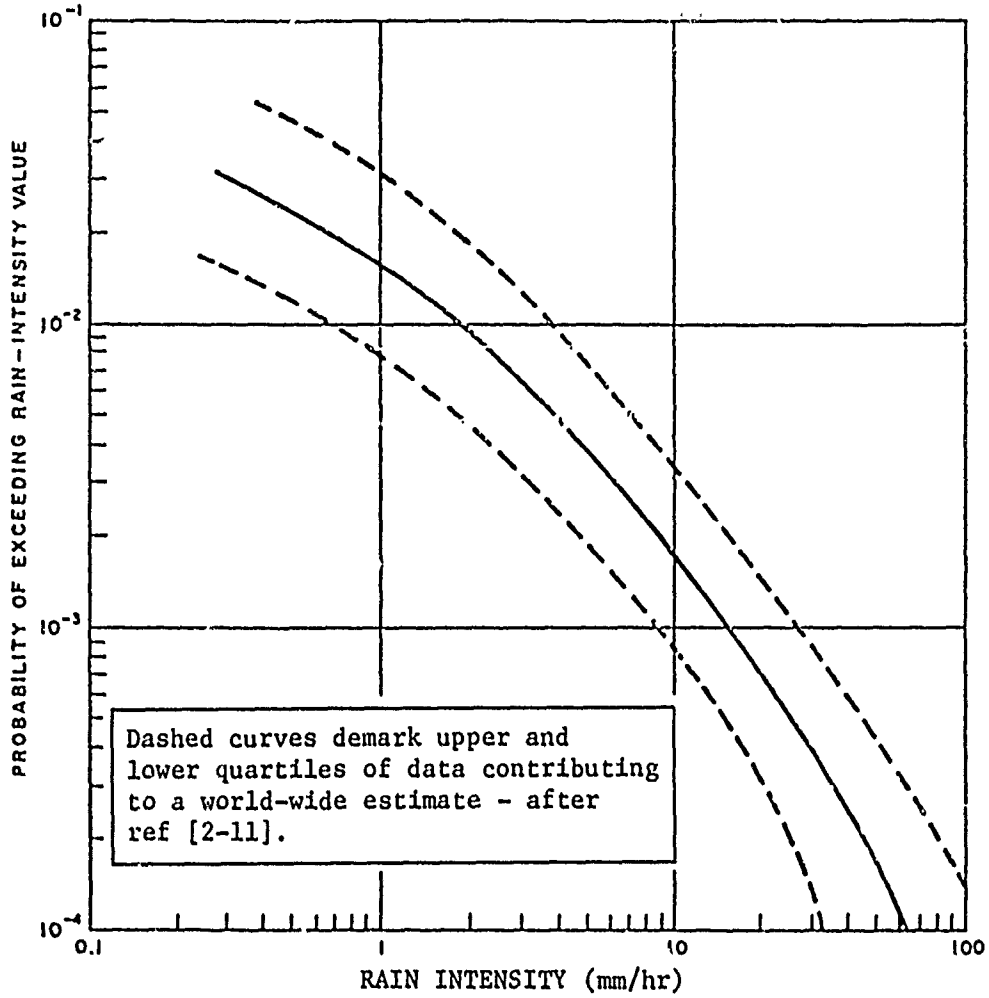

Figure 2-7

World Average Probability That Rain Intensity at a Given Point Will Exceed a Specified Value

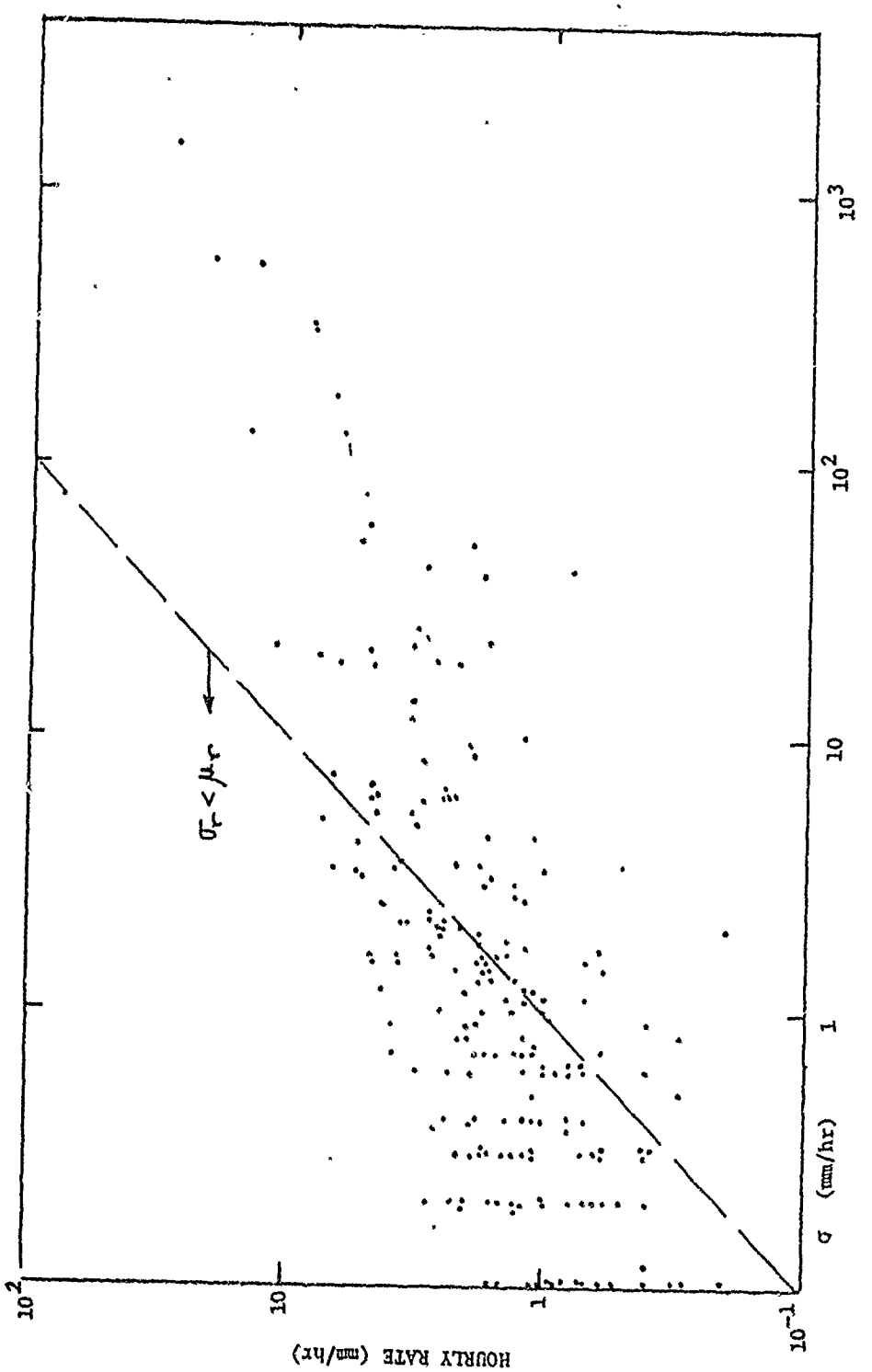

Figure 2-8

Standard Deviations of 120 30-Second Rates vs Hourly Rates for a Number of Storms in 1962

Storm cells are spatial regions of rain characterized generally by greatest density at their center and monotonic fall-off radially outward. Let A be the area included within a contour along which r is the rain rate. Then

$$r = r_c\, e^{-1.38\, x}$$

where r_c = the rain rate at the center of the cell at the same altitude as r, and

$$x = \left(\frac{A}{17.5\ \text{nm}^2}\right)^{1/3} = \left(\frac{A}{60\ \text{km}^2}\right)^{1/3}$$

The shape of a contour with area A is approximately elliptical. If the dimensions of the ellipse are a and b, $a \geq b$, such that $A = \frac{\pi}{4} ab$, then the most probable value of $a/b = 1$, and its median is 1.7 [2-14].

For some cells, the rain rate in a cell decreases monotonically with altitude. For others, the density may increase from the surface to a certain altitude and fall-off above it. If r_{cs} is the surface center rain rate, and the center rain rate at altitude h is $r_c(h)$, the fall-off with altitude can be typified by

$$r_c(h) = r_{cs}\, e^{-b\, h^2}$$

Clearly this distribution approximates the case when the rain cell has its base at the surface [2-15]. The parameter b varies depending on the type of storm, over the range of 0.2 km^{-2} (0.018 kft^{-2}) [2-11] to 3.329 km^{-2} (0.0033 kft^{-2}) [2-15].

The cells of a storm are separated by distances that vary over a range, but the distribution of separations is unimodal, as seen in figure 2-10. This distribution is very close to Rayleigh,

$$p(y)\, dy = y \exp\left\{-\frac{y^2}{2}\right\} dy$$

$$P(Y<y) = 1 - \exp\left\{-\frac{y^2}{2}\right\}$$

in which $y = \delta/\delta_m$, $\delta_m \approx 28.3$ km or 15.3 nm [2-15].

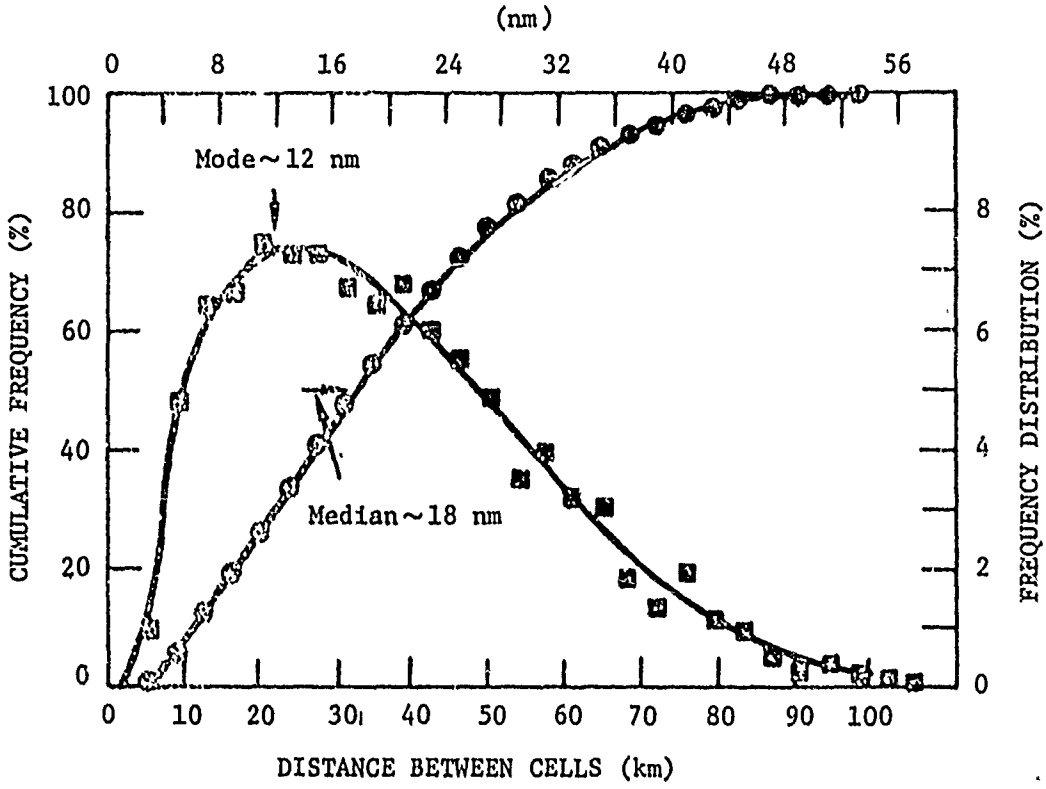

Figure 2-10

Distribution of Distance Between Rain Cell Centers [2-15]

2.4 Chaff Design Characteristics

The objective in chaff design is to obtain the largest radar return and the slowest fall rate with the least weight of chaff material. A number of exotic chaff techniques such as absorbers and aerosols have been considered from time to time, but the half-wave dipole has proven to be a very efficient scatterer and is the most widely used chaff element. It will likely remain so for many years.

The two most common materials for both US and Soviet chaff are aluminum foil and aluminum-coated glass filaments. The trend is to the coated glass which exhibits a larger cross section per pound of material and falls at a slower rate than foil chaff. The trend in glass filament chaff is to smaller diameters of filaments to improve its characteristics even more. Presently 1 mil diameter filaments are the most common for frequencies above approximately 3 GHz. Below this frequency, larger diameter filaments are used to give the dipoles more rigidity. A resilient chaff consisting of bonding together several glass filaments to form a composite strand about 3 mils in diameter has also been used for lengths over 2 inches (below 3 GHz). Foil chaff having a thickness of 0.45 mil is commonly used (1 mil $\cong$ 0.025 mm).

2.4.1 Reflectivity Characteristics of Chaff Dipoles

The radar cross section of a single half-wavelength dipole is maximum when the dipole is parallel to the incident electric field.

For a high conductivity dipole element, the maximum cross section is given by,

$$\sigma_{max} = 0.86\ \lambda^2 \ . \qquad (2\text{-}1)$$

For a random orientation, the average cross section per dipole is, approximately,

$$\sigma_d = 0.18\ \lambda^2 \ . \qquad (2\text{-}2)$$

In the absence of shadowing and clumping effects, the cross section of a collection of chaff dipoles is linearly related to the total number of dipoles N_t, resulting in a total cross section of,

$$\sigma_t = 0.18\ \lambda^2\ N_t \qquad (2\text{-}3)$$

In practice, the cross section predicted by the above is rarely achieved. Effects which tend to reduce the cross section actually obtained include:

1. Finite conductivity of the chaff material.
2. The radar frequency may not be precisely at the resonant frequency of the chaff.
3. The effective number of dipoles may be considerably less than the actual number as a result of clumping and screening effects.

The combined effects of the finite conductivity of a practical dipole and frequency are shown in figure 2-11. This curve from [2-16] is based on the variational procedure devised by C.T. Tai and calculated numerically by Brown [2-17]. The results obtained by this procedure are reported to be in close agreement with experimental measurements. The peak cross section is given by approximately $0.14\ \lambda^2$ rather than $.18\ \lambda^2$ as predicted by (2-3). The cross section is also highly frequency sensitive with a 3 dB bandwidth of approximately 10 percent. The dipole exhibits a secondary peak of about one-third of the maximum at a frequency where the dipole is one wavelength long.

The response is also a function of the length/diameter ratio, $A = 2L/d$. Thin dipoles (large A) tend to be more narrow band than thick dipoles (small A).

The percentage of dipoles actually dispersed is a complex phenomenon which depends on the type of chaff, the dispenser, location, and the environment into which the chaff is dispensed. This percentage is defined as a dispersal efficiency, E_d. Field measurements indicate the dispersal efficiency is rather small, approximately 0.1-0.3 in the first second or so after dispensing when the cloud is small and screening effects are severe [2-18], to a value of 0.6 or more several minutes after dispensing.

Even though the frequency of the chaff may not coincide exactly with the radar frequency, the radar may be required to handle the worst case wherein the two are tuned to the same frequency. A realistic expression for the maximum cross section is then given by

$$\sigma = 0.14\ \lambda^2\ E_d\ N_t\ . \qquad (2\text{-}4)$$

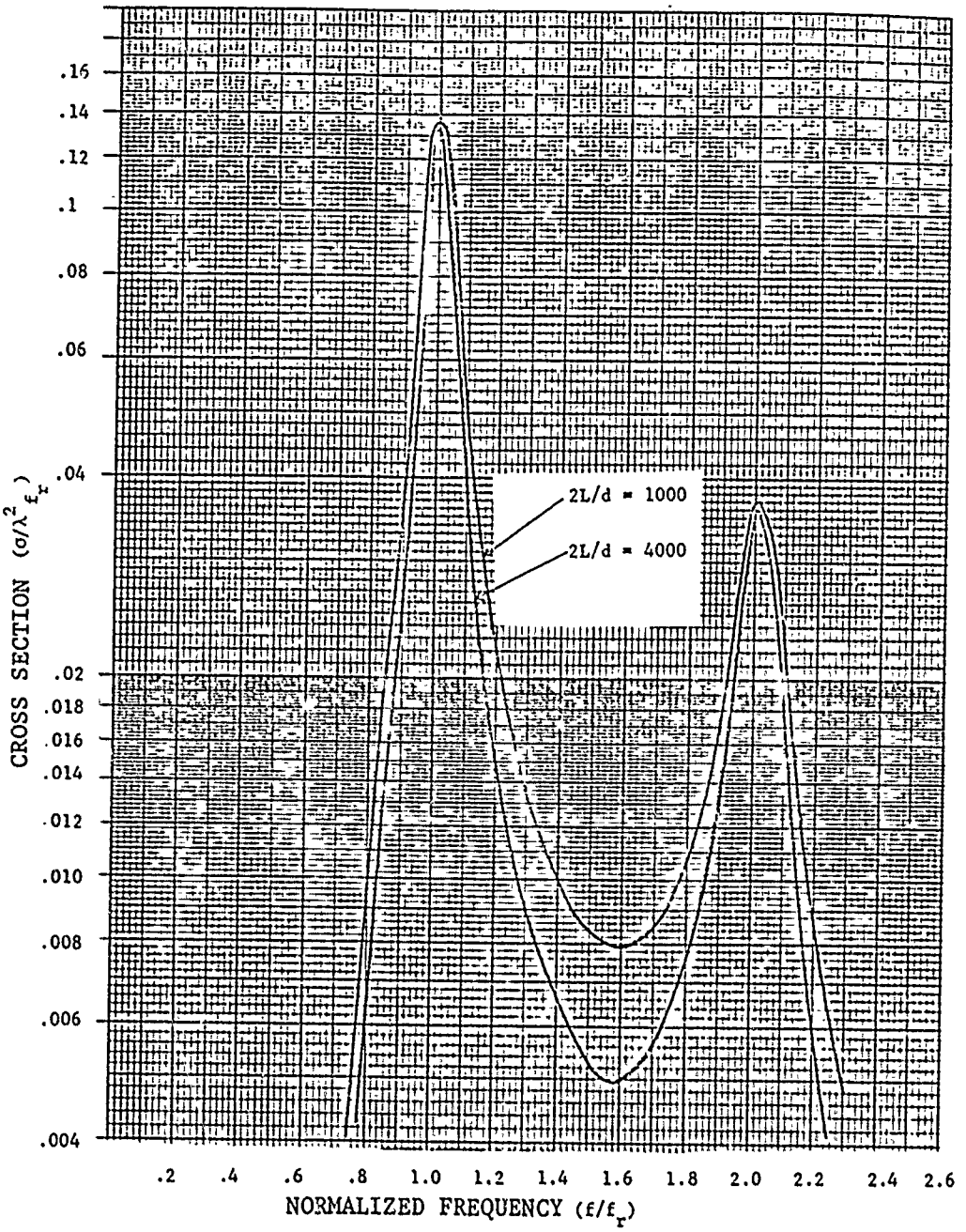

Figure 2-11

Dipole Cross Section in Square Wavelengths as a Function of Frequency (Random Orientation)

A plot of the above in terms of the total number of dipoles effectively dispersed, $E_d N_t$, required for a 1 m^2 cross section is shown in figure 2-12.

2.4.2 Cross Section per Unit Weight

Since the total chaff radar cross section is related to the total number of dipoles through equation (2-4), one can also relate the radar cross section to the weight of chaff material dispensed. For aluminum-coated glass filament chaff, it is assumed that 1 mil filaments are used for frequencies of 3 GHz and above and 2 mil filaments below 3 GHz in order to provide greater rigidity for the longer lengths. Similarly, 6 mil wide by 0.45 mil thick foil is assumed above 3 GHz and 10 mil foil below.

For the above chaff dimensions, the cross section at the resonant frequency per pound of material is given by the following. For glass chaff,

$$f < 3 \text{ GHz} \qquad \sigma = 7700\, E_d/f\ (\text{GHz})\ m^2/\text{lb} \tag{2-5}$$

$$f \geq 3 \text{ GHz} \qquad \sigma = 31{,}000\, E_d/f\ (\text{GHz})\ m^2/\text{lb} \tag{2-6}$$

and for foil,

$$f < 3 \text{ GHz} \qquad \sigma = 5000\, E_d/f\ (\text{GHz})\ m^2/\text{lb} \tag{2-7}$$

$$f \geq 3 \text{ GHz} \qquad \sigma = 8300\, E_d/f\ (\text{GHz})\ m^2/\text{lb} \tag{2-8}$$

where E_d is the dispersion efficiency.

Referring to figure 2-1, it is obvious that if coverage over a band of frequencies is desired, a number of different length chaff elements spaced at 10-15 percent intervals in frequency are required. Generally, it is not necessary to cover a broad frequency band, but only those relatively narrow portions of the spectrum corresponding to the operational bands of known radars. A curve which relates the dipole length to the desired resonant frequency is shown in figure 2-13.

The cross section per unit weight when coverage of a number of discrete frequencies is desired may be computed by observing that the weight of material required for a unit cross section at a given frequency is the reciprocal of (2-5) - (2-8). If coverage at N frequencies above 3 GHz is desired with glass chaff, the resulting cross section per pound of total material is given by,

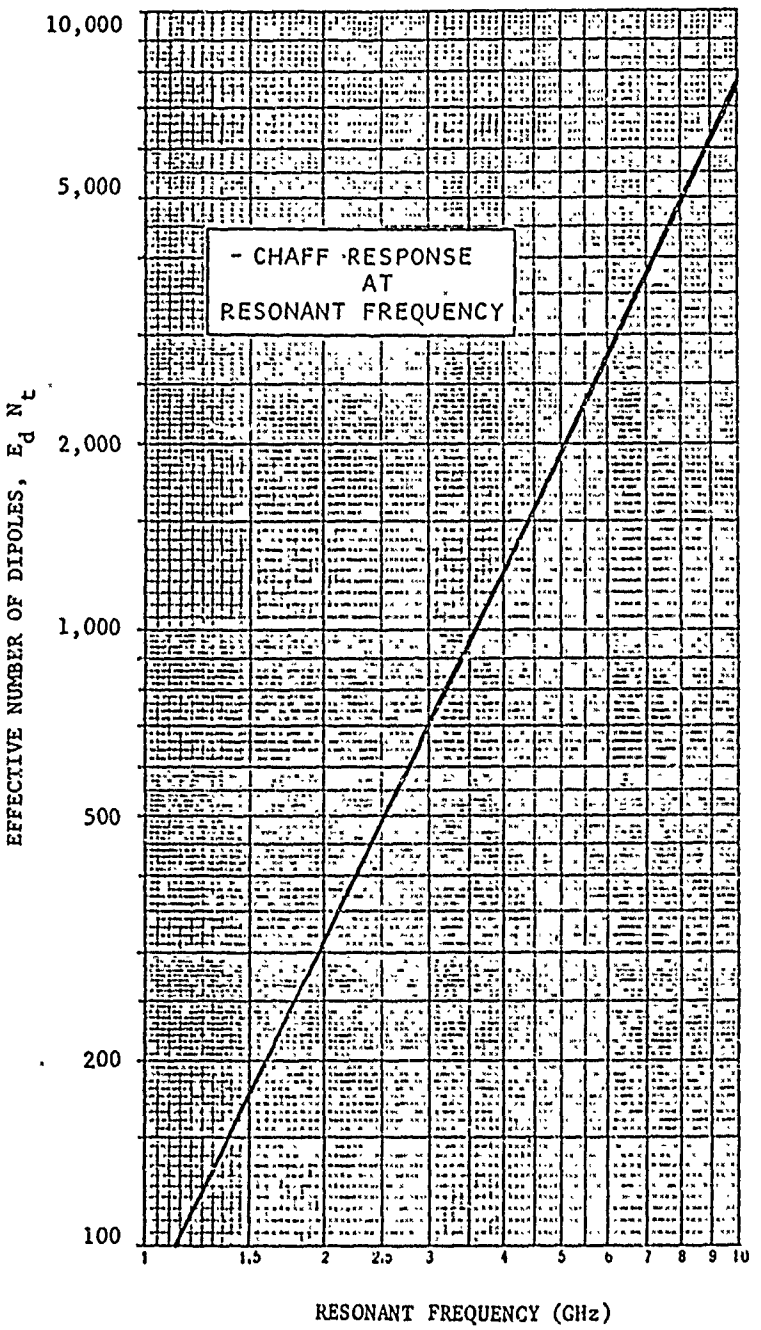

Figure 2-12

Effective Number of Dipoles Required for 1 m^2 Cross Section

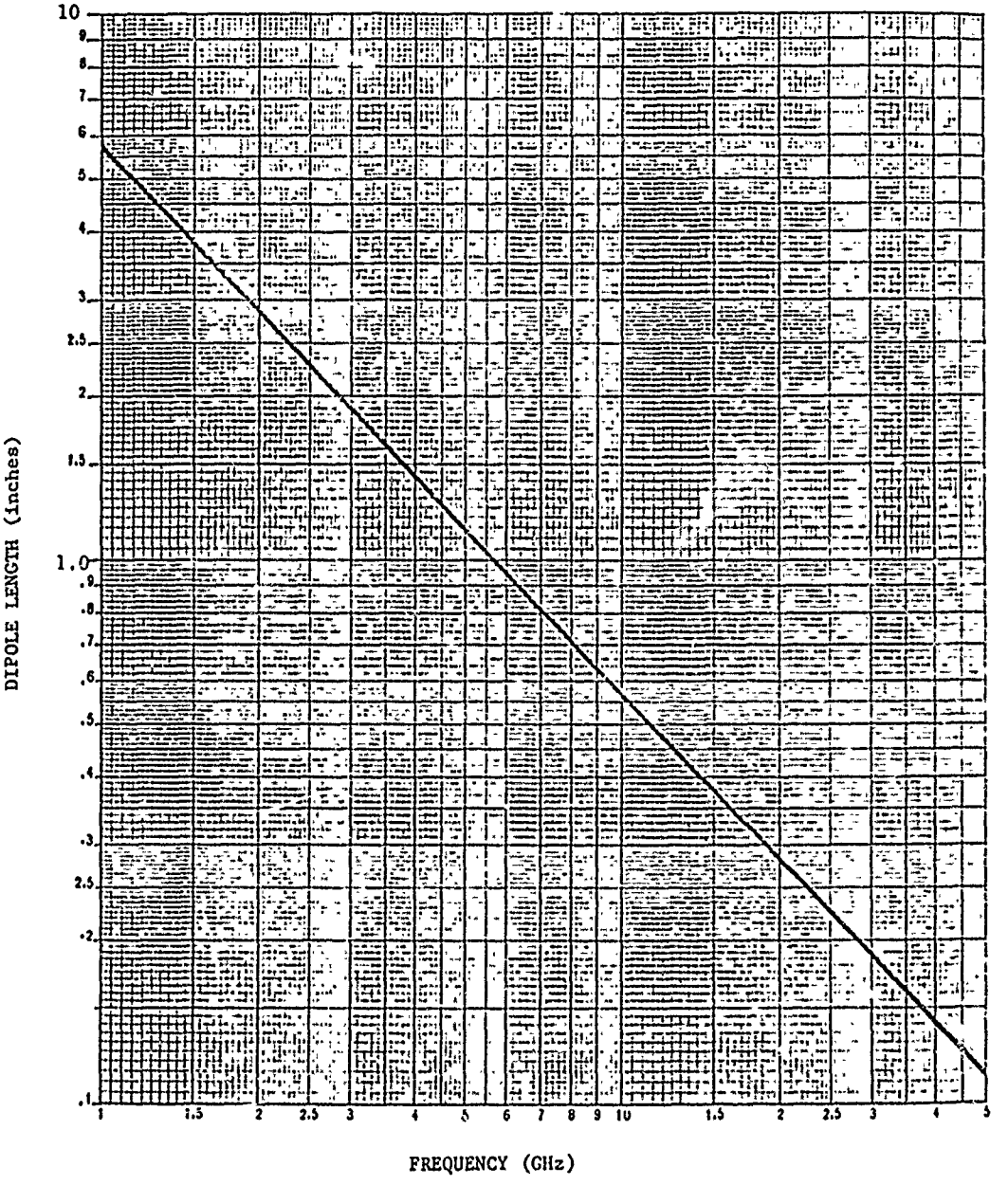

Figure 2-13

Resonant Frequency of Half-Wavelength Metalized Glass Dipoles

$$\sigma = \frac{1}{\sum_{i=1}^{N} f_i/(31{,}000\ E_d)} \quad m^2/lb \qquad (2\text{-}9)$$

In table 2-6 are shown the total cross sections of glass filament and aluminum foil chaff in m^2/lb where a dispersion efficiency of 0.65, typical of large area dispersal, is assumed. In order to cover a band of frequencies, it is assumed that a portion of the chaff is cut to resonate at frequencies spaced every 15 percent resulting in a fairly uniform cross section over the band. The cross section ranges from a maximum of 6,700 m^2/lb for a 10 percent band at 3 GHz to 190 m^2/lb for coverage of the entire 1-10 GHz band. Values for coverage of other portions of the frequency spectrum are also given.

It should be emphasized that chaff cross section specifications should be examined with care to avoid an incorrect interpretation. The highest values of cross section per unit weight are associated with narrow band ($\approx$ 10%) coverage. Using different length dipoles in order to broaden the frequency coverage reduces the cross section per unit weight accordingly. The other highly variable parameter is the dispersion efficiency, or the fraction of the total number of dipoles effectively dispersed. This parameter must be determined from field measurements for a particular dispenser configuration and can range from at least 0.1 to 0.8 depending on the conditions and the time from being dispensed. The values of E_d used in this study are approximately 0.2 in the first second and 0.65 several minutes after being dispensed.

2.4.3 Attenuation Characteristics of Chaff

It is sometimes suggested that a chaff cloud can produce sufficient attentuation of a radar signal to hide an aircraft flying on the opposite side of the cloud. It turns out, however, that the density of chaff required to produce significant attenuation of the signal is extremely large; so large that its backscatter potential is reduced significantly.

Kownacki [2-19] computes the two-way attenuation of a uniform chaff cloud with depth D and a dipole density of N dipoles/unit volume as,

$$\text{Atten.} = e^{-\bar{\sigma}_s ND} \qquad (2\text{-}10)$$

Table 2-6

Chaff Cross Section (m^2/lb., Assumed Dispersion Efficiency = 0.65)

		Glass Filament 2 mil dia - f < 3 GHz 1 mil dia - f ≥ 3 GHz	Foil .45 x 10 mil - f < 3 GHz .45 x 6 mil - f ≥ 3 GHz
Single Frequency (BW ≈ 10%)	f < 3 GHz	5000/f (GHz)	3200/f (GHz)
	f ≥ 3 GHz	20,000/f (GHz)	5400/f (GHz)
D through I Bands (1-10 GHz, 15% spacing)		190 m^2/lb	73 m^2/lb
D and E Bands (1-3 GHz, 15% spacing)		360	240
G and H Bands (4-10 GHz, 15% spacing)		450	120
F through I Bands (3-10 GHz, 15% spacing)		390	105
F through J Bands (3-18 GHz, 15% spacing)		190	52

Unclassified

SECURITY CLASSIFICATION OF THIS PAGE (When Data Entered)

REPORT DOCUMENTATION PAGE

1. REPORT NUMBER: FS-77-144	2. GOVT ACCESSION NO.
3. RECIPIENT'S CATALOG NUMBER	
4. TITLE (and Subtitle): ASSESSMENT OF REQUIREMENTS OF 1985-2000 ERA US NAVY SURFACE SHIPS FOR SURVEILLANCE RADAR INFORMATION, Book II, Volume II, Radar Clutter	5. TYPE OF REPORT & PERIOD COVERED: technical report
	6. PERFORMING ORG. REPORT NUMBER
7. AUTHOR(s): G. Emch et al	8. CONTRACT OR GRANT NUMBER(s): Contract N00024-78-C-5384 Task B98A
9. PERFORMING ORGANIZATION NAME AND ADDRESS: The Johns Hopkins University, Applied Physics Lab, Johns Hopkins Road, Laurel, MD 20810	10. PROGRAM ELEMENT, PROJECT, TASK AREA & WORK UNIT NUMBERS: PE 63516N, Project S0168-AA
11. CONTROLLING OFFICE NAME AND ADDRESS: Chief of Naval Operations, Surface Combat Systems Division, OPNAV 35, Pentagon, Wash., D.C.	12. REPORT DATE: March 1978
	13. NUMBER OF PAGES: 153
14. MONITORING AGENCY NAME & ADDRESS (if different from Controlling Office): Naval Sea Systems Command, Weapons Systems & Engineering Directorate, SEA 652, Washington, D.C. 20362	15. SECURITY CLASS. (of this report): unclassified
	15a. DECLASSIFICATION/DOWNGRADING SCHEDULE: GDS (3) (Indefinite)

16. DISTRIBUTION STATEMENT (of this Report)

Approved for public release; distribution unlimited

17. DISTRIBUTION STATEMENT (of the abstract entered in Block 20, if different from Report)

18. SUPPLEMENTARY NOTES

Prepared for use in Concept Formulation Phase of Shipboard Surveillance Radar Systems Program
See Book I and Book II, Volumes I-V
For summary, see FS-78-155/DRC U-G733

19. KEY WORDS (Continue on reverse side if necessary and identify by block number)

radar clutter, models, weather, chaff, radar propagation

20. ABSTRACT (Continue on reverse side if necessary and identify by block number)

Appendix III presents models of radar clutter for use on the program for evaluation purposes and for making design trade-offs.

DD FORM 1 JAN 73 1473 EDITION OF 1 NOV 65 IS OBSOLETE

Unclassified

where $\bar{\sigma}_s$ is the average scattering cross section per dipole. The product $\bar{\sigma}_s N$ is the volume reflectivity density $\Sigma\,\sigma$ in m^2/unit volume. Expressing the above in dB per meter,

$$\text{2-way Aten. (dB/m)} = -4.34\ (\Sigma\sigma) \qquad (2\text{-}11)$$

where $\Sigma\sigma$ is in the units of m^2/m^3. A heavy chaff threat may consist of a chaff reflectivity density of about 3000 m^2/nm^3, corresponding to 475 x 10^{-9} m^2/m^3. This results in an attenuation of 2 x 10^{-6} dB/m. Therefore, to attenuate a radar return by only 3 dB with a heavy chaff cloud of 3000 m^2/nm^3 would require a chaff cloud thickness of 1500 km (or 800 nm) clearly indicating an impractical approach to screening a target.

Laboratory chaff experiments confirm the fact that radar signals undergo significant attenuation only when the chaff dipoles are extremely dense, in the order of a wavelength or less apart on the average [2-18]. Such a situation exists only in the short period of time immediately after being dispensed. Significant attenuation of target returns resulting from a chaff cloud, therefore, appears to be virtually nonexistent for conventional chaff.

2.4.4 Rope Chaff

Rope chaff is a continuous filament of conducting material whose length is many wavelengths. The material may be a solid metal wire or foil strip, a metallized dielectric fiber, or a multifilament lay of part metallized and part uncoated fibers. Backscattering from such a long filament is characterized in terms of "scattering width" or cross section per unit length of rope. The scattering width is frequency dependent and varies with the size and type of filament, as shown in figure 2-14. "10/20 Stringball Rope" is a loose multifilament lay of 10 metal-coated and 10 uncoated glass fibers, with an overall diameter (if compressed radially) of 3.5 mils [2-8].

Reflectivities of 100-m ropes of three possible materials are compared in table 2-7 for a frequency of 450 MHz. The cross section-per-unit-weight figures shown are for chaff that is actually dispersed, and they do not reflect dissemination, packaging, or system weight efficiencies. Scaling the figures to other frequency bands should be according to the curves of figure 2-14, which have a slope of $f^{-2/3}$ [2-8].

2.4.5 System Weight Efficiency

Aircraft payload weight allocated to chaff systems must be broken down into portions which dispense chaff packages and the chaff packaging itself. Thus, a system handling efficiency factor,

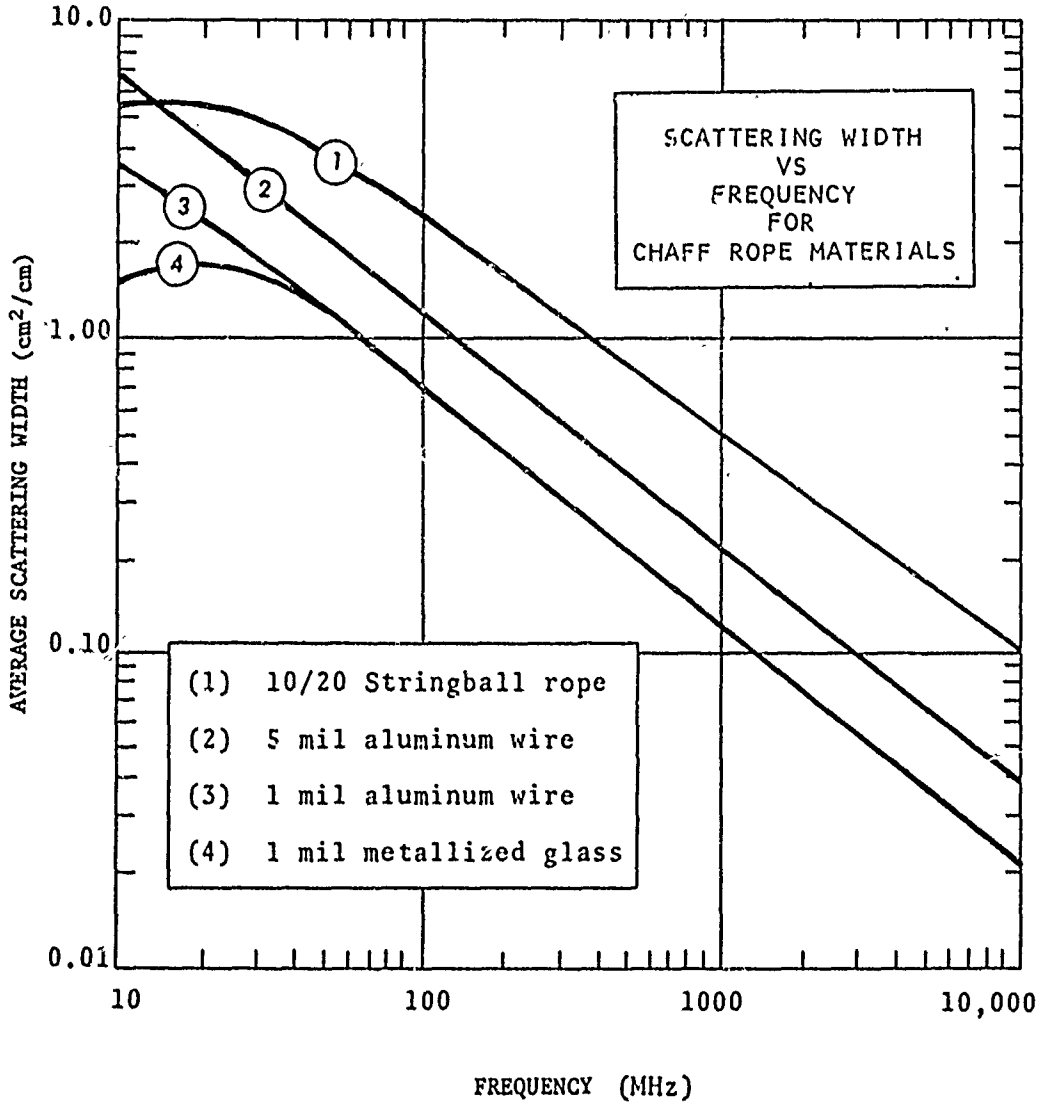

Figure 2-14

Equivalent Scattering Width of Metalized Glass Rope Chaff and Solid Aluminum Wires [After Reference 2-8]

Table 2-7

A Comparison of Rope Chaff Types

Type	Density	Scattering Width @ 450 MHz	Per 100 m Strand		Cross Section Per Unit Weight (unpackaged)	Ref.
			Cross Section @ 450 MHz	Weight		
5 - Mil Al. Wire	0.033 g/m	0.4 cm	0.4 m^2	3.3 g	121 m^2/kg	2-8
1 - Mil Met. Glass	0.0022 g/m	0.22 cm	0.22 m^2	0.22 g	1000 m^2/kg	2-8
10/20 Stringball Multifilament	0.011 g/m	0.95 cm	0.95 m^2	1.19 g	864 m^2/kg	2-8
6 mm wide Al. Foil	0.7-1.5 g/m	4.5 cm	30 m^2	50-100 g	300-600 m^2/kg	2-38

NOTES:

1. 10/20 stringball rope is 10 uncoated + 10 coated fibers parallel and loosely twisted.
2. Scattering width is scattering cross section per unit length, length >> wavelength, average overall orientations.
3. At frequencies above resonance, scattering width (and cross section of a given length) varies as $\approx f^{-2/3}$.

apart from the dispersion efficiency factor, must be applied to compute usable chaff weights in the air that result from a given aircraft payload. Typical estimated system factors are listed in table 2-8 for cartridge monofilament, roll-packed continuous dispersal, and mono-filament-rope systems.*

2.4.6 Chaff Cloud Growth

After dissemination, a cloud of chaff dipoles will increase in size under the influence of atmospheric turbulence, wind shear and differences in fall rate. Although the qualitative effects of these mechanisms are understood, their quantitative results are as uncertain as the properties of a real atmosphere and of real chaff are variable. Atmospheric turbulence produces local mixing of air parcels so that chaff from regions of higher density is moved statistically toward regions of lower density. Turbulent diffusion results in a growth law for a cloud dimension of

$$r_c(t) = \sigma_v k_v t^{1/2}$$

for values of cloud radius r_c greater than about a hundred meters, in which σ_v is the rms turbulence velocity and k_v is a constant of the order of 110 sec $^{1/2}$ for spherical clouds (see Section 2.1.3 for typical values of σ_v) [2-34].

Wind shear acts to transport air (and chaff) at one altitude at a faster rate or in a different direction from air and chaff at another altitude, thus developing an increased overall dimension of the cloud in the direction of the vector shear. Shear growth is linear in time and is proportional to the shear vector magnitude (the gradient of wind speed) and the cloud dimension in the direction of that gradient (generally height). Thus, a shear growth law such as

$$x_c(t) = z_c \frac{d\vec{u}}{dz} t$$

might apply. Here x_c and z_c are the cloud dimensions in the horizontal along-wind-shear and the vertical directions, respectively, and $\vec{u}$ is the vector wind velocity (see Section 2.1.2 for typical values of $d\vec{u}/dz$).

Chaff dipoles fall under influence of gravity and air drag at rates that are determined by their mass, their diameter, and

* Estimates based in part on data in [2-8, 20-23].

Table 2-8

Estimated Weight and Efficiency Factors of Chaff Systems

SYSTEM TYPE	UNIT ON-BOARD EQUIPMENT[1]		CHAFF WT/PACKAGE WT[2]	SYSTEM EFFICIENCY (EXCEPTING DISPERSION)
	NOMINAL GROSS WT	NET DISPOSABLE WT		
Cartridge Dispenser	150 lb	55 lb	0.7 - 0.8	26%
Roll-Packed Chaff	550 lb	300 lb	0.95	52%
Stringball Rope (Fiber-Type)	See Cartridge Dispenser		0.1 - 0.2	4 - 8%

NOTES: [1] Includes estimated allowance for carriers, drives and controllers.

[2] Includes factor of 0.9 to account for imperfectly coated chaff.

shape-induced aerodynamic effects. This latter can produce a large spread in fall rates, but when all fibers fall in the same aerodynamic mode, a spread in fall rate of the order of 10% (1- σ) is created by tolerance variation in fiber diameter alone (mostly attributed to coating thickness variation). The corresponding tolerance effects for more typical production chaff may be $\pm$30%[2-7, 2-35]. Figure 2-4 showed some fall rate data for homogeneous chaff of several types. When chaff is disseminated in mixtures having a range of diameters or cuts of different lengths, or when the packing or dissemination produced dipole distortion that induces different aerodynamic fall modes, then large variations in fall rate should be expected. For example, Chemring has been reported to have identified 14 dipole fall modes in vertical wind tunnel observations [2-36], and Puskar of AFAL has identified 6 major modes [2-38]. However, in spite of the large number of modes possible, it may be the case either that one or at most a few modes predominate or that fall rates and average orientations may be similar for groups of modes, so that a simpler description of chaff fall is possible statistically. Puskar observed one batch of foil dipoles, 90% of which fell in one mode, a flat spin with a predominantly horizontal dipole orientation. Vakin and Shustov [2-37] suggest that the modes split into two main groups, one of which falls slowly and is oriented predominantly horizontal, while the other falls faster and is more steeply inclined toward the vertical. The difference in fall rate caused by mode differences seems to be of the order of 2:1.

2.5 Other Airborne Scatterers

Clouds are characterized by generally low reflectivities because of their low water density compared to rain. Typical reflectivities are 25 dB below that of light rain (see table 2-9). An exception is the Nimbo-Stratus form in which reflectivity resembles that of light rain, but with a horizontal distribution of a storm model. The vertical distribution of that cloud differs from a continous quasi-uniform rain model only in its lower boundary: about 2 km for the cloud and sea level for the rain model [see also reference 2-24].

The larger birds have cross sections below those of most Naval tactical targets, but within a few tens of miles of land, gulls abound at some times of the day, and their backscatter will be well above noise in some shipboard radars. Typical cross sections are depicted in figures 2-15 and 2-16.

Table 2-9

Reflectivity Statistics for Clouds

	Cirrus (Ci)		Alto-Cumulus Ac or Alto-Stratus As		Strato-Cumulus (Sc)		Nimbo-Stratus (Ns)	
$\overline{Z}\left(\frac{mm^6}{m^3}\right)$	0.20		0.53		0.50		106.7	
σ_z (variation)	0.54		1.24		0.60		262.0	
Z_{mode}	0.05		0.05		0.50		50.0	
$\overline{Z}$ in db below 1 mm/hr rain	-30		-26		-26		-3	
Specific Examples of Vertical Profiles	Hgt (meters)	$\overline{Z}$	Hgt (meters)	$\overline{Z}$	Hgt (meters)	$\overline{Z}$	Hgt (meters)	$\overline{Z}$*
	7460	0.11	4880	0.35	900	0.5	1250	3.4
	7820	0.09	5210	0.80	1150	0.43	1750	5.9
	8180	0.07	5540	1.16	1370	0.31	2250	9.0
	8540	0.07	5880	1.14	1600	0.31	2750	36.0
	8900	0.07	6250	0.58	1800	0.31	3200	272.5†
							3400	199.0
							3600	84.5
							3800	28.5
							4000	15.6
							4200	3.1
Peak Cloud Hgt	9000 (meters)		6500		2000		4000	
Min. Cloud Hgt	6900 (Meters)		4400		700		750	

*$\overline{Z}$ = 200 for 1 mm/hr rain

† Bright Band (0°C)

Data from Reference [2-25] Ignatova, Petruskevskii, and Sal'man

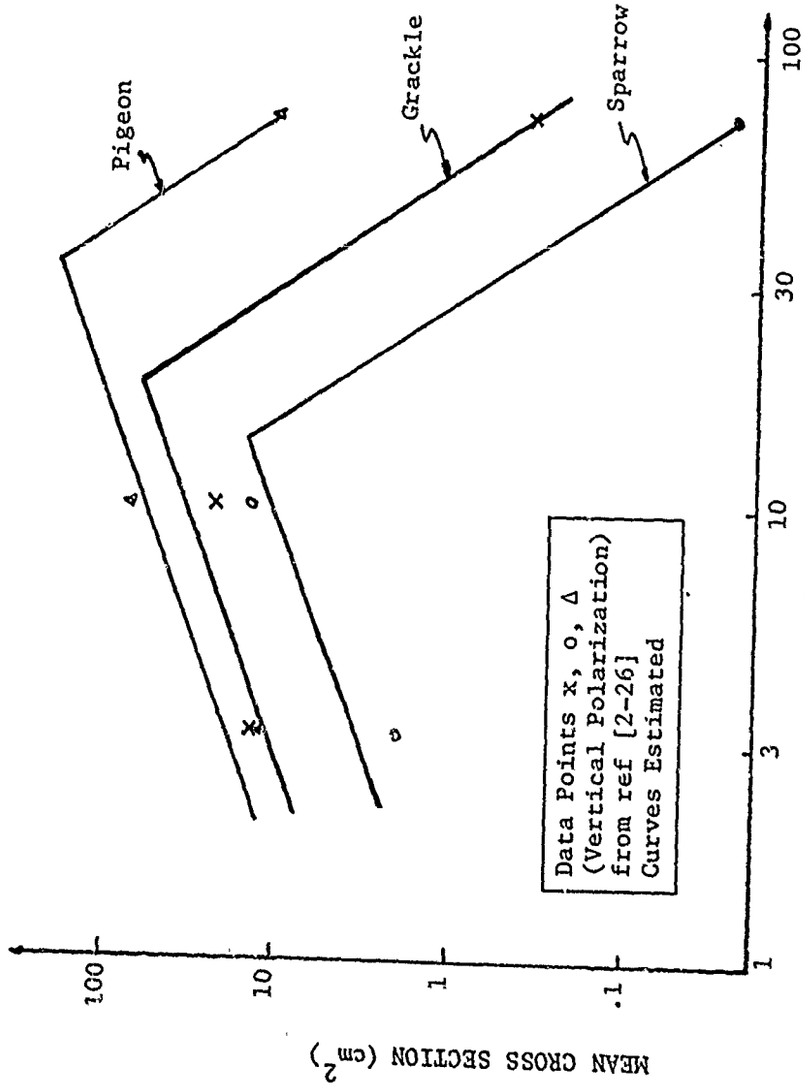

Figure 2-15
Bird Mean Radar Cross Sections

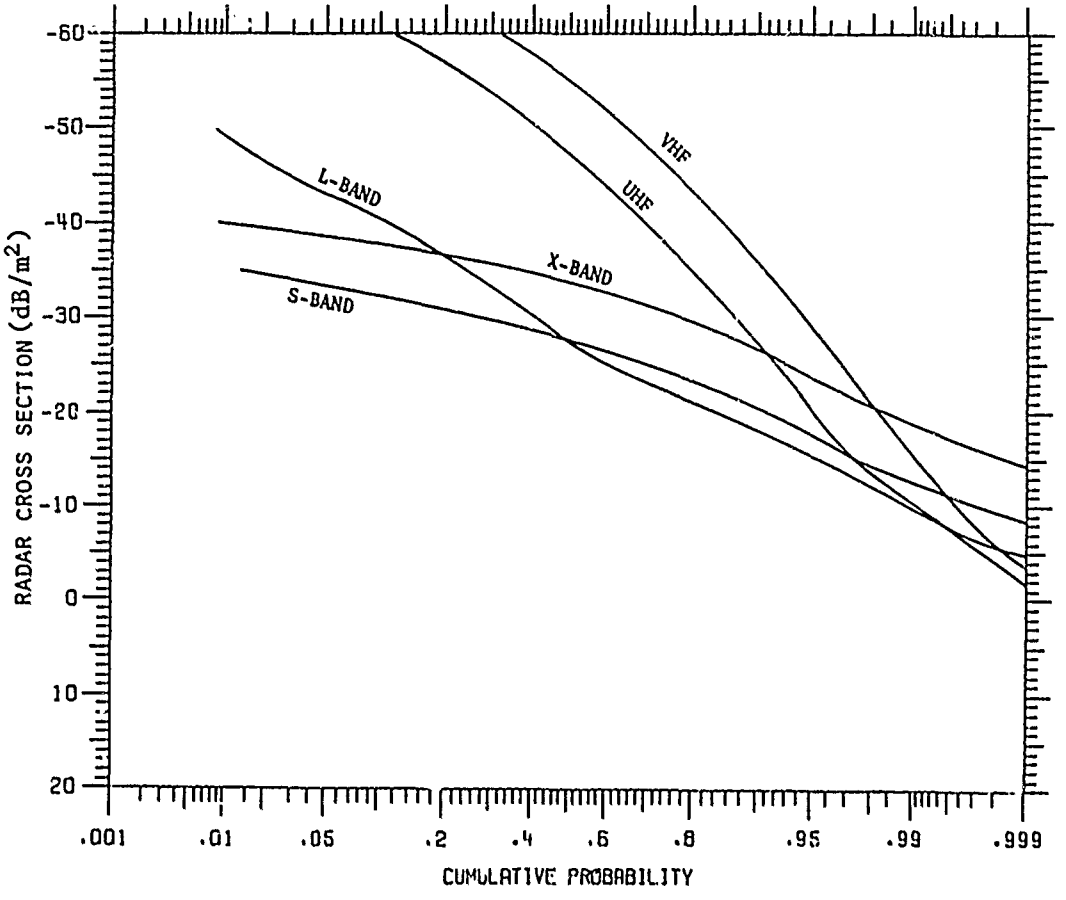

Figure 2-16

Derived Bird Mean Radar Cross Section Distribution [2-27]

2.6 References, Chapter 2

2-1 J. S. Marshall, and W. Mck. Palmer, "The Distribution of Raindrops with Size," J. Meterology, 1948.

2-2 J. Joss and A. Waldvogel, "A Method to Improve the Accuracy of Radar-Measured Amounts of Precipitation," Fourteenth Radar Meteorology Conference, November 1970.

2-3 I. Katz, et al., "Radar Derived Spatial Statistics of Summer Rain; Vol. I: Experiment Description," NASA Contractor Report CR-2592 (APL/JHU), September 1975.

2-4 F. E. Nathanson, Radar Design Principles, McGraw-Hill Book Co., 1969.

2-5 J. R. Scoggins and M. Susko, "FPS-16 Radar/Jimsphere Wind Data Measured at Eastern Range," NASA TMX-53290, George C. Marshall Space Flight Center, Huntsville, AL, 19 July 1965.

2-6 P.R. Brooks and L.W. Brooks, "Survey of Weather Clutter Literature," Memo No. TSC-W2-41, Technology Service Corporation, Silver Spring, MD, August 1974.

2-7 J. E. Jiusto and W. J. Eadie, "Terminal Fall Velocity of Radar Chaff," J. of Geophysics Research 68, May 1963.

2-8 "Advanced Chaff Materials," Lundy Technical Center, Technical Note D12106, February 1973.

2-9 S. H. Lin, "Statistical Behavior of Rain Attenuation," BSTJ52, p. 557, April 1973.

2-10 S. H. Lin, "A Method for Calculating Rain Attenuation Distributions on Microwave Paths," BSTJ54, p. 1051, July-August 1975.

2-11 H. H. Burroughs, "Rain Intensity-Time Distributions," NOLC Report 729, 15 January 1967.

2-12 P. M. Austin, "Some Statistics of the Small-Scale Distribution of Precipitation," Goddard Space Flight Center, Contractor Report X-751-72-149 (Department of Meteorology, MIT), July 1971.

2-13 (Unused.)

2-14 J. S. Marshall and C. D. Holtz, "Rainshower Statistics from a Montreal Radar," McGill University, October 1969, AD 860 954.

2-15 T. G. Konrad and R. A. Kropfli, "Radar Derived Spatial Statistics of Summer Rain; Vol. II: Data Reduction and Analysis," NASA Contractor Report CR-2592 (Applied Physics Laboratory, JHU), September 1975.

2-16 Bjorksten Laboratories, "Design of Chaff Units," Technical Memorandum D1200-1, Lundy Technical Center, Pompano Beach, Florida, July 1965.

2-17 Brown, B. M., "Dipole Cross-Sections Calculated by Variational Techniques," AF-TM-59, University of Texas Defense Research Laboratory, April 1961.

2-18 Puskar, R. J., "Radar Reflector Studies," Proceedings, IFFF 1975 NAECON, pp. 177-183, May 1974.

2-19 Kownacki, S., "Screening (Shielding) Effect of a Chaff Cloud," IEEE Transactions on Aerospace and Electronic Systems, Volume AES-3, pp. 731-734, July 1967.

2-20 "How Chaff Protects Aircraft," Microwave System News, October/November 1976.

2-21 "AN/ALE-41 Chaff Dispersion," MB Associates, Undated.

2-22 "Performance/Design and Qualification Requirements: QRC-530 Countermeasures, Chaff," Specification LC 20,005, Lundy Technical Center, May 1971.

2-23 "Chaff Systems Directory," Lundy Technical Center, Technical Memo. D12201, January 1973.

2-24 F. A. Berry, et al., Handbook of Meteorology, McGraw-Hill Book Co., 1945.

2-25 R. V. Ignatova, V.A. Petrushevskii, and E. Sal'man, "Radar Echo Characteristics of Clouds," Tr. by American Meteorological Society, 1965.

2-26 T. G. Konrad, J. J. Hicks and E. B. Dobson, "Radar Characteristics of Birds in Flight," Science 195, 19 January 1968.

2-27 G. E. Pollon, "Distribution of Radar Angels," IEEE Transactions, AES-8, November 1972.

2-28 J. O. Laws and D. A. Parsons, "The Relationship of Raindrop Size to Intensity," Am. Geophys. Union Trans., Vol. 24, p. 452-460, 1943.

2-29 E. A. Mueller and A. L. Sims, "Raindrop Distributions at Franklin, North Carolina," Illinois State Water Survey (Urbana) Technical Report TR-ECOM-02071-RR3, 1967.

2-30 E. A. Mueller and A. L. Sims, Raindrop Distributions at Island Beach, New Jersey," Illinois State Water Survey (Urbana) Technical Report TR-ECOM-02071-RR3, 1967.

2-31 R. K. Crane, "Virginia Precipitation Scatter Experiment-Data Analysis," Goddard Space Flight Center Report X-750-73-55, October 1973 (Rev.).

2-32 R. K. Crane, "Propagation Phenomena Affecting Satellite Communication Systems Operating in the Centimeter and Millimeter Wavelength Bands," Proc. IEEE, Vol. 59, p. 173-188, 1971.

2-33 R. Wexler and D. Atlas, "Radar Reflectivity and Attenuation in Rain," J. Applied Meteorology, Vol. 2, p. 276-280, 1963.

2-34 G. Rose and F. E. Nathanson, "Chaff Model for U. S. Navy Surveillance Radar Calculations," Naval Ship Engineering Center Report, October 1974.

2-35 E. R. Coleman, "Chaff Meteorology," International Countermeasures Handbook, p. 518-522, June 1976.

2-36 G. S. Sundaran, "Expendables in Electronic Warfare," International Defense Review 9, p. 1045, December 1976.

2-37 S. A. Vakin and L. N. Shustov, Principles of Jamming and Electronic Reconnaissance, Idz-vo, "Sovetskoye Radio," Moscow, 1968; FTD Translation FTD-MT-24-115-69, AD-692-642.

2-38 C. C. Pinson, "Chaff," JTCG/AS Countermeasures Handbook for Aircraft Survivability, JTCG/AS-76-CM-001.

3.0 AREA CLUTTER

3.1 Sea Backscatter

Sea Echoes (After Pidgeon & Nathanson [3-1 to 3-3])

The early users of radar soon discovered that when transmitting microwave signals in the presence of the sea, large signal returns were received from the ocean surface. In many instances this sea return signal completely masked the target signal that the radar operation was trying to detect. This discovery prompted scientific investigators to commence a most extensive program of studying the effects of the ocean as a rough surface on radar propagation. As early as the closing years of World War II, many research centers such as the Radiation Laboratory of the Massachusetts Institute of Technology were investigating this effect [3-4]. In the years to follow, the method of making measurements of radar scattering from the sea became more and more sophisticated. Extensive programs involving the precise measurement of the physical surface of the ocean by means of stereophotography and free floating spar buoy wave gauges were coupled with elaborate research radars especially designed for the purpose of measuring time, frequency, and spatial correlation characteristics of radar sea return [3-1].

After these many years, considerable understanding of the microwave scattering properties of sea has been obtained. This understanding has become enough to reverse the trend of this research - radar is now used as a research tool in the field of physical oceanography to study ocean wave heights, lengths, periods, their distributions, wave dynamics, and the state of the sea.

From information taken from Kinsman [3-5] and Pierson [3-6] relationships can be obtained relating significant wave height (average of the highest one-third of the waves) to average wave "periods," "lengths," and "velocities." A fully arisen sea is assumed.

$$H_{1/3} = H_s = 0.103 \quad T^{5/2}$$

$$= 0.0218 \quad L^{5/4}$$

$$= 0.0047 \quad C^{5/2}$$

and

$$H_{1/3} = 0.0045 \quad W^{5/2},$$

where W = wind speed in kts and H_s is significant wave length, L is ocean wave length, T is wave period and C is average wave "velocity." Dimensions of feet, seconds, and feet-per-second are used.

3.1.1 Description of the Sea Surface

The quantitative interpretation of radar scatter from the sea requires the use and appreciation of certain properties of ocean waves. A brief review is undertaken here of the ocean-wave physics and characteristics which we will need later; also, common oceanographic nomenclature pertaining to ocean waves is defined and explained. A readable but detailed treatment of all aspects of ocean wave physics can be found in the text by Kinsman [3-5]; a more elementary introduction to water waves is the concise soft-cover booklet by Bascom [3-7].

Sea State

This term, as used here, refers to the state of the sea, or roughness, as determined by the heights of the largest waves present. Numbers have been assigned to sea states by the International Mariners Codes, and these are related to wave heights. Sea state should not be confused with Beaufort scale, which is a measure of wind force only.

Significant Wave Height

This term is a common maritime descriptor referring to the average of the heights - from crest to trough - of the 1/3 highest waves; it is denoted $H_{1/3}$.

RMS Wave (or Roughness) Height

This is a term describing root-mean-square height (above the mean surface level) used in rough surface scatter theories; it is denoted here by h. While there is no exact general relationship between h and $H_{1/3}$, a common approximation frequently used for wind waves is $H_{1/3} = 4.0h$.

Length

The length or spatial period of a single ocean wave is the distance from one crest to another; it is denoted by L.

Period

Unless denoted otherwise, this refers to the temporal period, and is the length of time it takes two successive crests of a single wave to pass one point. It is denoted by T.

Spatial Wavenumber

This is defined in terms of the length of an ocean wave as $K = 2\pi/L$.

Temporal Wavenumber

This radian wavenumber is given in terms of the period by $\omega = 2\pi/T$.

Fetch

The fetch is the horizontal distance over which a nearly constant wind has been blowing. (It is also defined by its duration).

Duration

This term refers to the length of time during which a nearly constant wind has been blowing.

Wind Waves

This term refers to a system of ocean waves which is being, or has very recently been, aroused by winds blowing locally above that area of the ocean. Wind waves result in a random appearing ocean height profile.

Fully Developed Seas

This is an equilibrium sea state condition reached after sufficient duration and fetch at a given wind speed. The estimated duration and fetch versus wind speed required to produce fully developed seas is given in figure 3-1.

Swell

When wind waves move out of the area in which they were originally excited by the winds, or after winds have ceased to blow, these waves change their shape and settle down to what is known as "swell." Swell appears less random and more nearly sinusoidal, of great length, and with great width along the crestlines. The usual

SEA STATE [1]	SEA-GENERAL DESCRIPTION [2]	(BEAUFORT) WIND FORCE	WIND [3] DESCRIPTION	WIND [3] RANGE (KNOTS)	WIND [3] VELOCITY (KNOTS) AVERAGE	WIND [3] VELOCITY (KNOTS) SIGNIFICANT	SEA [3] WAVE HEIGHT FEET AVERAGE 1/10 HIGHEST	SEA [3] WAVE HEIGHT FEET SIGNIFICANT	SEA [3] SIGNIFICANT RANGE OF PERIODS (SECONDS)	SEA [3] PERIOD OF MAXIMUM (ENERGY OF SPECTRUM) T_{max}	SEA [3] $\bar{T}$ (AVERAGE PERIOD)	SEA [3] T_L (AVERAGE WAVE LENGTH)	SEA [3] MINIMUM FETCH (NAUTICAL MILES)	SEA [3] MINIMUM DURATION (HOURS)
0	See like a mirror.	0	Calm	Less than 1	a) 0	0	0	0	–	–	–	–	–	–
	Ripples with the appearance of scales are formed, but without foam crests.	1	Light Air	1 - 3	2	0.05	0.08	0.10	up to 1.2 sec	0.7	0.5	10 in.	5	18 min
1	Small wavelets, still short but more pronounced; crests have a glassy appearance, but do not break.	2	Light Breeze	4 - 6	5	0.38	0.29	0.37	0.4-2.8	2.0	1.4	6.7 ft	8	39 min
	Large wavelets, crests begin to break. Foam of glassy appearance. Perhaps scattered white horses.	3	Gentle Breeze	7 -10	8.5	0.6	1.0	1.2	0.8-5.0	3.4	2.4	20	9.8	1.7 hrs
					10	0.88	1.4	1.8	1.0-6.0	4	2.9	27	10	2.4
2	Small waves, becoming longer, fairly frequent white horses.	4	Moderate Breeze	11-16	12	1.4	2.2	2.8	1.0-7.0	4.8	3.4	40	16	3.8
					13.5	1.8	2.9	3.7	1.4-7.6	5.4	3.9	52	24	4.8
3					14	2.0	3.3	4.2	1.5-7.8	5.6	4.0	59	28	5.2
					16	2.9	4.6	5.8	2.0-8.8	6.5	4.6	71	40	6.6
4	Moderate waves, taking a more pronounced long form, many white horses are formed. Chance of some spray.	5	Fresh Breeze	17-21	18	3.8	6.1	7.8	2.5-10.0	7.2	5.1	90	55	8.3
					19	4.3	6.9	8.7	2.8-10.6	7.7	5.4	99	65	9.2
					20	5.0	8.0	10	3.0-11.1	8.1	5.7	111	75	10
5	Large waves begin to form, the white foam crests are more extensive everywhere. (Probably some spray).	6	Strong Breeze	22-27	22	6.4	10	13	3.4-12.2	8.9	6.3	134	100	12
					23	7.9	12	16	3.7-13.5	9.7	6.8	160	130	14
					24.5	8.2	13	17	3.8-13.6	9.9	7.0	164	140	15
6					26	9.6	15	20	4.0-14.5	10.5	7.4	188	180	17
	Sea heaps up and white foam from breaking waves begins to be blown in streaks along the direction of the wind. (Spindrift begins to be seen).	7	Moderate Gale	28-33	28	11	18	23	4.5-15.5	11.3	7.9	212	230	20
					30	14	22	28	4.7-16.7	12.1	8.4	250	280	23
					30.5	14	23	29	4.8-17.0	12.4	8.7	258	290	24
					32	16	26	33	5.0-17.5	12.9	9.1	285	340	27
7	Moderately high waves of greater length; edges of crests break into spindrift. The foam is blown in well marked streaks along the direction of the wind. Spray affects	8	Fresh Gale	34-40	34	19	30	38	5.5-18.5	13.6	9.7	322	420	30
					36	21	34	44	5.8-19.0	14.3	10.3	363	500	34
					37	23	37	46.7	6-20.5	14.9	10.5	376	530	37

*For hurricane winds (and often whole gale and storm winds) required durations and fetches are rarely attained. Seas are therefore not fully arisen.

a)A heavy bar around this value means that the values tabulated are at the center of the Beaufort range.

b)For such high winds, the seas are confused. The wave crests blow off, and the water and the air mix.

1)Encyclopedia of Nautical Knowledge, W.A. McEwen and A.H. Lewis, Cornell Maritime Press, Cambridge, Maryland, 1953, p. 483

2)Manual of Seamanship, Volume II, Admiralty, London, H.M. Stationery Office, 1952, pp. 717-718

3)Practical methods for observing and forecasting Ocean Waves, Pierson, Neumann, James, N.Y. Univ. College of Engin, 1953.

This was compiled by Wilber Marks D T M B

Figure 3-1

Wind and Sea for Fully Arisen Sea

period of swell is from six to sixteen seconds. Swell, while an occasional phenomenon, can arise from storm areas thousands of miles distant.

Deep-Water Waves

When the water is sufficiently deep that the effect of the bottom on the propagation characteristics of the waves can be neglected, they are called "deep-water" waves. Generally, if the depth is greater than 1/2 the length of a given wave, the deep-water approximation is valid. Except near beaches, ocean waves are deep-water waves, and we utilize this assumption throughout.

Gravity Waves

This term refers to waves in which the chief restoring force upon the perturbed water mass is gravity. Waves whose lengths, L, are greater than 1.73 cm [3-8] are gravity waters.

Capillary Waters

This term refers to waves in which the chief restoring force acting on the perturbed water mass is surface tension. (Less than 1.73 cm in length).

Care must be taken in specifying the state of the sea by a sea state scale, because many of these scales have been defined in the past, and more than one scale is in use today which disagree in the wind speeds and surface roughness regions which apply to a sea state scale index number. Two of the current scales are compared in figure 3-2. For a given index number, wind speeds can be different by as much as a factor of 2, although wave heights correspond closely. The windspeed difference is significant in radar models because sea return is influenced strongly by wind generated capillary waves, as well as the gross structure reflected by wave height. In the models documented here, the sea state scale of Pierson, et al., has been used [3-6].

3.1.2 Cross Section of Sea Backscatter

Sea Backscatter Models for Low Grazing Angles (0^o - 20^o)[1]

In determining sea or land backscatter, the term σ_o is used to represent the normalized mean (or median) omnidirectional backscatter from a surface area illuminated by a pulse radar. To a first approximation this area (A) is R θ_2 ($c\tau/2$) for small grazing angles, narrow

[1]From "Radar Design Principles," F. E. Nathanson, McGraw-Hill, 1969.

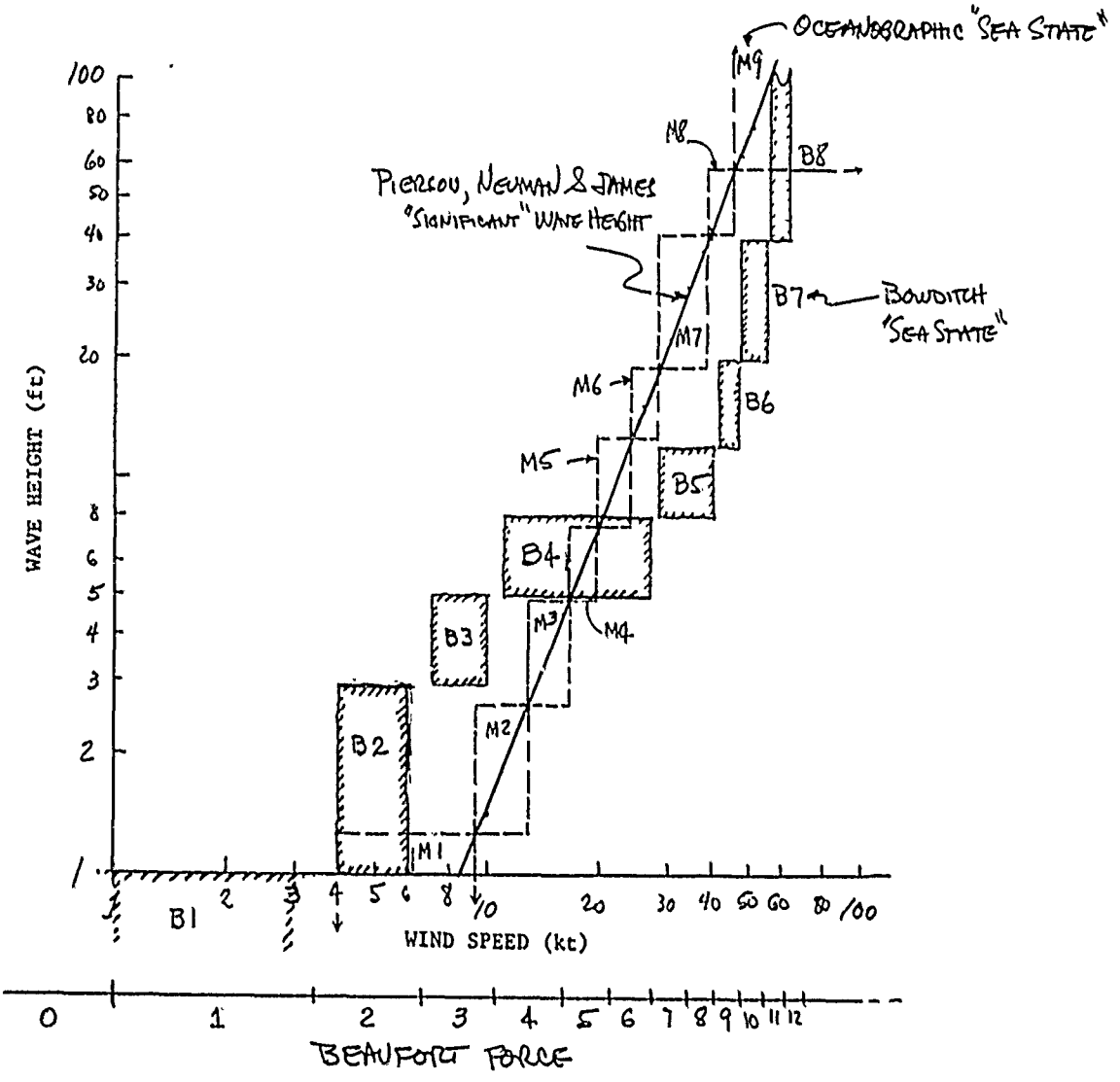

Figure 3-2

Comparison of Two "Sea State" Definitions

azimuth beamwidths, and full antenna gain on the water. In this formula, R = range from radar to center of cell, θ_2 = azimuth beamwidth (3 dB two-way), and $(c\tau/2)$ = pulse length in distance units for a two-way path (12.34 μsec = 1 nm). The conventional backscatter parameter, σ, for radar can be approximated from $\sigma_o = d\sigma/dA$. Then:

$$\sigma \approx R\theta_2 \ (c\tau/2)\sigma_o$$

for a beamwidth that is small compared to a radian, and for low grazing angles.

Obviously, the above discussion did not take lobing and forward scatter into account. These items are virtually always inseparably included within the "models" for σ_o. The term σ_o is also called the "normalized reflectivity" and is generally given as a mean value of cross section per unit area, in decibels. If σ_o = -30 dB, the average "radar cross section" (σ) is 30 dB below a 1 m^2 target for every square meter of the sea that is illuminated. Since the power density on this surface is proportional to the sine of the incident angle, another term (γ) is often used for reflectivity, where $\sigma_o = (\gamma)(\sin \psi)$, where ψ = incident angle.

Tables 3-1 through 3-7 are models for the backscatter coefficient σ_o. These tables were compiled using experimental data from numerous sources. They provide a complete and somewhat consistent set of numbers for the radar designer and system planners and evaluators. No attempt has been made to develop the theory of scattering from the sea surface or explain the anomalies in certain data. On the other hand, the points have been derived from a more extensive set of experiments than was the case previously. In assembling such models it has been found that only a few extra data points make the tables converge rapidly. Separating by frequency, polarization, depression angle, and sea state in the tables seems to make the data more consistent. When further data are available, it will also be useful to separate out data by wind and wave direction. Until that time, the models refer to:

1. An average of the upwind, crosswind, and downwind values where available.
2. Pulse lengths in the 0.5 to 5 μsec region with echoes having approximately Rayleigh distributions.

Data points not conforming to these assumptions have been crudely adjusted to conform. An asterisk is shown where data are questionable or where there is a severe conflict, leading to an expected error of 5 dB or more.

Table 3-1

Normalized Mean Sea Backscatter Coefficient σ_o

for Grazing Angle of 0.1°

SEA STATE	POL.	Reflection Coefficient in db Below 1 m^2/m^2 at Indicated Carrier Frequency						
		UHF 0.5 GHz	L 1.25	S 3.0	C 5.6	X 9.3	Ku 17	Ka 35
0	V							
	H			90*	87*			
1	V			(77)	(70)	65*	(59)	(51)
	H			80	75*	71*	(62)	(55)
2	V	90*	(85)	72*	64	56	(50)	(45)
	H	95*	90*	75*	67*	61*	(52)	(46)
3	V		(73)	(65)	(57)	51	(45)	(41)
	H	90*	82*	68	60*	53*	(45)	(40)
4	V		(67)	(59)	53*	(47)	(42)	(37)
	H		72	(61)	55	(47)	(41)	(35)
5	V		(62)	(56)	(49)	44	(39)	(34)
	H		65*	57	(49)	42*	(37)	(32)
6	V		(59)	(53)	(47)	(41)	(36)	(32)
	H		(61)	(54)	(46)	(39)	(34)	(30)

*5 dB error not unlikely
Values in parentheses are interpolated or extrapolated estimates.
After: Nathanson [3-3] Chapter 7

Monostatic radar
0.5 to 10 μsec pulse
Revised 2-77

Table 3-2

Normalized Mean Sea Backscatter Coefficient σ_o

for Grazing Angle of 0.3°

		Reflection Coefficient in db Below 1 m^2/m^2 at Indicated Carrier Frequency						
SEA STATE	POL.	UHF 0.5 GHz	L 1.25	S 3.0	C 5.6	X 9.3	Ku 17	Ka 35
0	V							
	H			83*	79	74*		
1	V			62*	60	58		
	H			74	71	66*		
2	V	80*		59*	55	52		
	H			66	60	56*		
3	V			55*	48	45		
	H		68*	58*	50	46		
4	V			54*		43		
	H			50*		42	39*	
5	V	75*		50*		39		
	H			47	41	39	39*	
6	V						37*	
	H			46			37*	

*5 dB error not unlikely

Monostatic radar
0.5 to 10 μsec pulse

After: Nathanson [3-3] Chapter 7

Revised 2-77

Table 3-3

Normalized Mean Sea Backscatter Cofficient, σ_o

for Grazing Angle of 1.0°

SEA STATE	POL.	Reflection Coefficient in db Below 1 m^2/m^2 at Indicated Carrier Frequency						
		UHF 0.5 GHz	L 1.25	S 3.0	C 5.6	X 9.3	Ku 17	Ka 35
0	V		68*			<60*	<60	56*
	H	86*	80*	73	70		<60	52*
1	V	70*	65*	56	53	50	47*	
	H	84*	73*	65	56	51	45	40*
2	V	63*	58*	53	47	44	42	38*
	H	82*	65*	55	48	46	41	38*
3	V	58*	54*	48	43	39	37	34
	H	76*	60*	48	43	40	37	36
4	V	55*	45	42	39	37	34	32
	H		52*	45	39	36	34	
5	V		43	38	35	33	32	31
	H	65*	50*	42	35	33	32	
6	V			33		29*	32	
	H			41		30*	32	

*5 dB error not unlikely

After: Nathanson [3-3] Chapter 7

Monostatic radar
0.5 - 10 μsec pulse
Revised 2-77

Table 3-4

Normalized Mean Sea Backscatter Cofficient, σ_o

for Grazing Angle of 3.0°

SEA STATE	POL.	Reflection Coefficient in db Below 1 m^2/m^2 at Indicated Carrier Frequency						
		UHF 0.5 GHz	L 1.25	S 3.0	C 5.6	X 9.3	Ku 17	Ka 35
0	V				60*	56*	52*	48*
	H	75*	72*	68*	63*	58*		53
1	V	60*	53*	52	49	45	43	41
	H	70*	62*	59	54	48	45*	43*
2	V	55*	53	49	45	41	39	37
	H	66*	59	53	48	42	38	40
3	V	43*	43	43	40	38	36	34
	H	61*	55*	46	42	39	35	37
4	V	38*	38	38	36	35	33	31
	H	54*	48*	41	38	35	32*	34
5	V		38	35	33	31	31*	30*
	H	53*	46	37	34	32	30*	
6	V					28	28	
	H			37		28	28	

*5 dB error not unlikely

Monostatic radar
0.5 to 10 μsec pulse

After: Nathanson [3-3] Chapter 7

Revised 2-77

Table 3-5
Normalized Mean Sea Backscatter Coefficient, σ_o
for Grazing Angle of 10°

SEA STATE	POL.	Reflection Coefficient in db Below 1 m^2/m^2 at Indicated Carrier Frequency						
		UHF 0.5 GHz	L 1.25	S 3.0	C 5.6	X 9.3	Ku 17	Ka 35
0	V		45*			49*	45*	44*
	H		60*			56*		
1	V	38			44	42	40	38
	H		56*		53	51		
2	V	35*	37	38	39	36	34	33
	H	54*	53	51	48	43	37	
3	V	34*	34	34	34	32	31	31
	H	50	48	46	40	37	32	31
4	V	32*	31	31*	32	29	28	29
	H	48*	45	40	36	34	29	29
5	V	30	30	28	28	25	23	26*
	H	46	43	38	36	30	26	27*
6	V	30*	29	28	27*	22*	18*	
	H	44*	40*	37	35*	27*	24*	

*5 dB error not unlikely

Monostatic radar
0.5 to 10 μsec pulse

After: Nathanson [3-3] Chapter 7

Revised 2-77

Table 3-6

Normalized Mean Sea Backscatter Coefficient, σ_o

for Grazing Angle of 30°

		Reflection Coefficient in db Below 1 m^2/m^2 at Indicated Carrier Frequency						
SEA STATE	POL.	UHF 0.5 GHz	L 1.25	S 3.0	C 5.6	X 9.3	Ku 17	Ka 35
0	V		42*					
	H		50*					
1	V	38*	38*	40	40	36	35*	35*
	H		46*		48			
2	V	30*	31*	32*	34	32	30*	30
	H	42*	41	40	42	44*	34*	
3	V	28	30	29	28	28	23*	23*
	H	40*	39	38	37	34	27	
4	V	28	28	27	25	24	21	22
	H	38*	37	37	35	29	23	
5	V	28	24*	23	22	18	17	20*
	H	35	34*	32	30	24	20*	20*
6	V	25*	23*	22*	21*	17	13*	
	H	33*	32*	30*	29*	21*	18*	

*5 dB error not unlikely

Monostatic radar
0.5 to 10 μsec pulse

After: Nathanson [3-3] Chapter 7

Revised 2-77

Table 3-7

Normalized Mean Sea Backscatter Coefficient, σ_o

for Grazing Angle of 60°

SEA STATE	POL.	Reflection Coefficient in db Below 1 m^2/m^2 at Indicated Carrier Frequency						
		UHF 0.5 GHz	L 1.25	S 3.0	C 5.6	X 9.3	Ku 17	Ka 35
0	V	32	33	31	35*	36*	28*	
	H	32	32	32		34*		26*
1	V	23*	22	24	28	24	20*	24*
	H	22	24	25	26	26		
2	V	20*	21	21	23	18	18*	19*
	H	22	21	21	22	23		
3	V	18*	18*	19	18*	16	14	14*
	H	21	20	20	20	21	14*	
4	V	14*	15*		15*	14*	11	10
	H	21*	18*				20*	
5	V	18*	15*	15	15	13*	8 *	4
	H	21*	18*	17	17	14	10*	
6	V	18*	15*	15*	14*	11*	10*	
	H	20*	18*	17*	16*	12*	10*	

*5 dB Error not unlikely

After: Nathanson [3-3] Chap 7

Monostatic radar
0.5 to 10 μsec pulse
Revised 2-77

The following ground rules have been observed and used for extrapolation and interpolation:

1. For a given entry on the table, the return from vertical polarization will equal or exceed that from horizontal and the deviation will increase at lower sea states, lower depression angles, and lower transmit frequencies. This does not appear to apply above 15 GHz.

2. The backscatter increases with depression angle from 0^o to 20^o as θ^n, where n may be as high as 3 for low angles, low sea states, and low frequencies. The value of n decreases in the tables towards the lower right-hand corner (high frequencies and sea states), where it approaches zero.

3. The backscatter coefficient at low grazing angles always increases with transmit frequency as f^m for horizontal polarization to at least 15 Ghz where m may be as high as 3 below 2 GHz for very low grazing angles (less than 1^o) and seas below state 3. As the angle, sea state, or transmit frequency exceeds these values, the exponent drops toward 0.

4. The backscatter increases with sea state by as much as 10 dB/sea state for low seas and low frequencies, but reduces to a smaller change at higher sea states and frequencies. Earlier studies by NRL (1965-1970) indicated a "saturation" at about sea state 4 for C and X band, but more recent studies by NASA at K_u band, Raytheon (for General Dynamics) [1976] indicate significant increases in σ_o up to 30-40 ft wave heights.

5. Sea state 0 arbitrarily corresponds to a significant wave-height less than 0.25 feet and winds less than 4 knots.

6. At small antenna depression angles the true grazing (incidence) angle on the ocean is smaller because of the curvature of the earth.

These generalizations were made to complete the tables; the generalizations should not be used for depressions angles of greater than 20 degrees.

3.1.3 Short-Pulse Sea Return

When a radar cell defined by beamwidth and pulse length, contains many scatterers of comparable size, the amplitude distribution of cross section is approximately Rayleigh, with cumulative distribution function:

$$P(\sigma>\sigma_t|\bar{\sigma}) = (1 - e^{-\sigma_t/\bar{\sigma}})$$

When the Rayleigh distribution is seen, the scatterers are generally distributed throughout the cell, and in the limit this leads to the condition of spatially uniformly distributed scatterers. This leads to a practice, in which this condition is invoked as necessary and sufficient that a Rayleigh section distribution will be observed. The sea surface does not fulfill this condition of uniformity, however, especially when viewed at low grazing angles, and the spatial structure is exposed when "snap shots" of the clutter are taken with sufficient resolution. Implicit in this statement is that the structure is visible for small cell sizes and short observation times but is washed out for large cell sizes or long observation times. The question is how short/small or long/large.

The effect of the gross surface structure is to present the short pulse[1] radar with three types (at least) of scatterers: patches of rough water thrust upward into view and tilted toward the radar, which presumably contain many incremental scatterers; patches not visible to the radar in troughs or the back sides of crests ; and large facets inclined steeply, with cross sections large compared to simple roughened surface. Evidence for the existence of each is available in signal observations. The upward raised scatterers are further structured spatially such that their regular appearance can be predicted approximately in the upwind/downwind (or -wave) directions. as indicated by the parameters of surface wavelength tabulated in table 3-1 and by the example of sea surface height displacement auto-coveriance function in figure 3-3. When a short pulse radar views the sea near grazing incidence, the wave crests are resolved and seen as a progression of isolated rapidly fluctuating moving scatterers, as seen in the sequence of figure 3-4. The crests are especially visible on radar because they are high and energy release (and small scale roughness) is maximum there. The radar return from crests generally fluctuates rapidly, presumably caused by the internal motion of the rough surface and consequent Doppler modulation. The return from regions between crests is much weaker, and in figure 3-4, is baseline clipped because of the limited

[1]Short title for "small cell size in both range and angle and non-integrating from scan-to-scan."

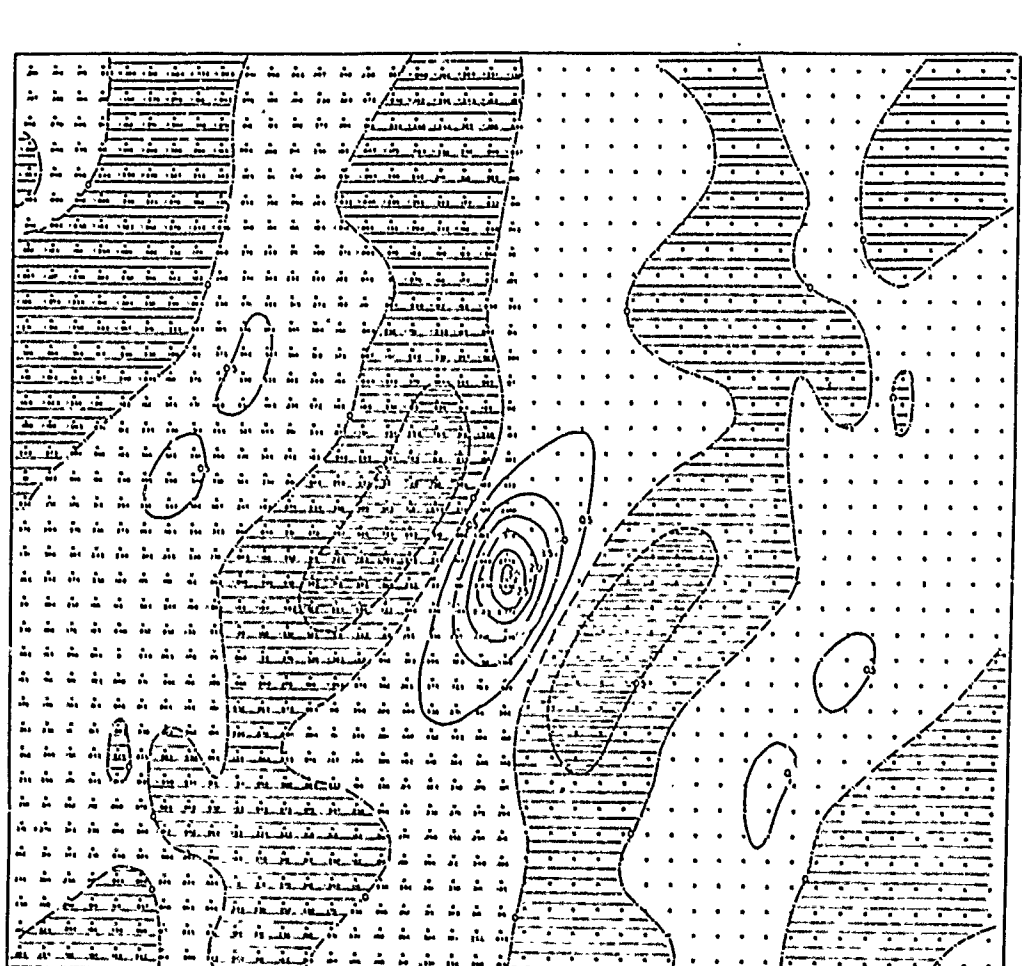

Figure 3-3

Auto Covariance Surface of the Sea [3-9]

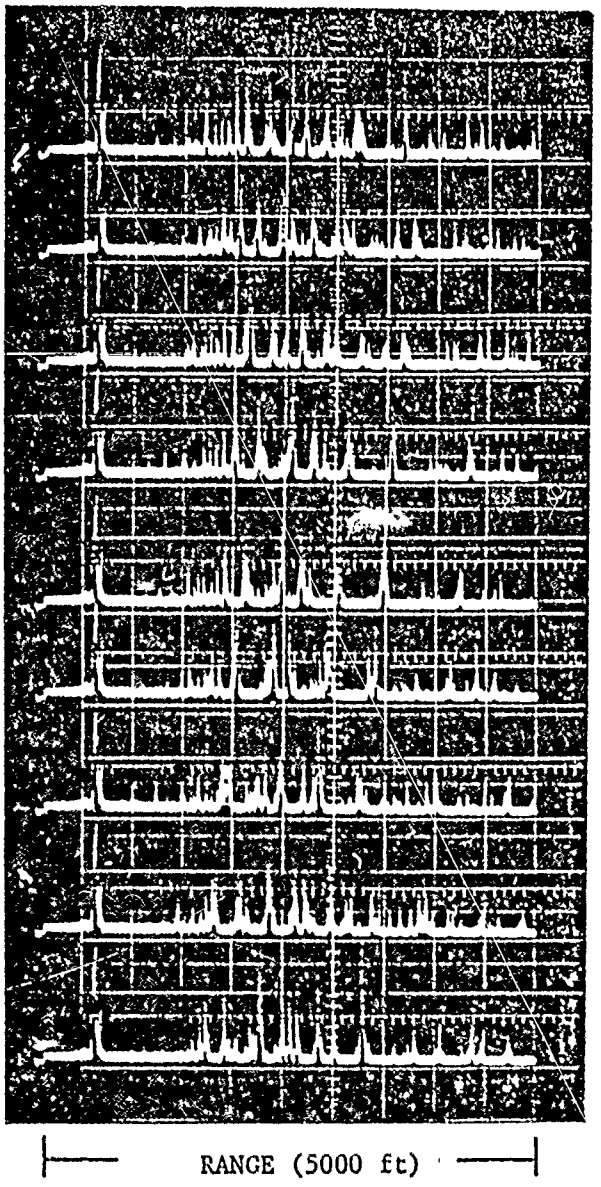

Figure 3-4

Range-Amplitude Displays of Radar Sea Return, Surface Radar, 0.1 Microsend Pulse [3-10]

dynamic range. When seen with wide-dynamic-range high-power radars, the trough regions also fluctuate rapidly. When the crests are viewed upwind when the wind and wave vectors are parallel, occasional Ricean or non-fluctuating echoes (over a period of a few tenths of a second) are seen, presumably associated with a wave curl.

The influence of this structure and resulting modulation of return is profound on the distribution function of cross section when all these returns from different spatial cells are ensembled. The dynamic range of return is much wider than Rayleigh, even though component cell contributions appear Rayleigh over short time scales. Three examples are shown in figures 3-5 through 3-7. They were recorded under the conditions listed in table 3-8. The plots are on arithmetic probability paper scaled so that normal distributions are straight lines. None of the three is strictly log-normal and the three vary considerably in character of their shapes. Slopes expressed as log-normal standard deviations are 7.5 dB(H) and 6 dB(V), 7 dB(H) and 11 dB(V) for the three figures, respectively, across the P_{F_A} = 1.0 to 1 percent region. Although comparison of data sets taken at different times and locations and with different equipment is risky, the spread illustrated here is typical for the parameters that apply. Standard deviations of 6 to 8 dB are frequently seen, with the 11 dB example about worst case. Horizontal polarization presents higher peak cross section than vertical at high sea states and low grazing angles in X-band, but at S-band the two should be about equal, with vertical exceeding horizontal below that band. In downwind directions, vertical will exceed horizontal by a few dB under the same conditions otherwise, but upwind will generally be worst case for both polarizations.

Analyses of detection of targets in clutter requires models of the decorrelation process of the clutter signals in addition to their distributions. The time autocovariance functions defined by

$$R^2(\tau) = E\{v_c(t)v_c(t + \tau)\} - E^2\{v_c(t)\},$$

where E{} implies expectation value and v_c is the clutter video voltage, reflect components of the physical model described earlier in the following way. Referring to figure 3-8, the total variance of the clutter is made up of two parts, a Rayleigh contribution and the non-Rayleigh part. The Rayleigh variance[1] of $(5.5\ dB)^2$ adds to the non-linear part, here shown as $(5.8\ dB)^2$ for the effect of the roughness/tilt/shadowing modulation in widening the distribution. The Rayleigh part decorrelates in milliseconds, with a slope representative of a Doppler process, proportional to frequency. The non-Rayleigh part decorrelates in 0.5 to 2 seconds and does not seem to be frequency

[1] A logarithmic video envelope transfer law has been assumed for this illustration.

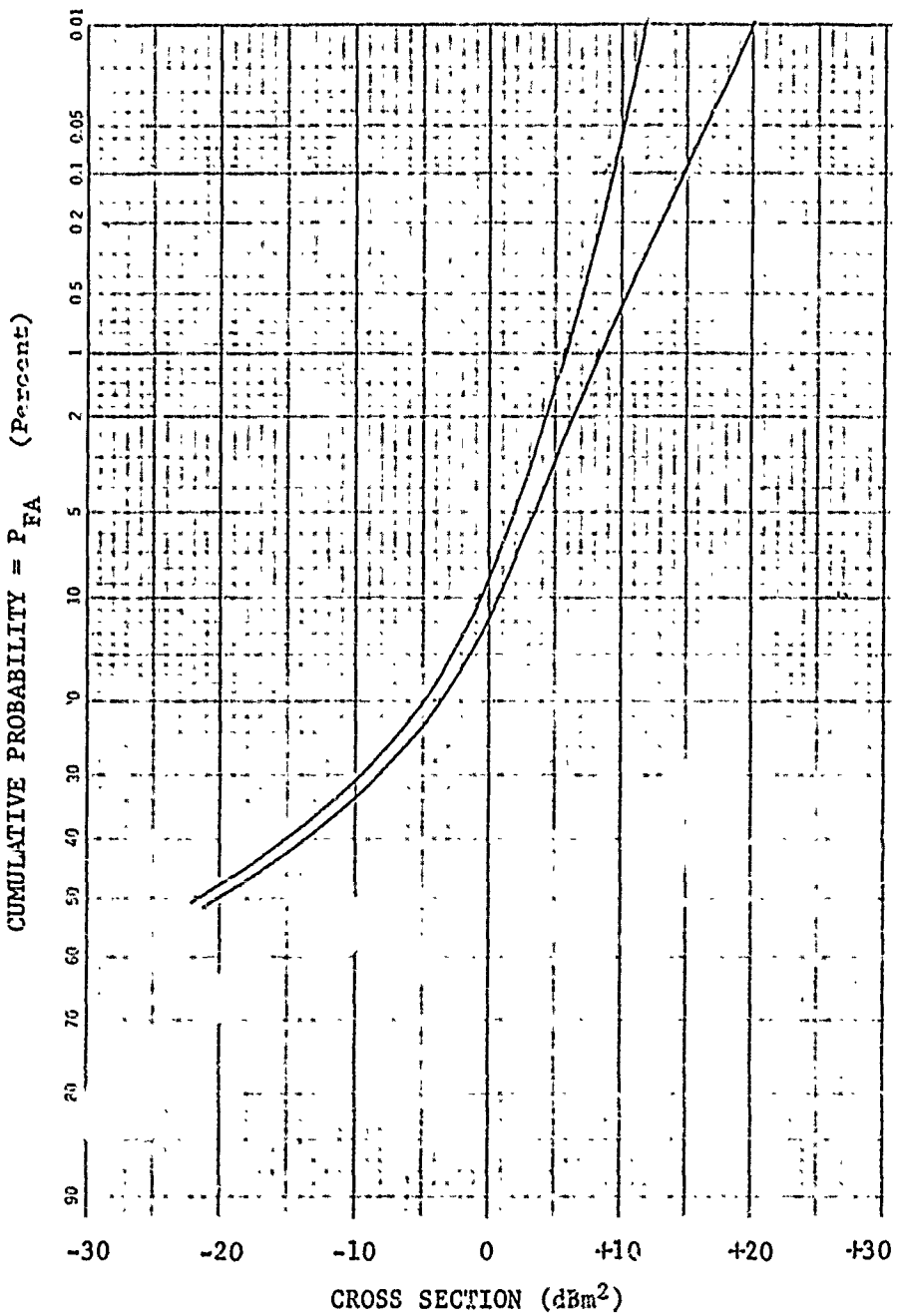

Figure 3-5

Distribution of Sea Return, τ = 0.07 μs, ψ = 1 deg [3-12]

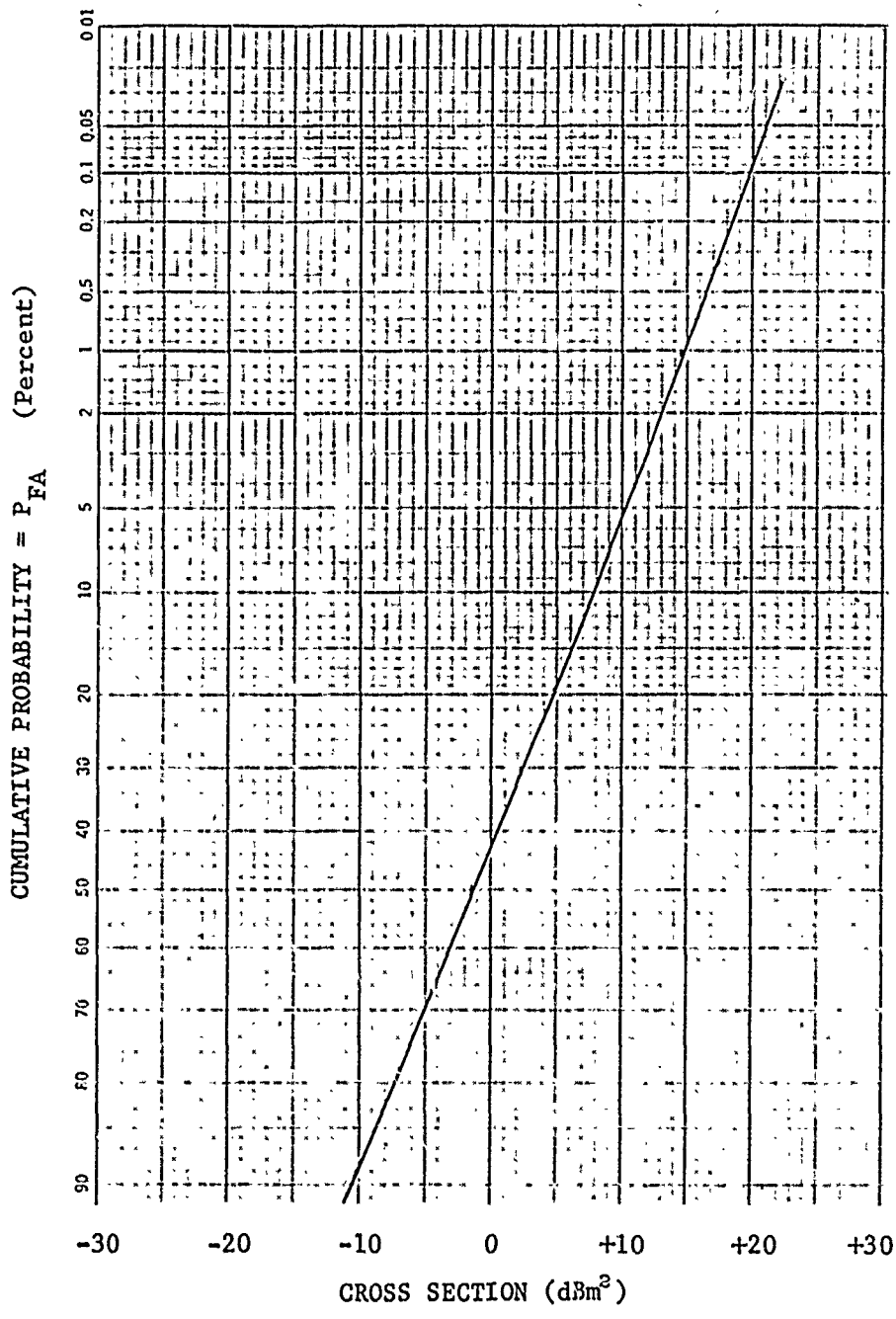

Figure 3-6

Distribution of Sea Return, τ = 0.25 μs, ψ = 0.12 deg [3-12]

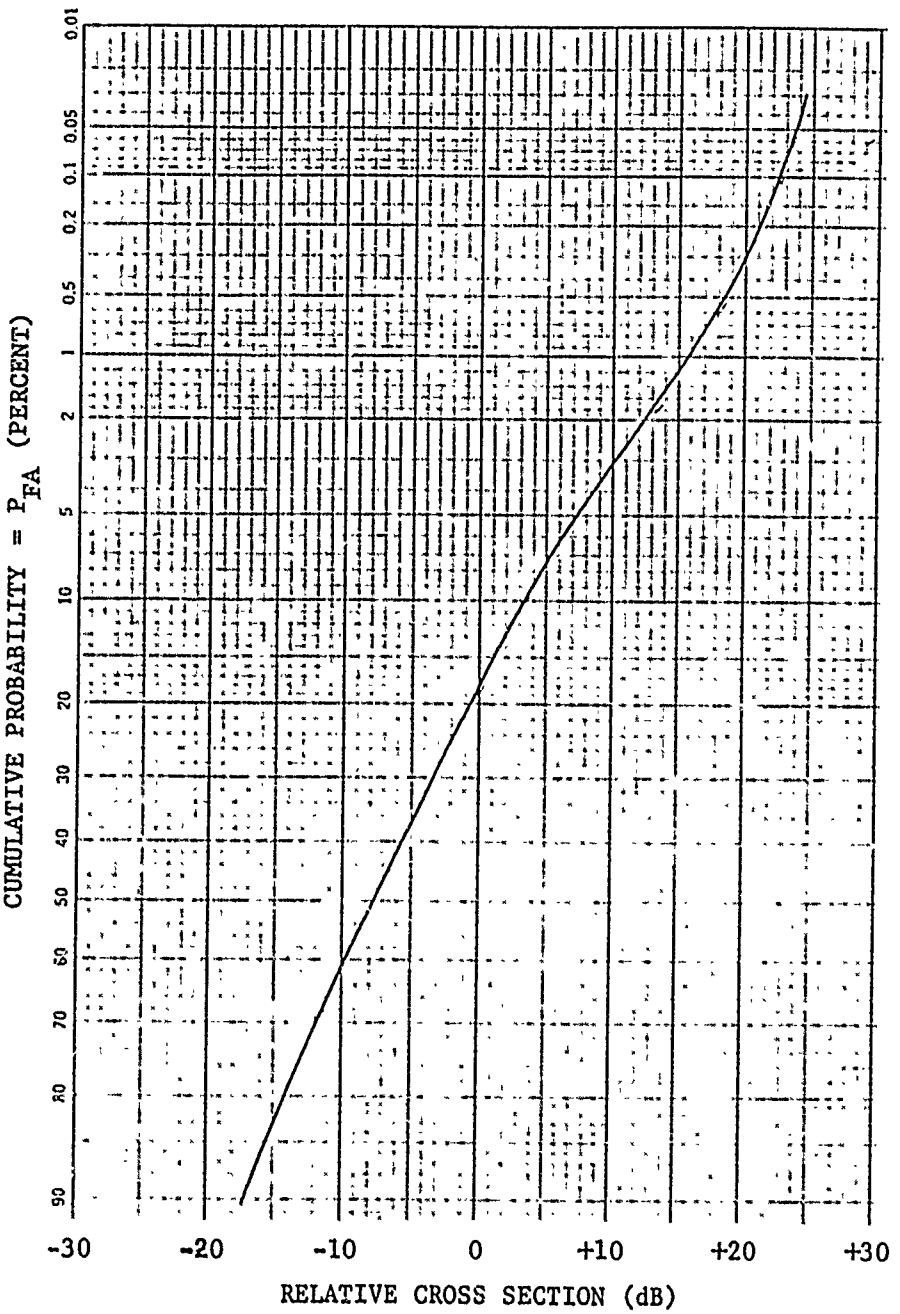

Figure 3-7

Distribution of Sea Return, τ = 0.1 μs, ψ = 0.16 deg [3-13]

Table 3-8

Parameters of Radar Sea Return Measurements

	FIGURE NO.		
PARAMETER	3-5	3-6	3-7
Reference	[3 - 11] (RRE)	[3 - 12] (GIT)	[3 - 13] (NRL)
Frequency	X-Band	X-Band	X-Band
Pulse Length	0.07 μs	0.25 μs	0.1 μs
Beamwidth	0.6 deg	1.6 deg	0.6 deg
Polarization	H & V	H	V
Antenna Height	250 ft	81 ft	75 ft
Range	2.4 nm	5.25 nm	4.7 nm
Grazing Angle	1 deg	0.12 deg	0.16 deg
Wind Speed	40 - 60 kt	22 kt	12 kt
Surface Roughness	3 - 5 ft rms	2 ft rms	0.6 ft rms (Wind Waves Only)
Direction of Look	Upwind	Upwind	30 deg off Upwind

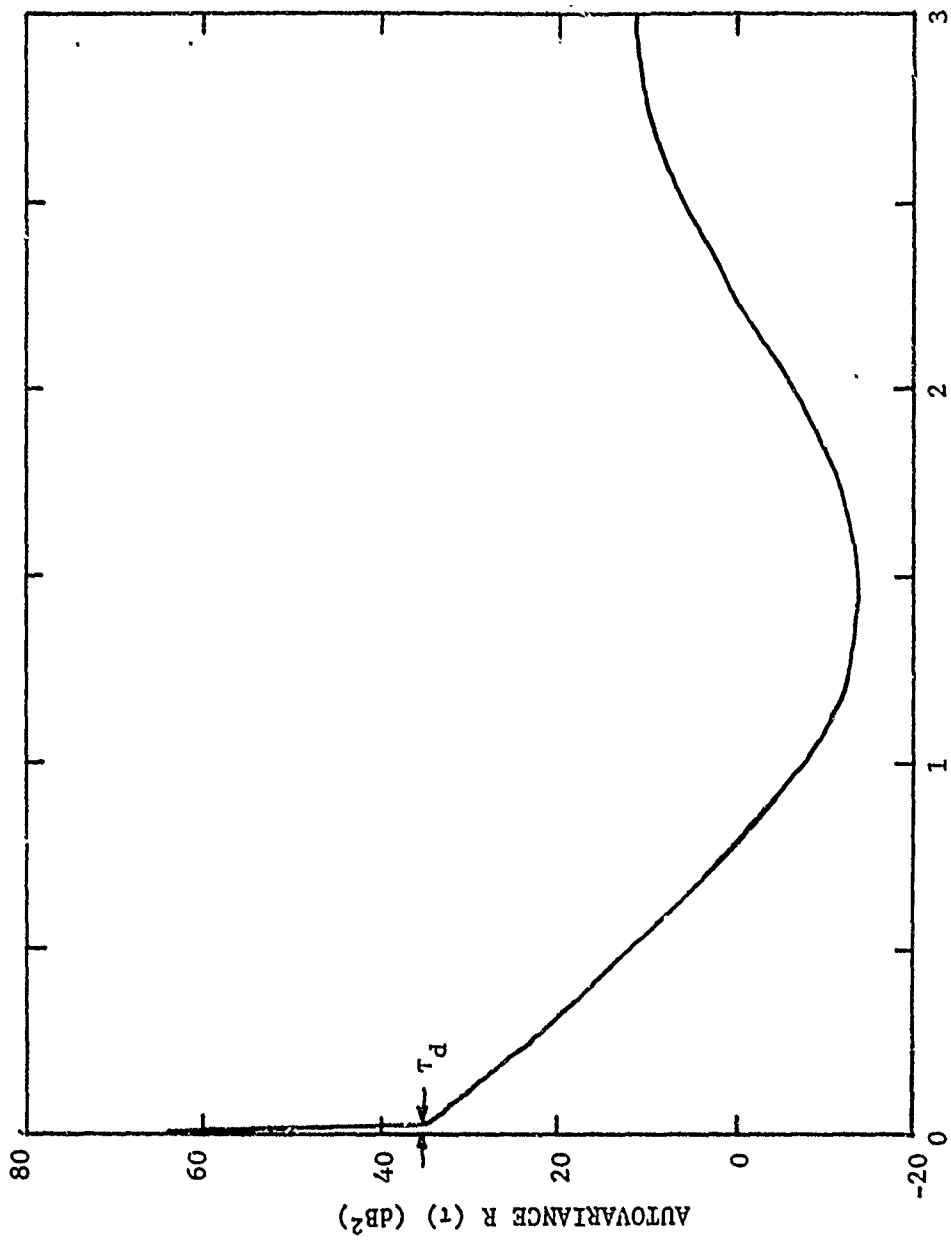

Figure 3-8

Autocovariance Function of Short-Pulse Sea Return in Upwind Direction, Standard Deviation of Distribution = 8 dB

sensitive [3-14]. The cyclic part, mostly seen only in up/down wind directions, has a period equal to the dominant wave period. The fast Doppler decorrelation time, τ_d, is approximately

$$\tau_d \approx \frac{790}{Wf},$$

where f is in GHz and wind speed W is in kt.

The Doppler peak has been shown to respond to frequency agility, such that samples from the same cell on pulses separated by about $1/\tau$ are found to be uncorrelated with respect to the fast mechanism (~ 30 dB^2 of variance reduction); however, the slower decorrelation mechanisms associated with gross surface structure rearrangement are unaffected [3-15]. Examples are shown in figure 3-9, in which lagged cross correlation products are summed for adjacent logarithmic video pulse samples spaced 250 ns. The lower curve, with the Doppler Rayleigh spike, is for a fixed frequency and the upper is for a pulse-to-pulse jump of 10 MHz. The radar was vertically polarized in X-band, and used pulse length and beamwidth of 0.25 μsec and 1.6 degrees, respectively. The curves have been separated vertically to eliminate confusing cross-overs.

Unfortunately, the data so far acquired at short pulse lengths and at low grazing angles typical of shipboard surface surveillance radars are not sufficient to formulate a definitive parametric model. No data have been acquired suitable for these purposes at any other band than X, and even there the amount of data and degree of qualitative control are inadequate to support a satisfactory model beyond the qualitative picture presented; however, even with the poor qualitative specification, analysis of processor performance can be pursued under an assumption that the distribution shape is log-normal with acceptable results, provided that reasonable values for its standard deviation are used [3-16].

3.1.4 Doppler Shift and Fluctuation of Sea Return

Coherent radar signals backscattered from the sea have been analyzed in terms of Doppler modulation caused by motion of scatterers [3-3, 3-7]. Parametric relations between the surface roughness or wind speed and the spectral spreading have been developed under the further assumption of a Gaussian-shaped spectrum and a similar shape of scatterer speed distribution. Examples of the results of analyses and fits to the data are given in the references and summarized in figure 3-10 for average velocity offset or drift and figure 3-11 for spectral width. Although land clutter fluctuation spectra are now available which definitely imply deviation from a Gaussian shape at low levels

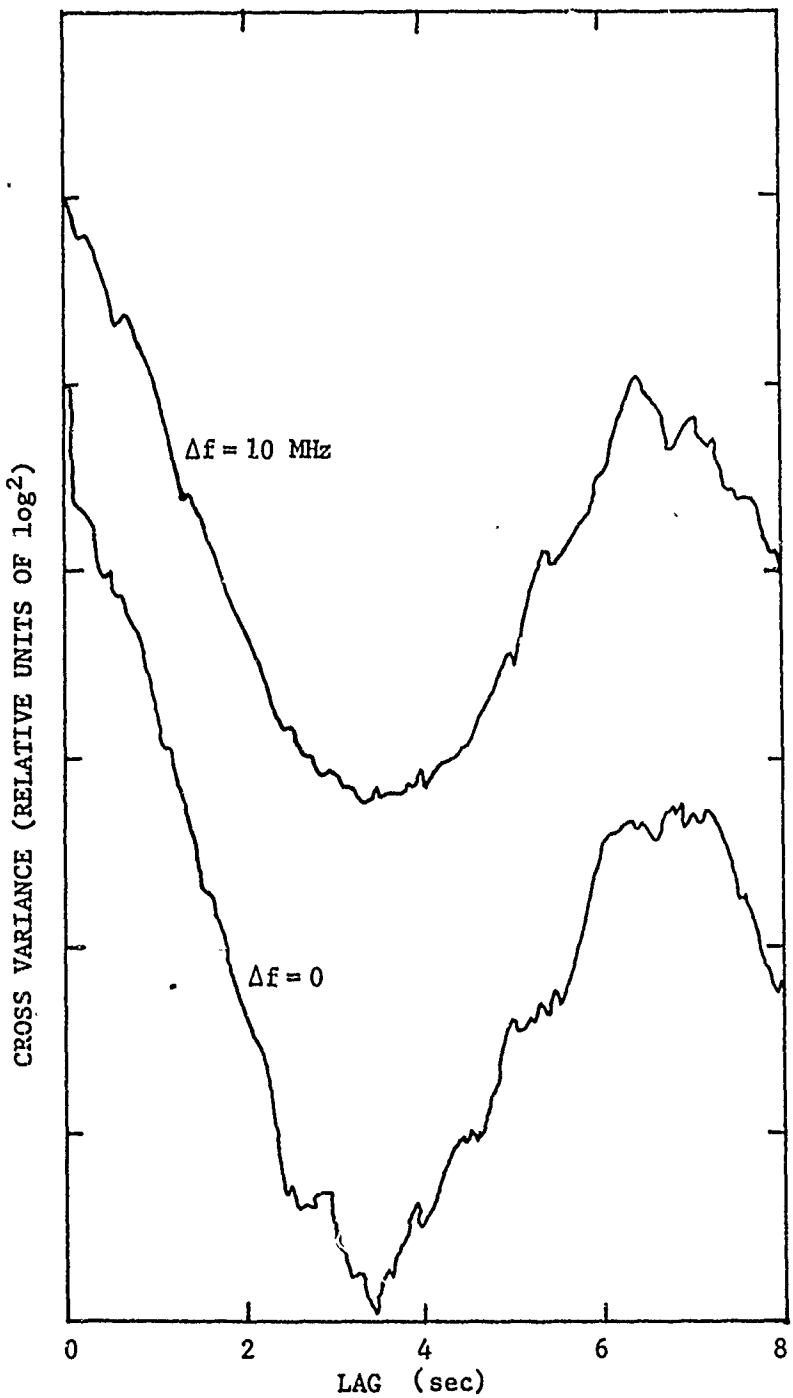

Figure 3-9

Decorrelation of Sea Return With Frequency Agility

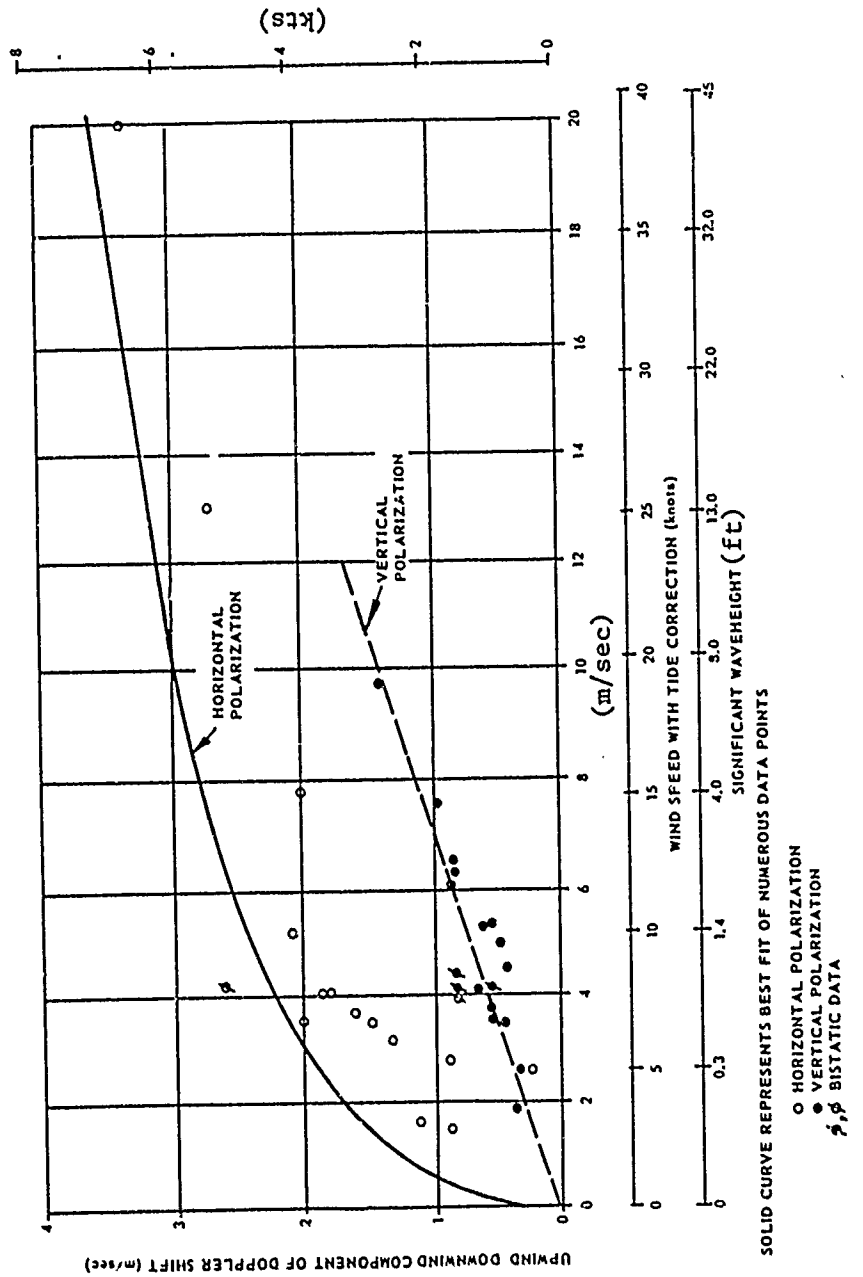

Figure 3-10
Mean Doppler Shift for Sea Clutter [3-3]

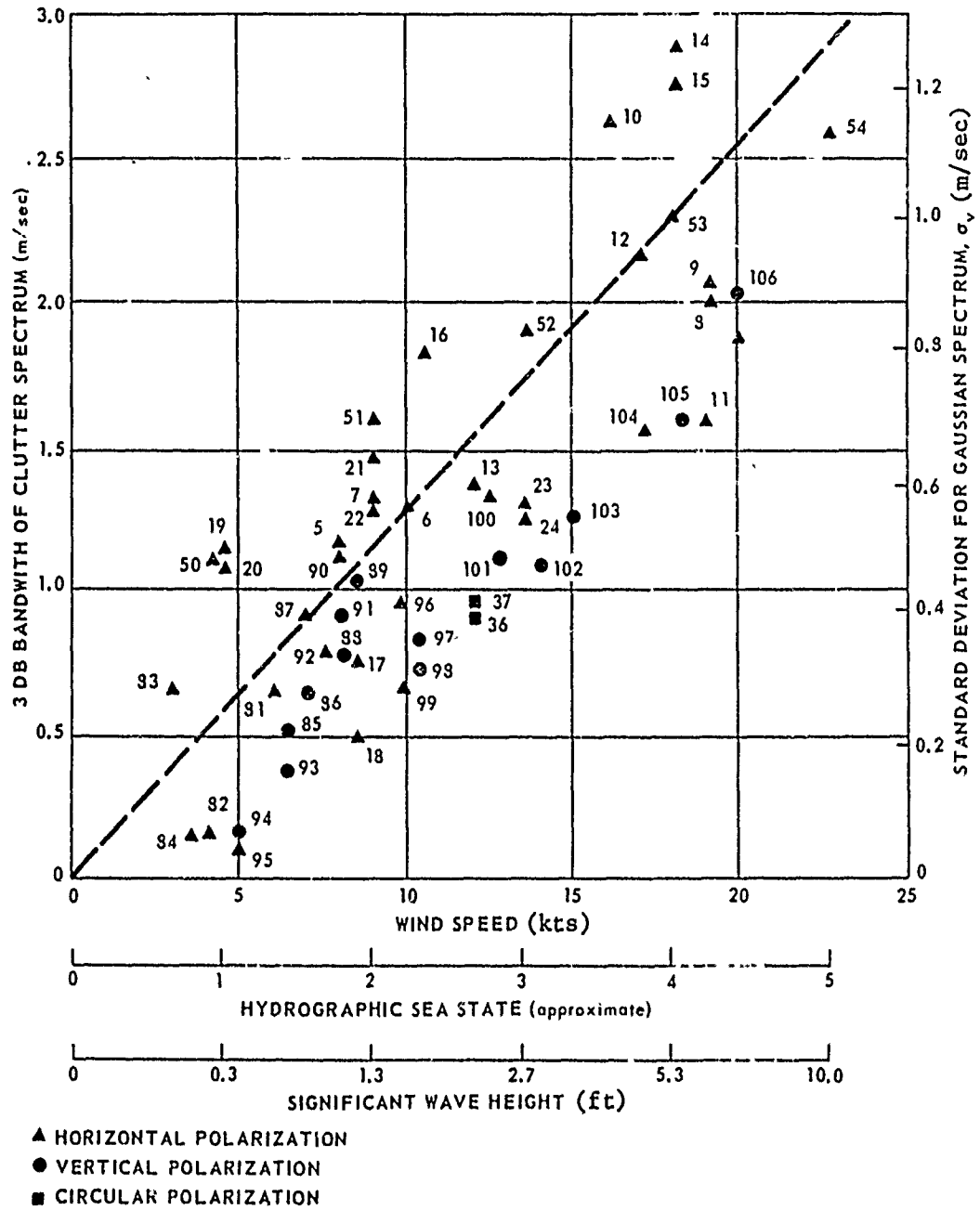

Figure 3-11

Variation of Bandwidth for Coherently Detected Sea Clutter Signals [3-3]

and give the reasons therefor, no comparable data are available for sea return fluctuation; however, it is anticipated that scatterer creation and annihilation or other dynamics would produce a similar deviation from Gaussian for the sea-echoes at some level.

3.2 Land Backscatter

3.2.1 The Modeling Problem

It is sometimes convenient to consider two land clutter characteristics separately; those characteristics that relate to clutter processing details, and those that relate to clutter backscatter coefficient characteristics. The former includes characteristics that are intimately associated with the details of clutter signal processing and include amplitude fluctuation statistics, spectrum, and frequency agility. The latter includes features of the backscatter coefficient σ_0 such as grazing angle, terrain, polarization and wavelength dependences, and spatial distribution.

For example, consider the question of clutter amplitude fluctuation statistics for a given value of σ_0, versus the (spatial) distribution of σ_0 itself, for a given terrain and wavelength. The former affects the radar system processing particulars such as CFAR (constant false alarm rate circuits), detection sensitivity, frequency diversity, and MTI, which are all under the control of the radar designer, whereas the latter tends more to specify the distribution of clutter magnitude external to the radar set. It has a secondary effect on CFAR design and the placement of detection threshold.

The distinction is also apparent in terms of specification of radar performance. It is normal to use false alarm rate and probability of detection to specify performance. For a given target location and known value of σ_0 the (local) false alarm rate and probability of detection are determined by consideration of clutter fluctuation and processing characteristics; yet these results depend critically on the value of σ_0. Consequently, it makes the most sense to require some minimum level of probability of detection, say 90 percent, that must be achieved over, say 95 percent, of the radar coverage. This approach allows one to separate, as much as possible, signal processing design considerations from environmental considerations. This concept is similar to Barton's "Interclutter Visibility."

The overall probability of detection of a radar set may be computed by averaging over these two types of limitations; however, how this is done depends on the application. In a mortar-locating radar where the target appears and disappears within a small region, the two

are almost interchangeable, whereas in an air surveillance radar case, where the target may traverse a large area, the overall computation is more difficult.

With a value for the average signal-to-clutter ratio as a parameter, the detection and false alarm probabilities can be obtained from the clutter and target fluctuation models, depending upon the effective number of independent target/clutter samples integrated by the radar video processing. It is often desirable to be able to make use of several target and clutter fluctuation models. Unfortunately, the computation of the statistics of clutter plus signal when the clutter is, e. g., Ricean and the target is Chi-Square, is not possible in closed form. Furthermore, even with computer solutions, the results are dependent upon the desired false alarm rate.

Fortunately, there is a greatly simplified approach which effectively isolates the interdependence of clutter and signal statistics. In the cases of most interest, i.e., high detection probability and low false alarm probability. This approach establishes the threshold setting based on clutter statistics and the desired false alarm probability, and then computes detection probability on the basis of this threshold (above the mean integrated clutter level) and signal statistics alone. The result is seldom in error by more than .5 dB. The resulting simplification in specifying performance characteristics and the subsequent insight gaines is usually more than worth this sacrifice in accuracy. Figures 3-12 and 3-13 show a comparison between the results obtained with this approach and the exact results for the Rayleigh (exponential) clutter [3-16].

Clutter Fluctuation Models

Three types of distributions are taken to be adequate to model observed fluctuation characteristics of ground and sea clutter. These are the Weibull family (of which the Rayleigh is a member), Rice, and log-normal distributions. The exponential statistic (Weibull with exponent parameter = 1) results in the case of many independent scatterers within a radar resolution cell. The Rice distribution results in the case of a single dominant nonfluctuating scatterer plus many smaller scatterers within a radar resolution cell. The log-normal and other Weibull distributions are not directly related to any known physical phenomenon, but because of their long tail characteristic they are useful in modeling "spiky" clutter. The log-normal distribution has been shown to affort a fairly good description of scattering from randomly oriented large simple shapes such as plates and cylinders [3-18].

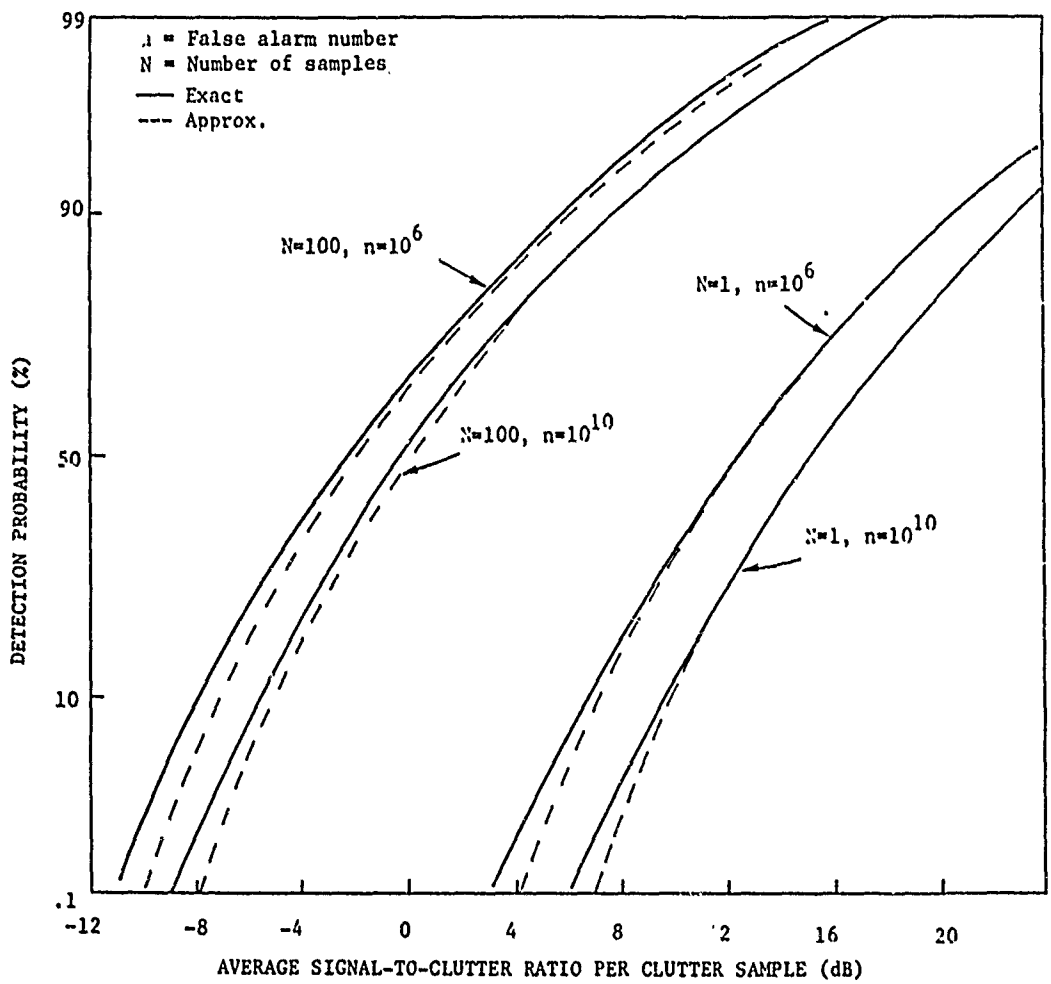

Figure 3-12

Comparison of Exact and Approximately Computed Detection Probability - Rayleigh Target (Swerling Case I), Rayleigh Clutter

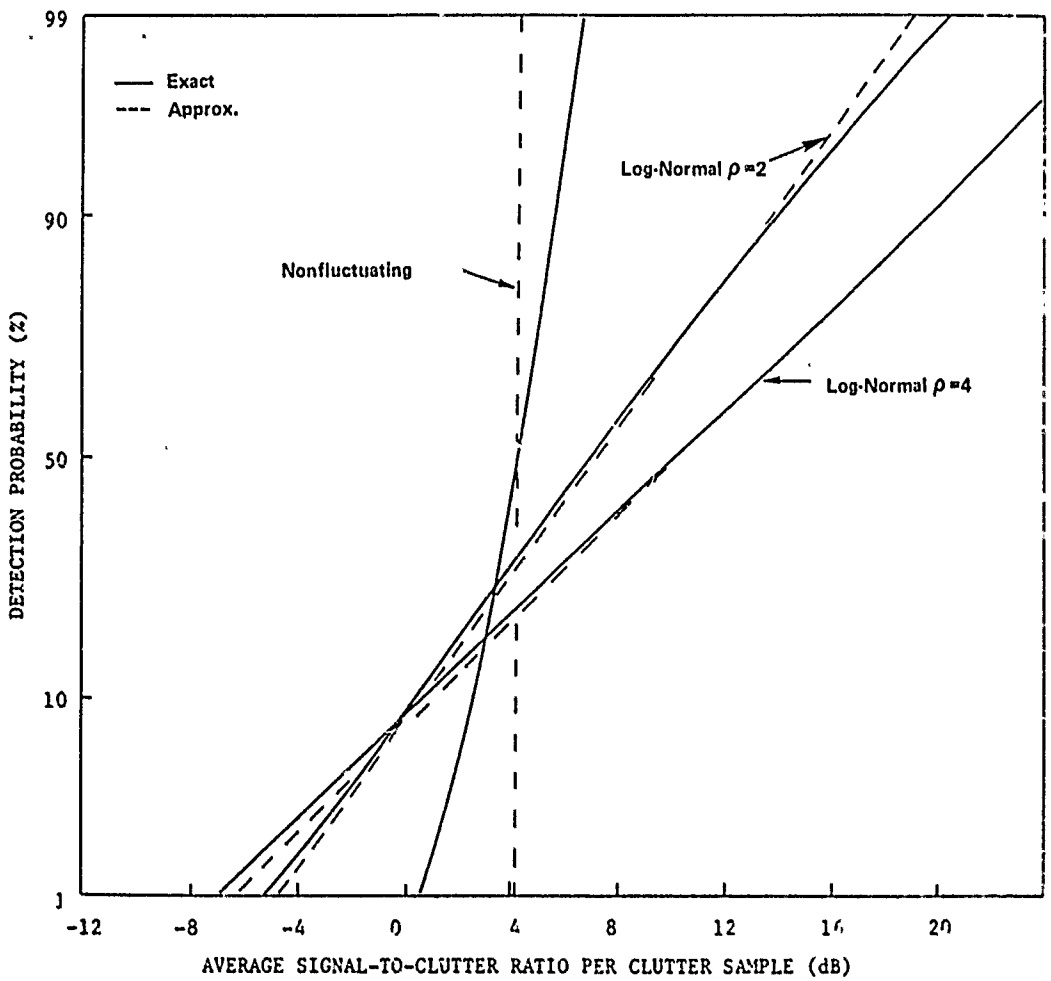

Figure 3-13

Comparison of Exact and Approximately Computed Detection Probability - Log-Normal and Nonfluctuating Targets, Rayleigh Clutter N=10, $n=10^8$

These distributions are given by:

$$p(\sigma)d\sigma = \frac{c\sigma^{c-1}}{\sigma_o^{\,c}} e^{-(\sigma/\sigma_o)^c} d\sigma, \qquad 0 \le c \le 1,\ \sigma \ge 0: \text{ Weibull (Exponential when } c = 1)$$

$$p(\sigma)d\sigma = \frac{1}{\sigma_o} e^{-(\sigma/\sigma_o + m^2)} I_o(2m\sqrt{\sigma/\sigma_o})d\sigma, \qquad \sigma \ge 0: \text{ Rice}$$

$$p(\sigma)d\sigma = \frac{1}{S\sigma\sqrt{2\pi}} e^{-\frac{\ell n^2\,(\sigma/\sigma_o)}{2S^2}} d\sigma,\ \sigma_o = \sigma_{50}e^{S^2/2};\ \sigma \ge 0: \text{ log-normal}$$

The exponential is a single parameter distribution and is invoked to represent uniformly distributed clutter. It is identical to the thermal noise case so that thermal noise performance curves may be used. In the Rice distribution, m^2 is the ratio of power in the fixed component to that in the fluctuating component. The log-normal is also a two parameter distribution; however, its parameters have no particular physical significance. The mean backscatter coefficient σ_o is given by $\sigma_o = \sigma_{50}\, e^{S^2/2}$, where σ_{50} is the median value, and S is the standard deviation of $\ell n(\sigma/\sigma_o)$.

Figures 3-14 through 3-16 show the threshold setting, in decibels above average integrated clutter level, needed to achieve various false alarm probabilities for the exponential, Rice and log-normal clutter distributions [3-19].

The parameter N in figures 3-14 and 3-16 is the effective number of independent clutter samples integrated. The most common ways in which independent samples result, are by use of frequency diversity and by noncoherent integration for a length of time greater than the reciprocal of the clutter spectral width. Frequency hops greater than the IF bandwidth are usually sufficient to decorrelate clutter of the exponential type which are the results of a uniformly distributed scatterer mechanism. Log-normal type clutter, however, is likely the result of an ensemble of point-like scatterers existing in only a fraction of range cells (or only partially filling a cell), and consequently even a frequency hop considerably greater than an IF bandwidth fails to achieve decorrelation.

When the signal processing integration time is greater than the clutter reciprocal bandwidth, additional effective decorrelated samples are obtained. The relationship

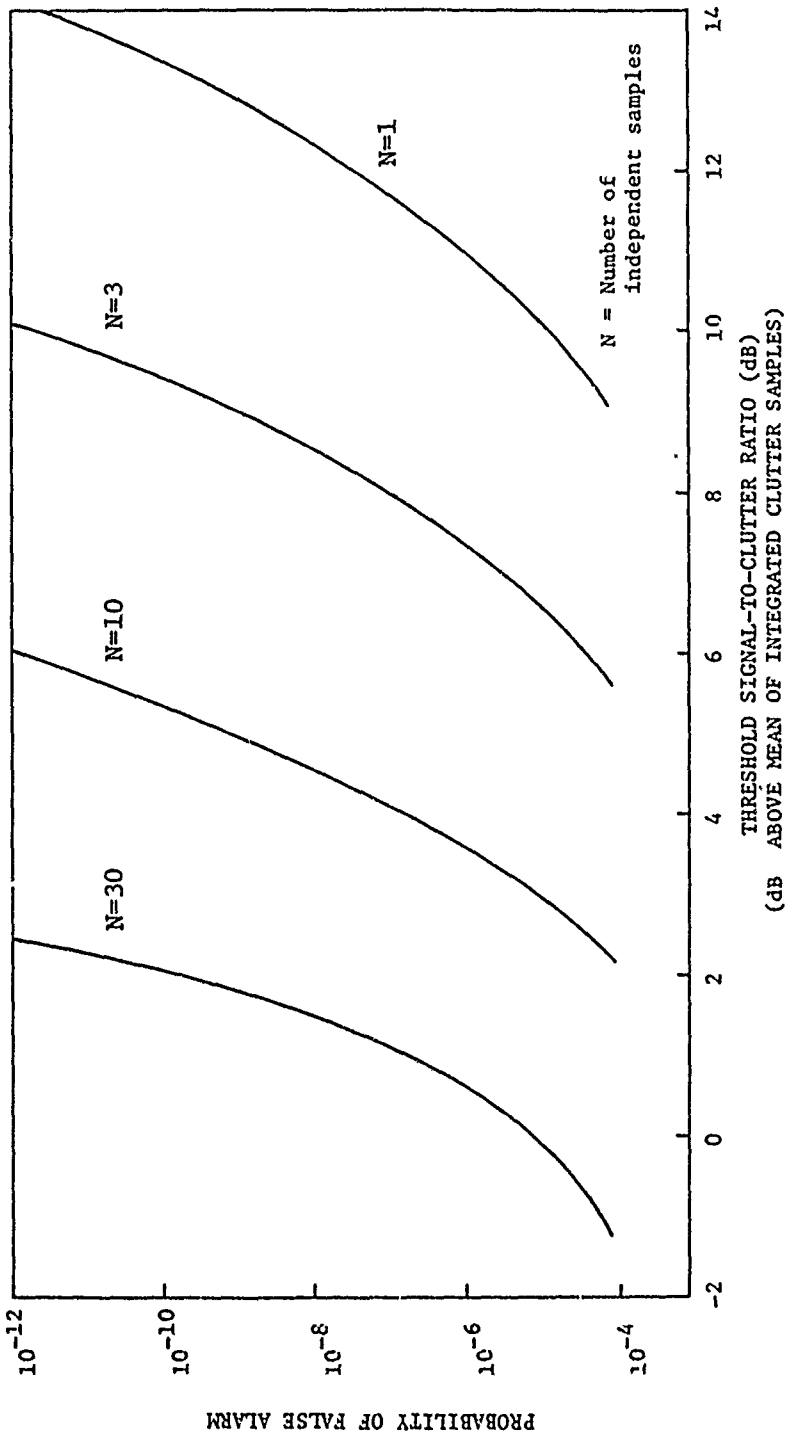

Figure 3-14

Threshold Settings Above Mean for Rayleigh Clutter

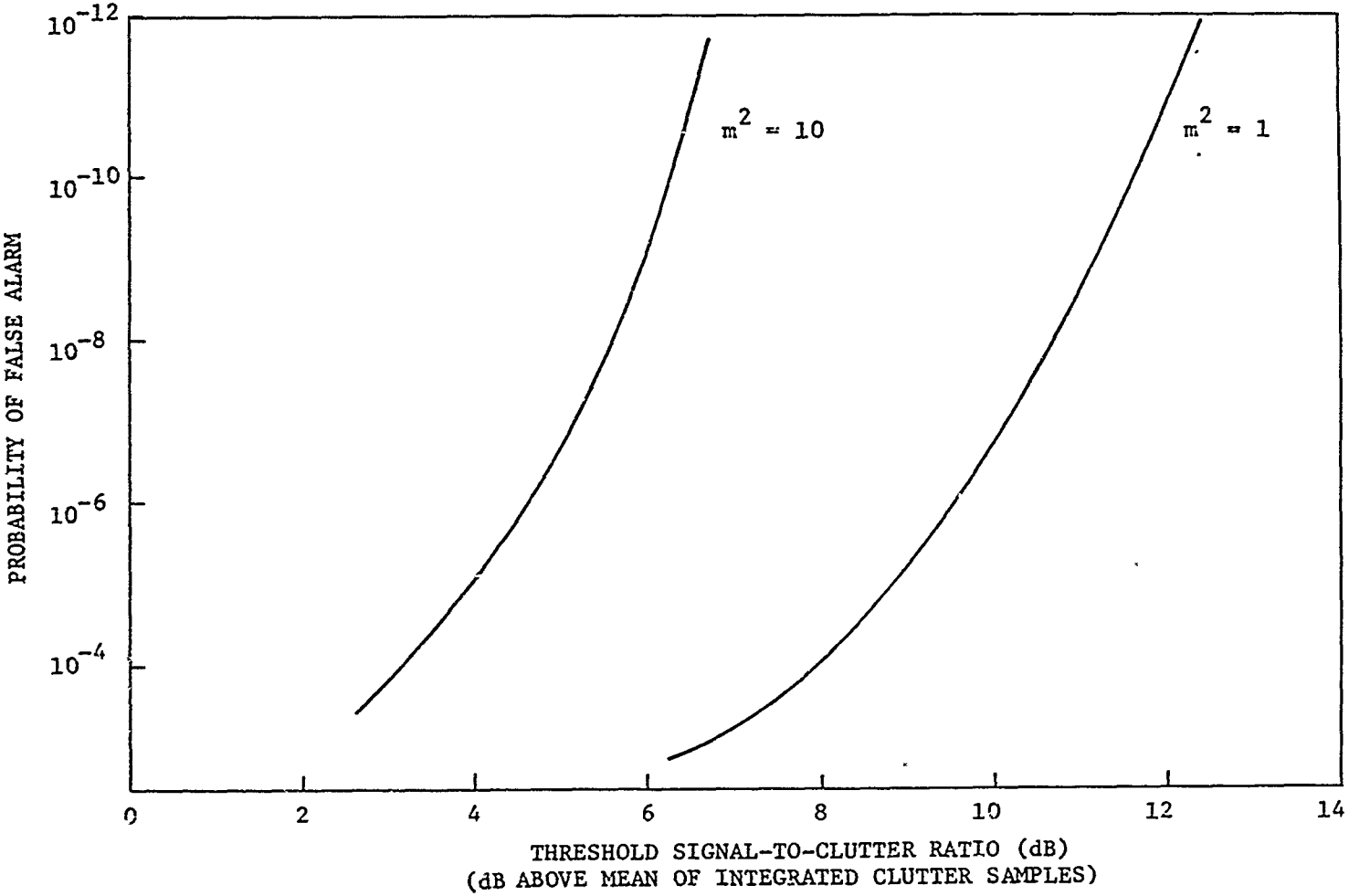

Figure 3-15

Threshold Settings for Rice Clutter

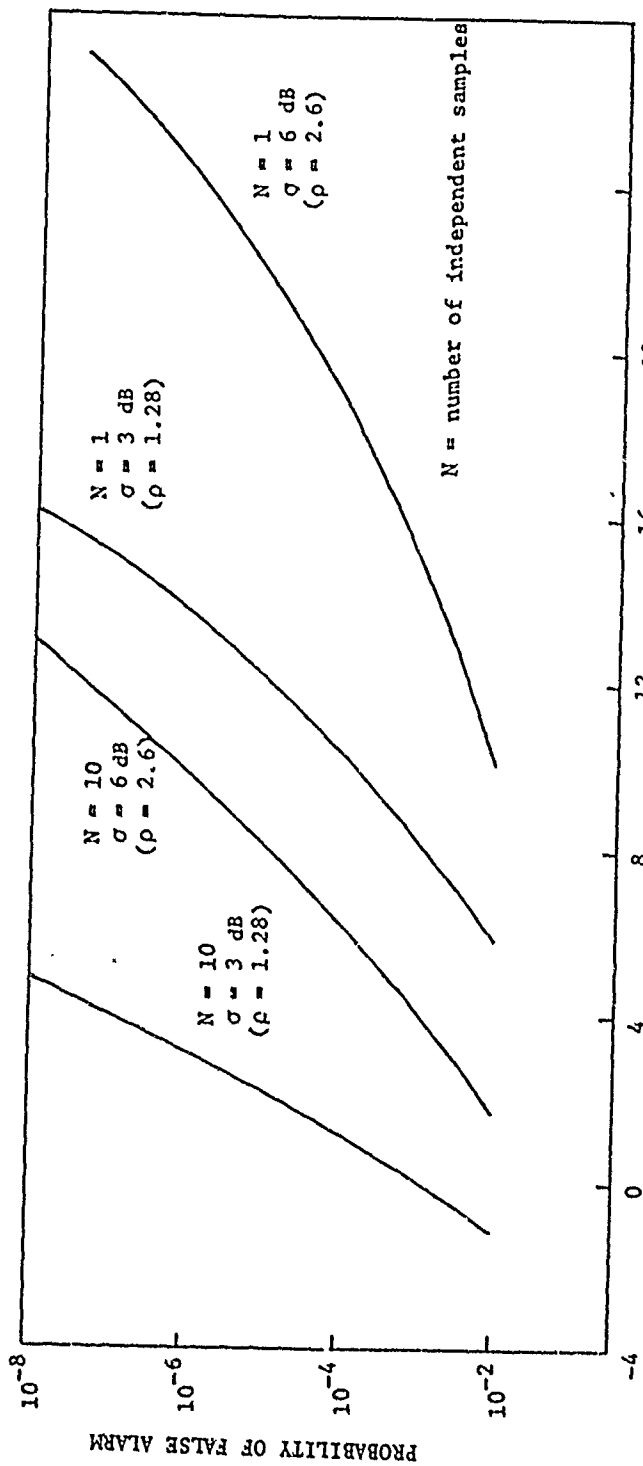

Figure 3-16

Threshold Settings for Log-Normal Clutter

$$N_e \approx 2\pi \sigma_f T$$

where N is the effective number of independent samples, T is the integration time, and σ_f is the rms spread of a Gaussian spectral model and can be used as a simplified but reasonable measure of this effect. N_e cannot be greater than the number of pulses integrated.

For the normal exponential or Rayleigh clutter assumption, a threshold setting of 12.7 dB is required to achieve 10^{-8} false alarm probability. With log-normal clutter when $\rho = 2$, a false alarm rate almost two orders of magnitude greater will result.

The exponential (Rayleigh) and Rice distributions represent land clutter only on a cell-by-cell basis. That is, if a cell contains many random scatters of equal amplitudes, it satisfies Rayleigh criteria. But another nearby cell which is also Rayleigh in type will not likely have an average cross section equal to that of the first, so that the same Rayleigh distribution cannot represent both cells. Similarly, two cells having a mix of non-fluctuating scatterer plus a distributed multiscatter component will not likely be representable by the same average values or ratio parameters m. Thus, these distributions can be used for detection performance predictions about a single cell characterized by a single value of average cross section (and m, in the Rice case), and the appropriate threshold to achieve any given value of P_{FA} will be different for any other cell. Application of these distributions, therefore, implies that availability of a threshold function of position that (adaptively) represents the surface that gives a constant value of P_{FA}, independent of position.

If the statistics of many cells are aggregated, or equivalently if the same value of threshold is to be applied to every cell to control P_{FA}, the log-normal and/or Weibull forms must be used to predict performance. Their use more accurately reflects the variation of the local average cross section from cell to cell, which tends to dominate the width of multicell distributions.

Adaptive Threshold CFAR

In order to regulate false alarm rates to the desired values of clutter limited areas, it is necessary to adjust the threshold (at least) in accordance with what the local mean clutter level is. In operator-controlled radars that is partially accomplished by adjustment of video gain until the clutter in the area being examined is mostly eliminated; however, in fast reaction or automatic systems, the (local) threshold adjustment to prevent false clutter detections must be accomplished automatically.

Automatic threshold adjustment for target direction in clutter include clutter mapping circuits, sliding window detectors, and limiters. The basic idea is to obtain several samples of the clutter level, either by several independent samples of clutter in the cell of interest or by sampling surrounding cells, or perhaps both. The effectiveness of cell (or time) averaging adaptive threshold CFAR for Rayleigh clutter in terms of a detection loss, i.e., the additional threshold increase required to compensate for the use of only a limited number of samples on which to base the estimate clutter level, is shown on figure 3-17. Note that on the order of at least 10 - 20 independent samples are required before the loss is held to a tolerable level. Because spatial decorrelation is fast for land forms (see table 3-9), cell averaging may not result in satisfying levels of threshold refinement.

Adaptive threshold or CFAR processing is of great value in preventing false alarms from increasing dramatically with increasing clutter level. Clutter mapping techniques are a sort of "all or nothing" version of adaptive thresholding. Conversely, as clutter levels decrease, adaptive thresholding allows maximum target detection sensitivity to be attained. Unfortunately, adaptive threshold design and performance characteristics are usually based on a homogeneous Rayleigh clutter assumption, such as would be the case over heavy vegetation; however, errors will result in the case of log-normal clutter. The curves cited earlier provide a measure of this sensitivity loss or change in false alarm rate. To date, adaptive threshold techniques that work efficiently in diverse types of clutter have not been implemented in production.

Finn [3-20, 3021] has considered the case in which there is mismatch between the actual and assumed spatial variation in clutter level. Figure 3-18 shows results for the case in which cell averaging is done including (unknowingly) areas in which there is no clutter. If, for example, there is a clutter-free shadow region comprising 25 percent of the cell averaging area, the false alarm rate may rise by as much as two orders of magnitude. Actually, this is still good considering the magnitude of this mismatch.

The major radar/environment characteristics of concern are terrain type, grazing angle, wavelength, and polarization. Taken together, there are approximately eight to ten possible terrain types, three or four separate grazing angle zones, about six radar bands, and two polarizations not counting cross-polarization characteristics, for a total of about 400 sets of conditions in which to specify just the backscatter coefficient σ_o. It is sometimes the case that in particularly sensitive applications, or for one of a kind fixed site radars, one is interested in examining the exact set of detailed conditions and interactions which lead to backscatter coefficient behavior. Nevertheless, in the vast majority of cases the radar design is more concerned with trends and an averaging of performance over a variety of conditions. This allows a more simplified specification of ground clutter characteristics.

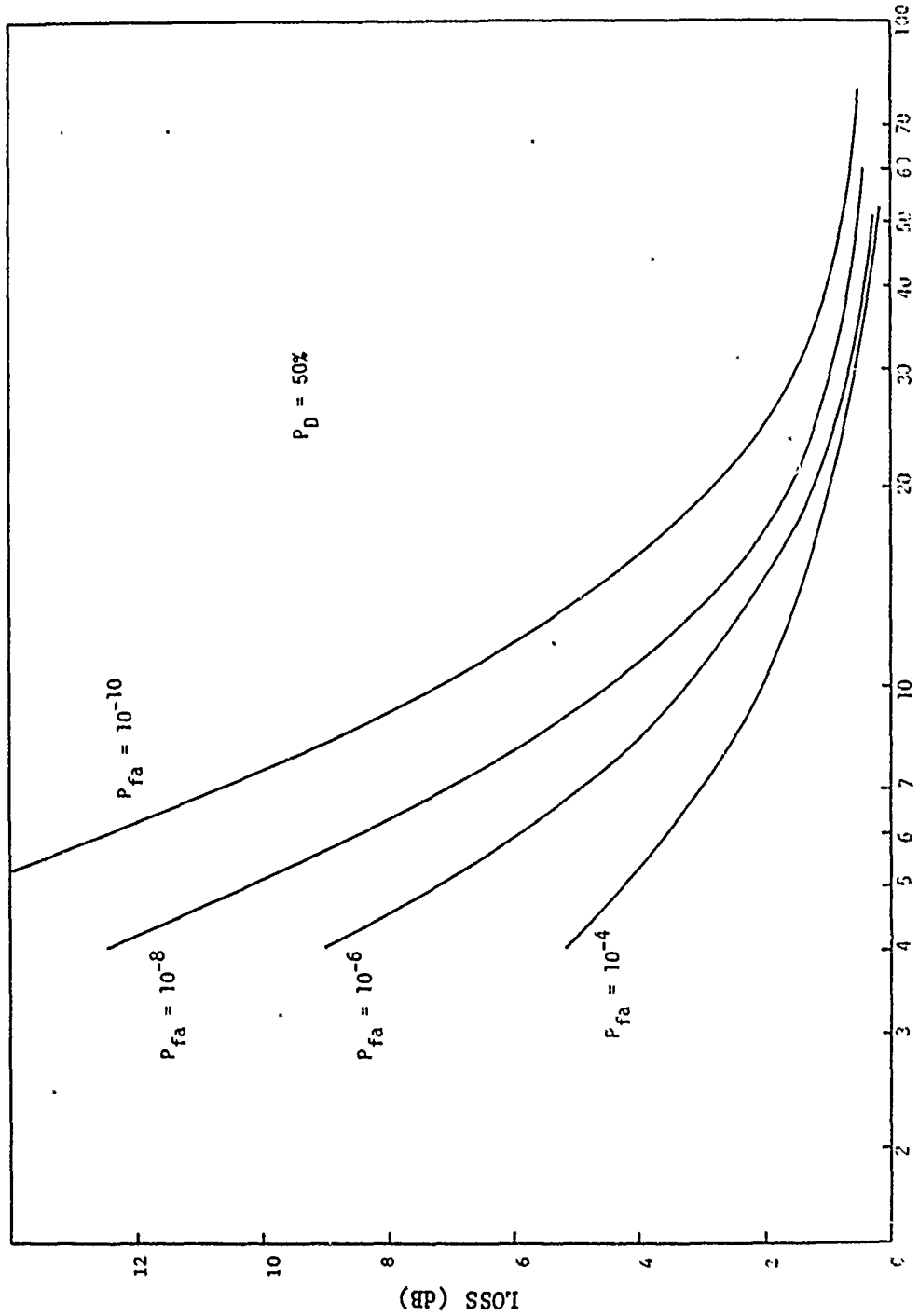

Figure 3-17

Loss of Adaptive Thresholding as a Function of Number of Reference Calls

Table 3-9

Empirical Clutter Shadowing Decorrelation Distances

TERRAIN	CORRELATION DISTANCE (m)
Plain Landforms	675
Low Hills	590
Low Mountains	670
High Hills	540
High Mountains	1030

[After References 3-22, 3-23, 3-24]

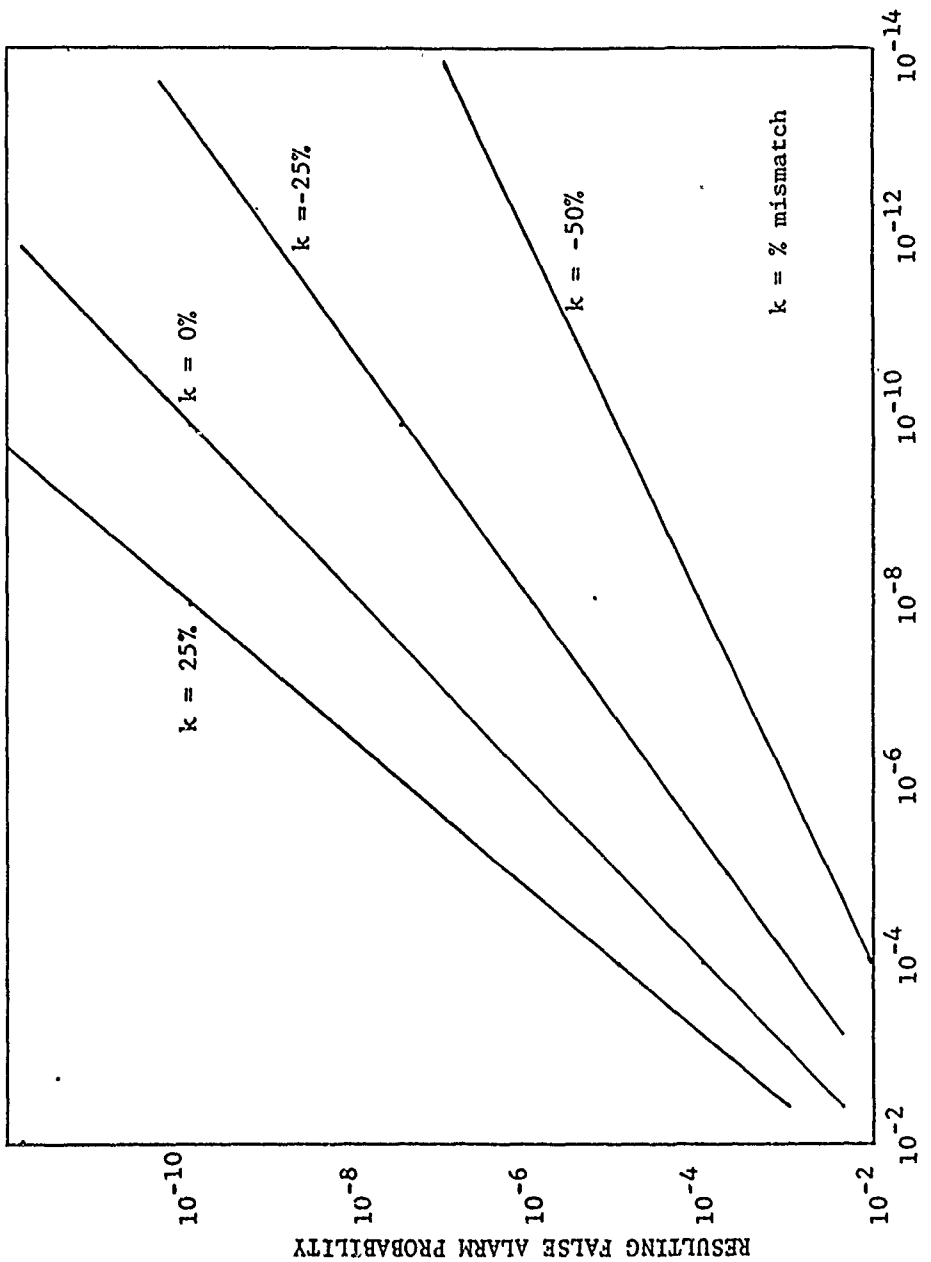

Figure 3-18
Effect of Mismatch in Cell Averaging CFAR

It is also of importance to note that the inclusion of a statistical spread parameter G, which acknowledges the real life inconsistency of σ_o even under the same terrain/grazing angle/wavelength/polarization conditions, to a large extent removes the importance of accurately specifying, say, the wavelength dependence of σ_o. For example, consider an application in which it is desired to have a radar operate over 90% of the clutter regions at a site at which, say, S = 8 dB, and it is desired to know the effect of the choice of, say, S-band or L-band as an operating wavelength on the clutter backscatter coefficient. If a σ_o independent-of-wavelength model is used there is no effect (except for possible changes in radar resolution) whereas if a λ^{-1} model is used (these are the two best substantiated possible models) then the 90% coverage figure drops to 81% from L-band to S-band. This difference may be significant, but it does not have the importance that is sometimes associated with a 4 dB (L- to S-band change) inability to meet "required" subclutter visibility performance.

3.2.2 Land Backscatter Statistics

It is difficult to give an adequate statistical distribution of the backscatter characteristics of land for the following reasons:

1. The statistical nature of the return from a given area cannot be related to the type of land as easily as the relatively convenient use of sea state descriptions. (Note that even sea state descriptions at any time are ambiguous.)

2. The land backscatter amplitude distribution at low grazing angles does not usually conform to the Rayleigh distribution because of the "shadowing" from hills, buildings, trees, etc.

3. The moisture content of the soil, or snow cover, can alter the backscatter coefficient.

4. The derivation of a mean or median value for σ_o differs between land and airborne measurements. The fixed radar sites essentially perform a time average of a given clutter cell while an airborne measurement performs a spatial average.

Figure 3-19 gives several cummulative distribution functions of σ_o from land-based radars. Two of the radars were operated at The Johns Hopkins University Applied Physics Laboratory in Maryland for the detection of low flying aircraft. Both of the profiles shown are for an azimuth angle for which the clutter return extended for several miles. The terrain consisted of rolling countryside with patches of 30-foot high trees and a number of small houses. The approximate peak values of the time fluctuation were plotted rather than the temporal average. The third distribution is from a Swedish forest area with a radar of similar parameters to the X band radar at APL. While the maximum values of σ_o for these two areas are similar, it can be seen that the median values of the backscatter coefficient for the two APL radars differ by about 11 dB for the same terrain. This is undoubtedly due to the shadowing effect, which almost completely obscures close to 50 percent of the terrain (but not necessarily 50 percent of radar cells, because of gap bridging by pulse or beamwidth). Essentially, the comparison of the median values of these two experiments would indicate a strong frequency dependence that other experimenters have not verified. The Swedish data, from Linell, do not have as marked a shadowing effect as do the APL data, probably because the radar used by Linell was located atop a 100-foot water-works tower; the APL radars are approximately 50 feet above the local terrain. A fourth cumulative distribution is shown for a mountainous area.

Various general classifications of terrain are arranged in tables 3-10 and 3-11 in order of increasing backscatter coefficient at low depression angles. The values of σ_m (median) for each frequency are the average of horizontal and vertical polarization unless otherwise stated. The results can be considered seasonal averages since the median return from vegetation and forests will vary by more than 9 dB, depending on the amount of foliage. The terrain backscatter was about 6 dB lower than the lowest seasonal average when there was a 4-inch snow cover at depression angles of about one degree.

The use of the term "σ_{84}" is an initial attempt to define the statistics of the backscatter coefficient for a pulse radar; σ_m refers to the median value and σ_{84} refers to the value of the backscatter coefficient that will <u>not</u> be exceeded in 84% of the range cells. The difference between these values (S) has been found to be as high as 18 dB. As the depression angle of the radar increases, the shadowing effect diminishes and the distribution standard deviation decreases. The following statements are tentative, but their general trends are indicative of low depression angles and homogeneous terrain:

1. The median backscatter coefficient increases somewhat with frequency for most terrain types, but usually not faster than linear (in power returned) with transmit frequency. The frequency effect on return from urban areas is quite small.

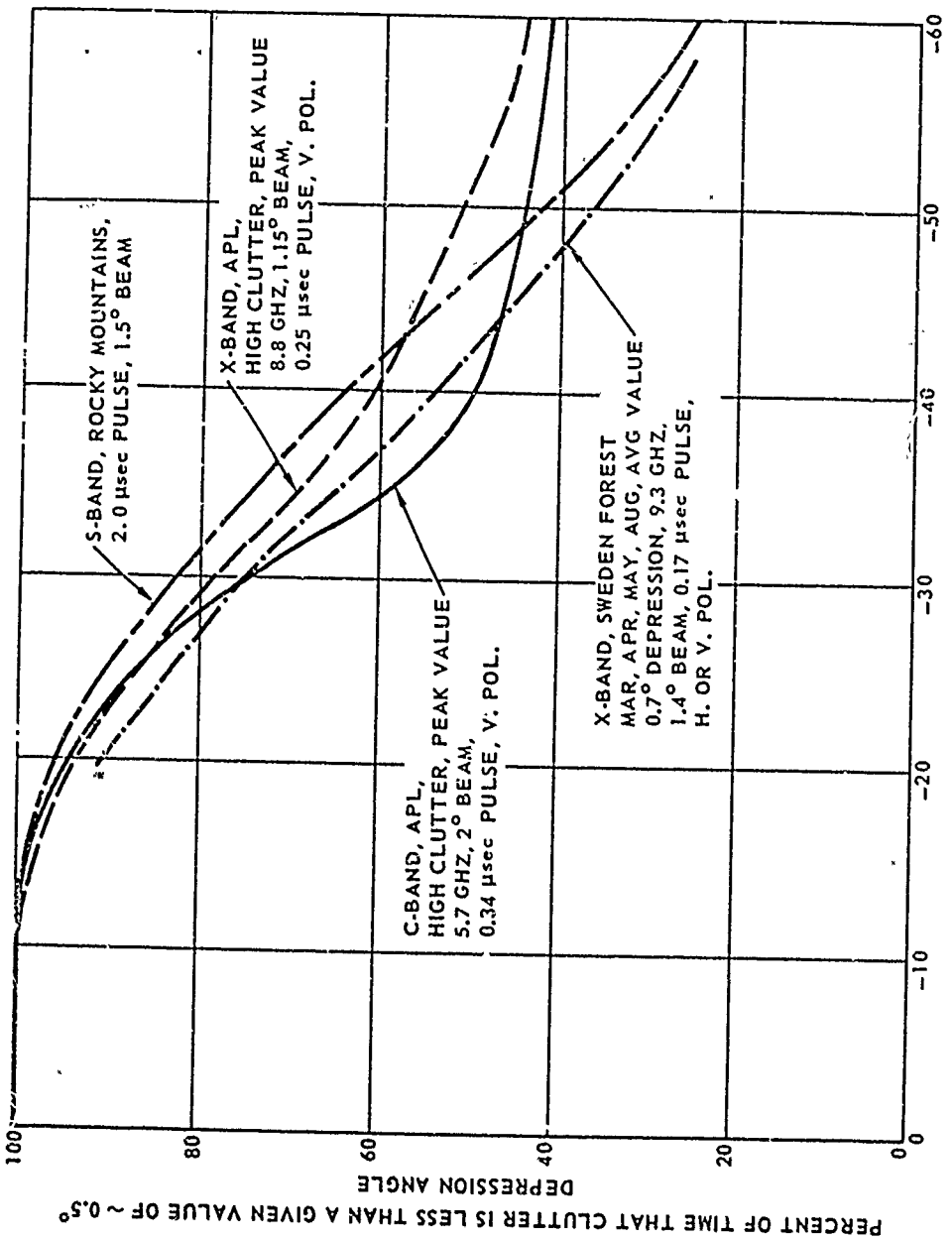

Figure 3-19

Land Clutter Backscatter Distributions from Surface Radars [3-3]

Table 3-10

Radar Land Backscatter – Grazing Angle = 0-1°

Non-Rayleigh Distribution

*6 dB error not likely

H = Horizontal Polarization
V = Vertical Polarization

Carrier Frequency

	L Band 1-2		S 2-4		C 4-8		X 8-12		Ku 12-18		Ka Band 31-36	
	σ_o	S	σ_o	S	σ_o	S	σ_o	S	σ_o	S	σ_o	S
1. Desert – Relatively Flat	45*		41*		40*		40*	8				
2. Farmland-Rural	39		34*	10	33*	8	30	13	23	13	18*	
3. Heavy Woods – Jungle		10	33*	13	28*	13	26	13		13	18*	
4. Mountainous			32*	10	28*	12	26	13		13		13
5. Urban	28*	10	25*		21*		18					

Table 3-11

Radar Land Backscatter – Grazing Angle = 3°

Non-Rayleigh Distribution

*6 dB error not likely

H = Horizontal Polarization
V = Vertical Polarization

Carrier Frequency

	L Band 1-2		S 2-4		C 4-8		X 8-12		Ku 12-18		Ka Band 31-36	
	σ_o	S	σ_o	S	σ_o	S	σ_o	S	σ_o	S	σ_o	S
1. Desert – Relatively Flat							34					
2. Farmland-Rural							31	8		8	18	
3. Heavy Woods – Jungle							26	8		8	18	
4. Mountainous							25					
5. Urban							18					

2. The median backscatter coefficient increases about linearly with grazing angle from 1/2° to 10°. In some cases a reduced value is found at 3° - 5° (see figure 3-20).

3. There are polarization differences on individual measurements, but there is not a strong general effect.

Backscatter from Composite Terrain

Most terrain appears to surface radar to be a composite, made up of a variety of scatterer types: some open fields; wooded areas; rough rocky patches; man-made artifacts; and shadowed regions. It is the ensemble of these types that results in the observed wide dynamic range of land clutter distributions. Some examples of distributions of cross section per unit area ensembled not only over heterogeneous cells but also over different ranges (incidence angles) are shown in figures 3-21 through 3-26. In the first three of these figures the probability axis is scaled so that log-normal functions would be straight lines; in the last three, Weibull distributions plot as straight lines. It is seen that in some cases the data deviate appreciably from log-normal (or Weibull, as the case may be), so there is no clear choice of a distribution function, only trends to guide analyses. These trends imply standard deviations of the log-normal fits to the region between median and 84 percent cumulative of about 12 dB (8 to 20 in various examples), and for Weibull fits in the same region, an exponent parameter of about 0.35 (0.5 to 0.2) is found.

The dominant independent variables which control the widths of distributions appear to be incidence angle and pulse length. The effects of incidence angle are illustrated for two data sets by figures 3-27 and 3-28. In the first, it is seen directly that as range to the clutter cells increases, the dynamic range of the clutter increases and saturates at a standard deviation (log-normal fit) of about 20 dB. In the second example, which corresponds to the composite curve labeled "Virginia Capes" in figure 3-21, it is seen that the widening of dynamic range of the cross section is caused by introduction at longer ranges of a second population of scatterers with median cross section about 30 dB below the higher level one, and in a way such that a greater number of cells belong to that lower-level group as range increases. This phenomenon is tentatively identified with shadowing, and a semantics in which the two groups are named "visible" and "shadowed" is defined.

The data set described in figures 3-29 and 3-30 illustrates the effect of pulse length on altering the fraction of cells that contain substantial clutter (the "visible" fraction) and on the shape of

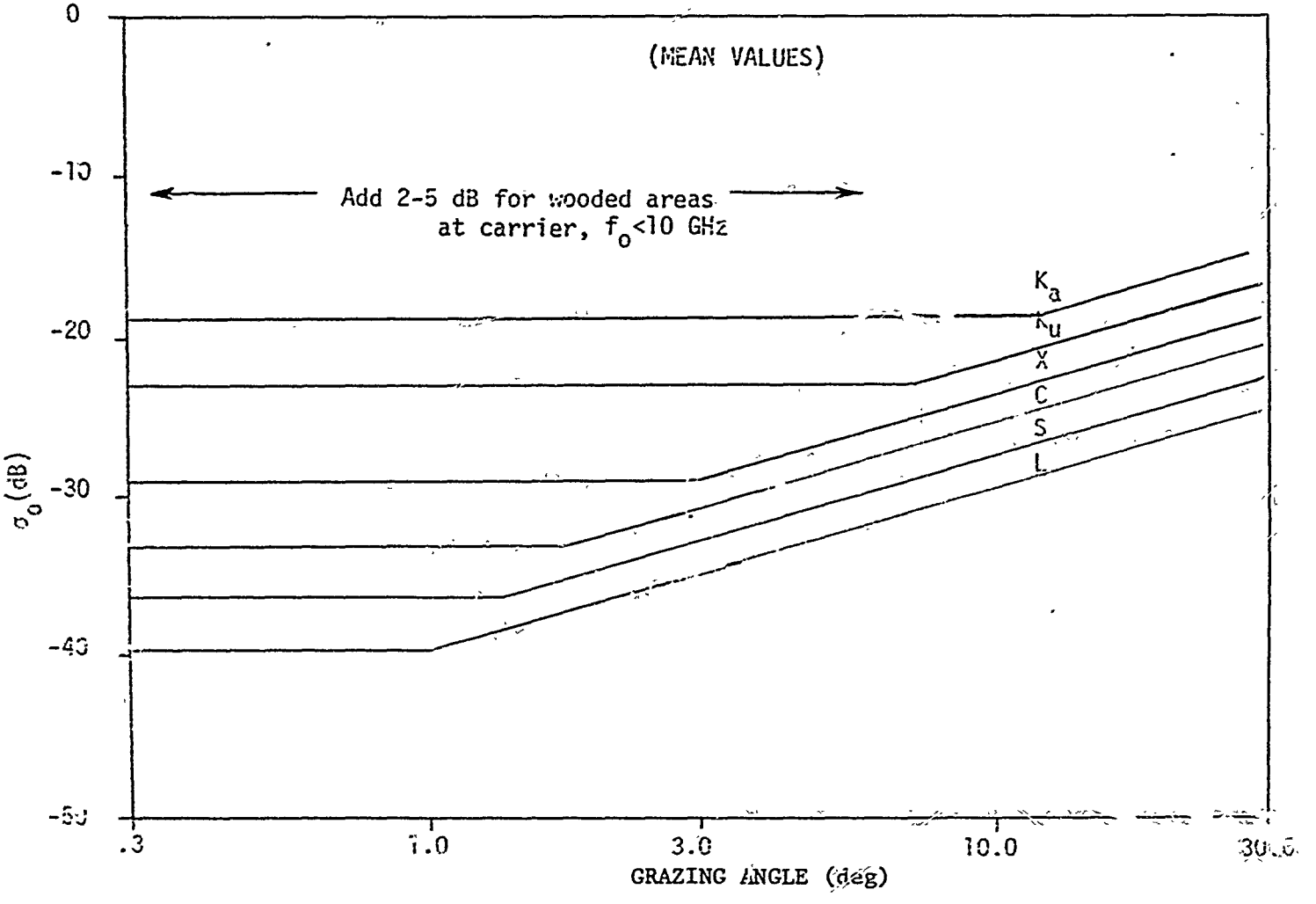

Figure 3-20

Reflectivity Values for Typical Rural Land Clutter

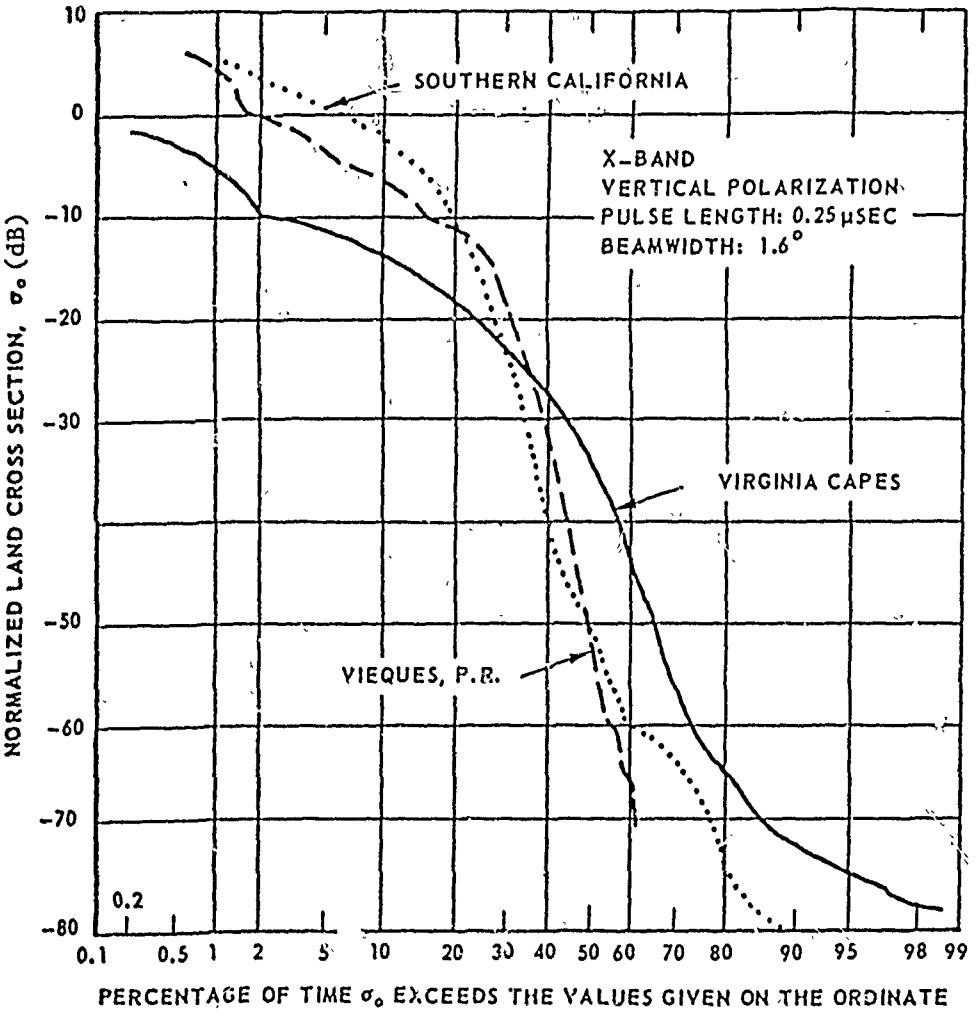

Figure 3-21

Probability Distribution of Land Cross Section per Unit Area, σ_o, at X-Band, Vertical Polarization [3-25]

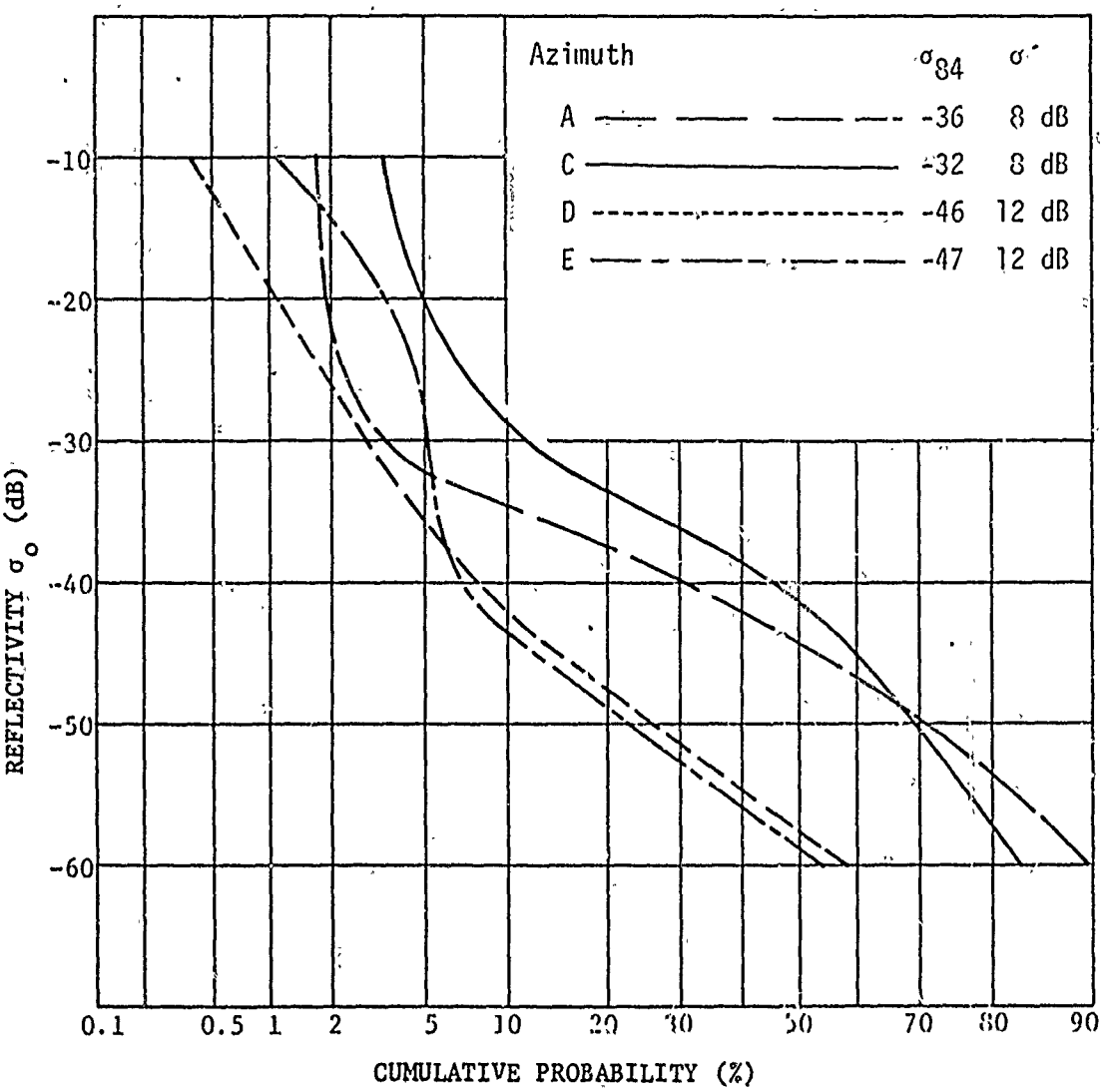

Figure 3-22A

Backscatter Distributions for Mountainous Desert WSMR C-Band, Vertical Polarization, τ = 1, $\psi < 0.1^{\circ}$ [3-26]

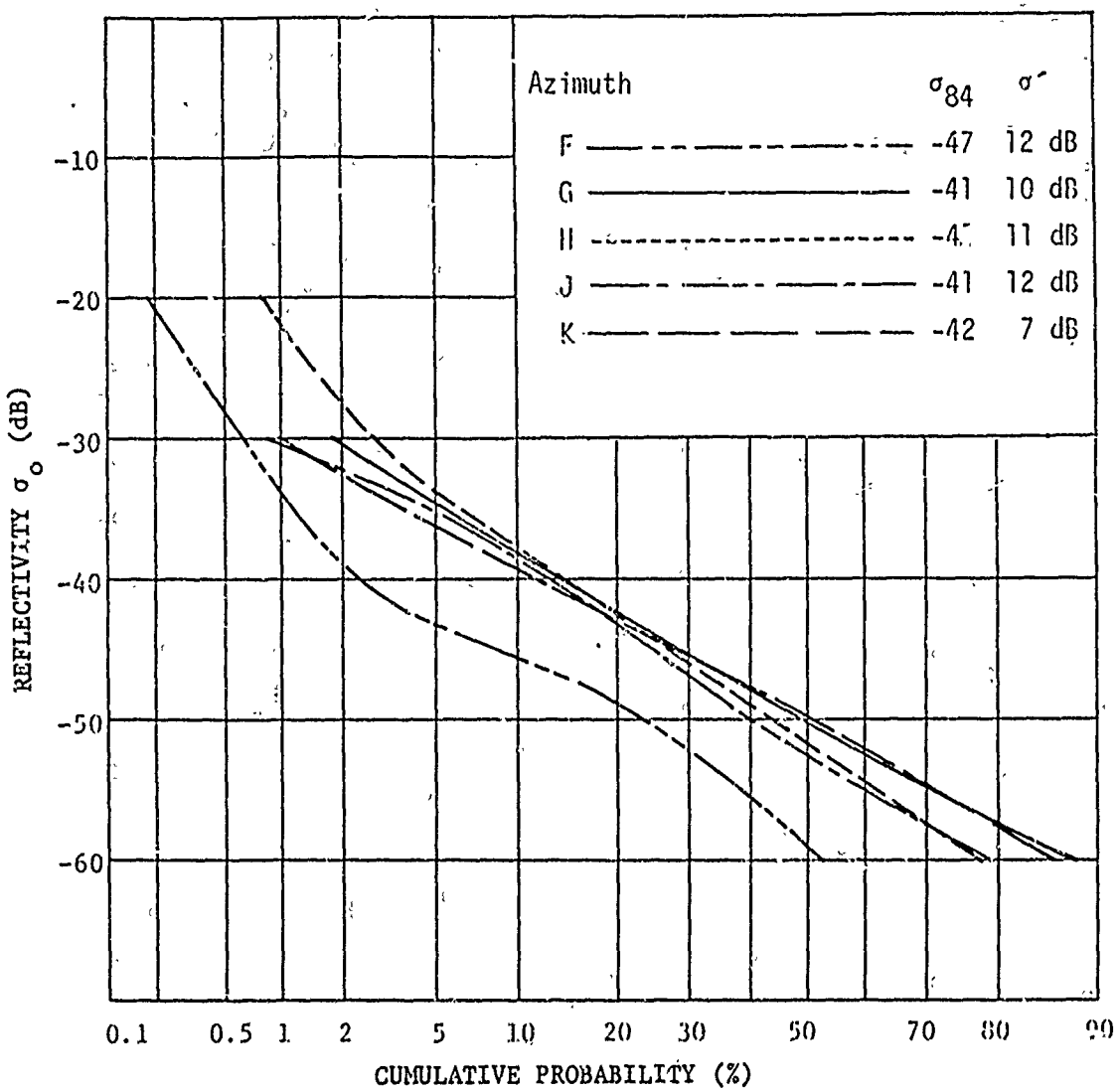

Figure 3-22B

Backscatter Distributions for Mountainous Desert WSMR C-Band, Vertical Polarization, $\tau = 1$, $\psi < 0.1^\circ$ [3-26]

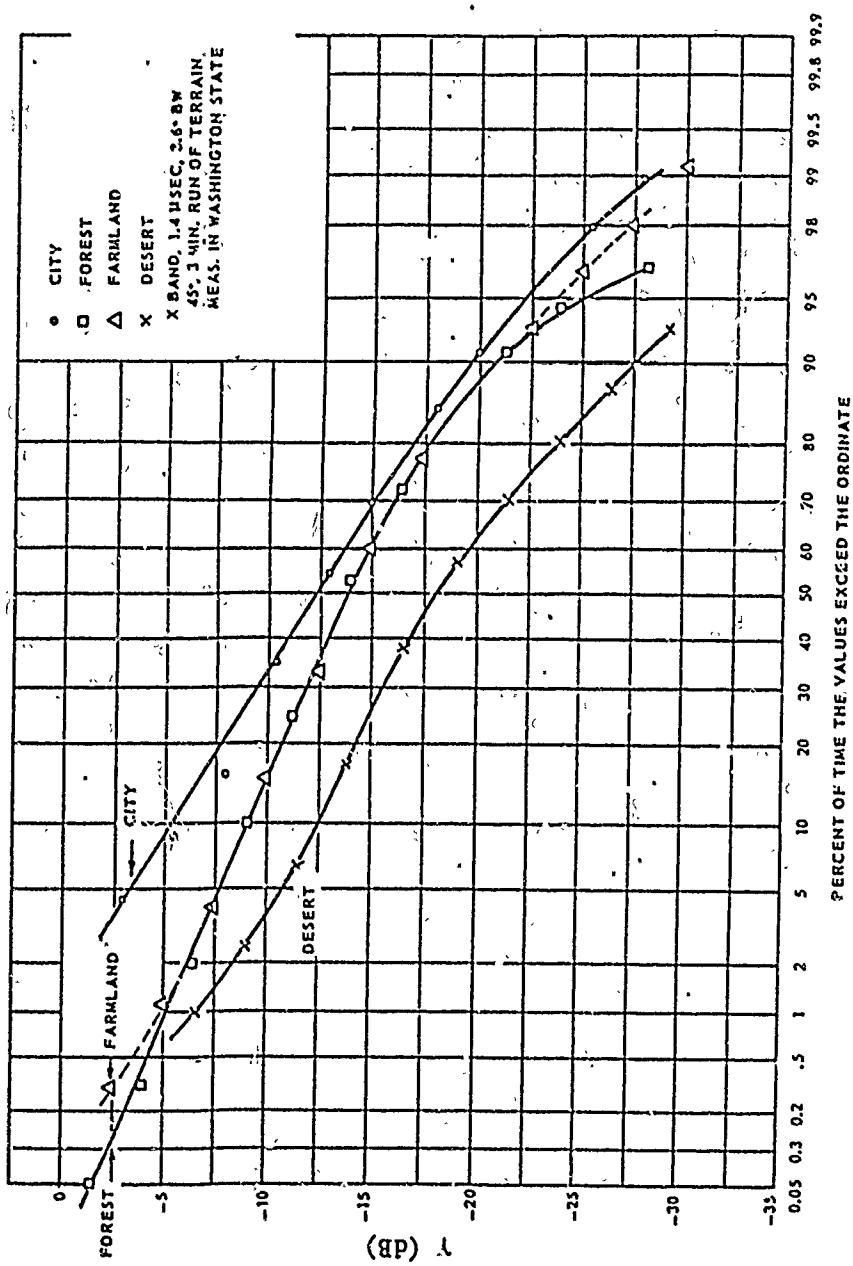

Figure 3-23
Distribution of γ - Boeing Data [3-27]

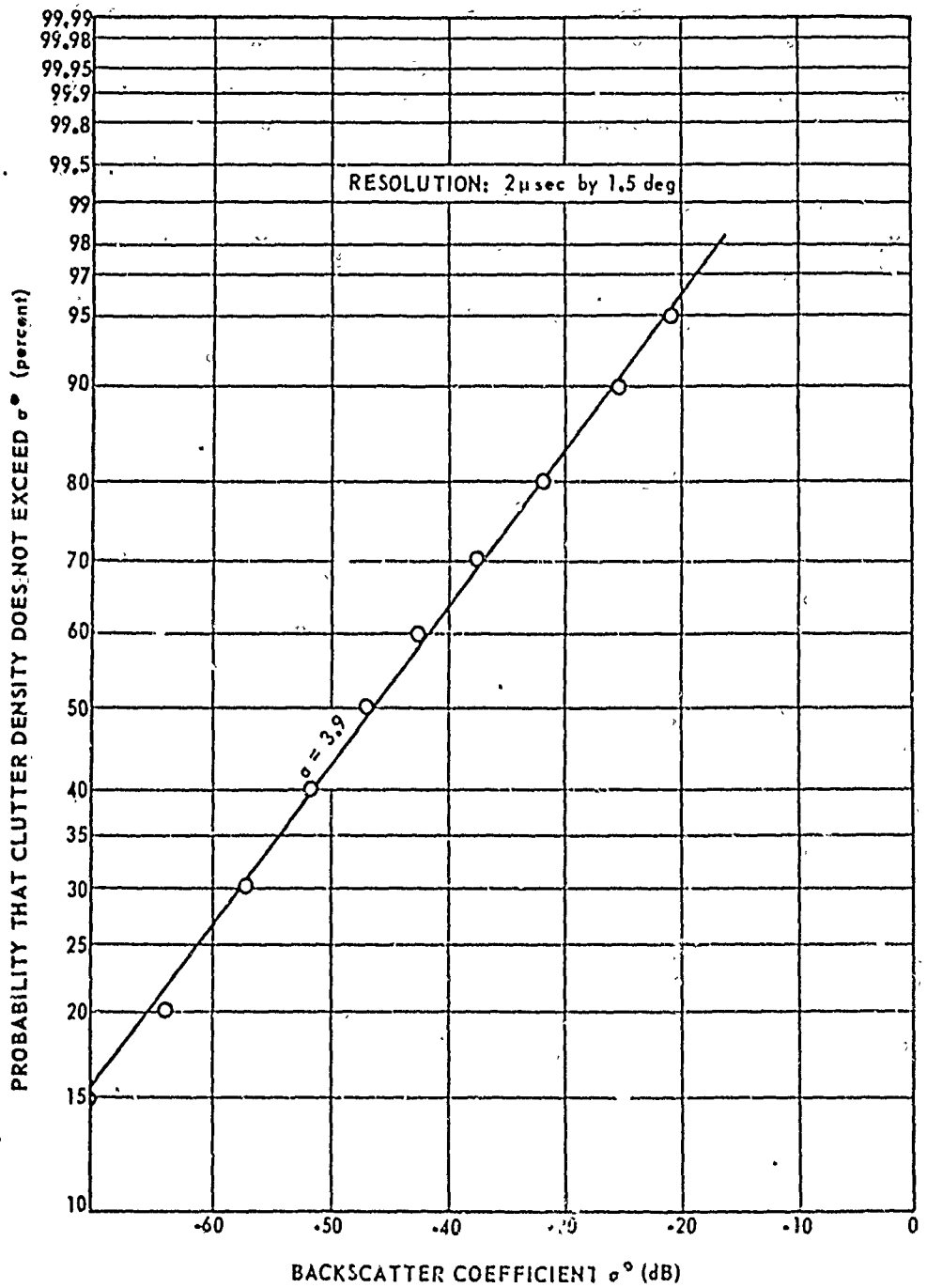

Figure 3-24

Ground Clutter Spatial Distribution
For Rocky Mountains at S-Band [3-28]

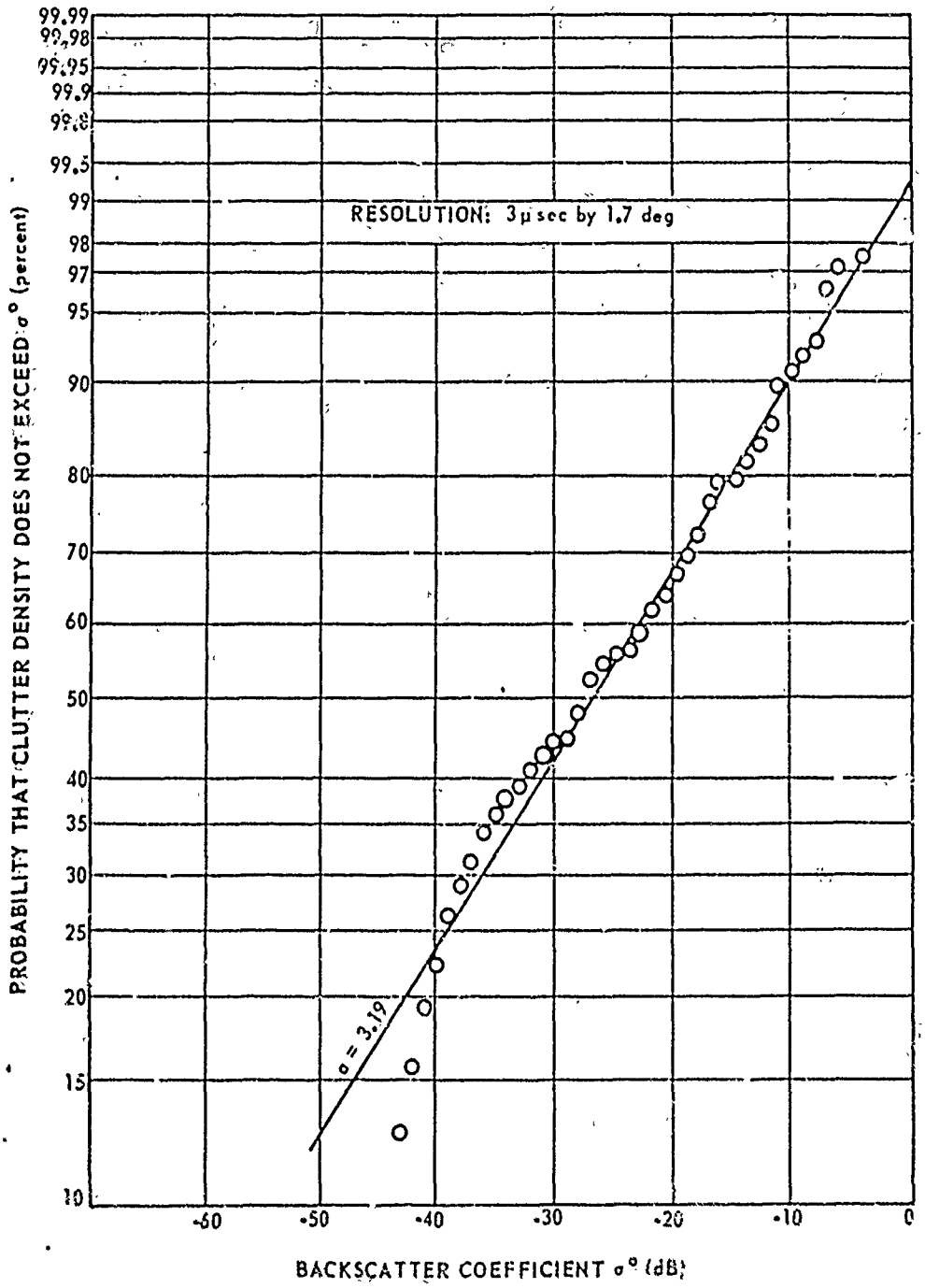

Figure 3-25

Ground Clutter Spatial Distribution For Wooded Hills and Grassland Near Huntsville, Alabama, at L-Band [3-28]

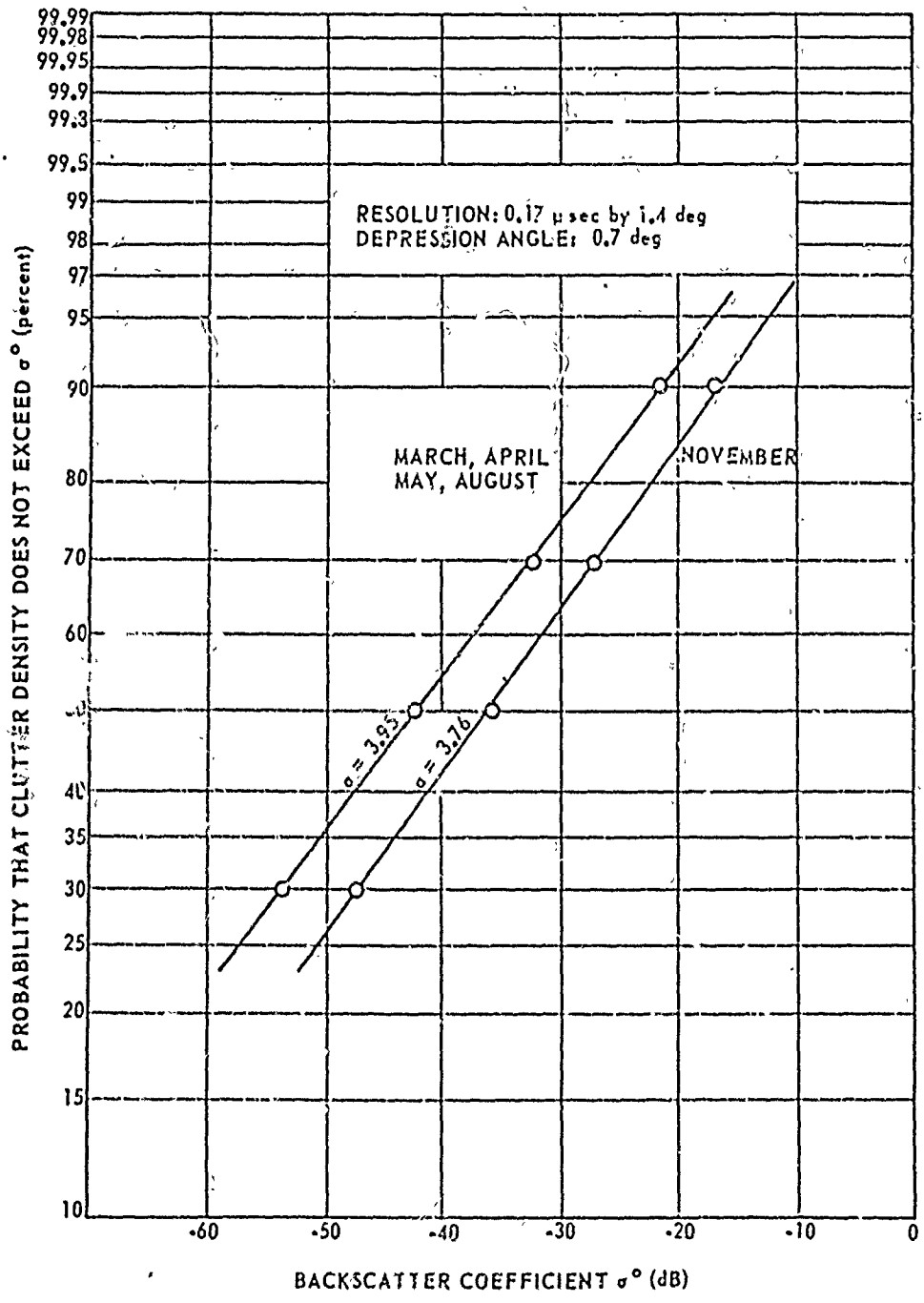

Figure 3-26

Ground Clutter Spatial Distributions
For Forest at Different Times of Year at X-Band [3-28]

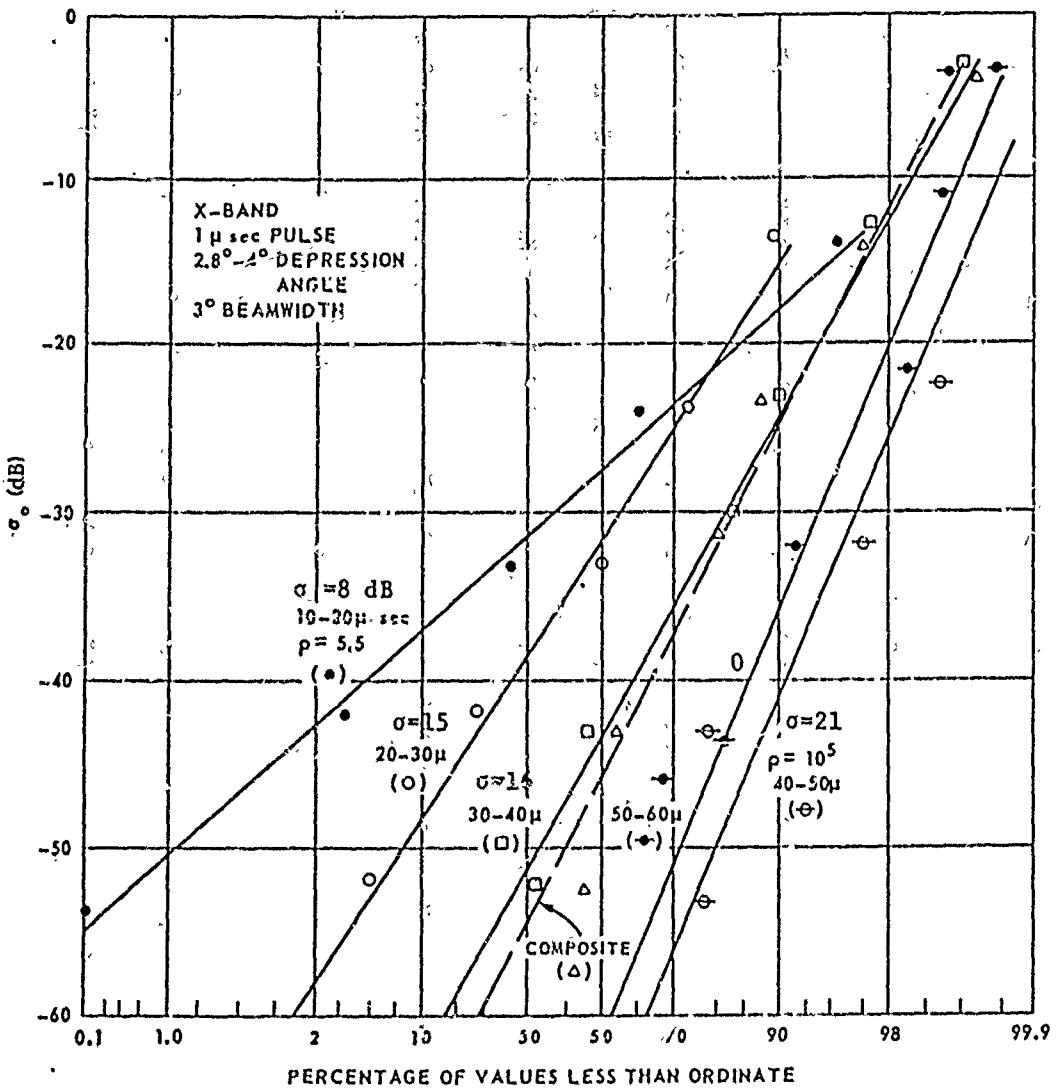

Figure 3-27

Distribution of Land Clutter as a Function of Range at Bedford Massachusetts [3-27]

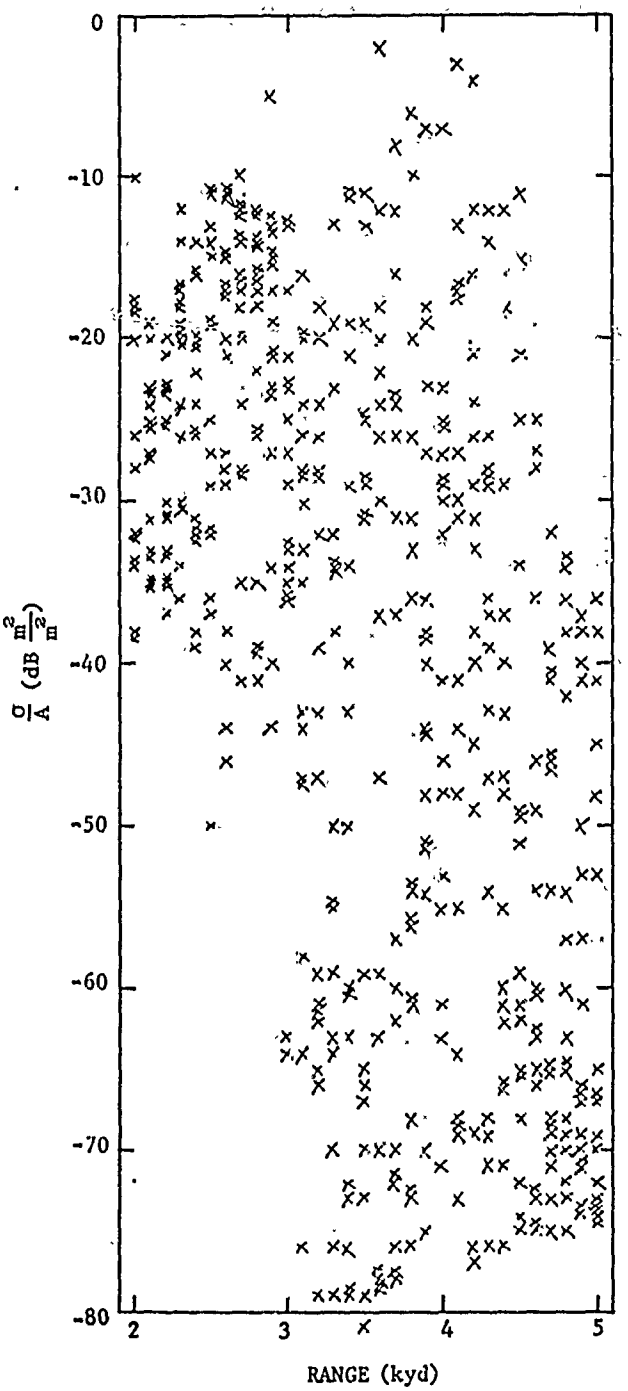

Data from "Resort" Case of [3-25]

Figure 3-28

Cross Sections per Unit area of Low Coastal Lands; X-Band, Vertical Polarization, 0.25 μ sec x 1.6° Cells

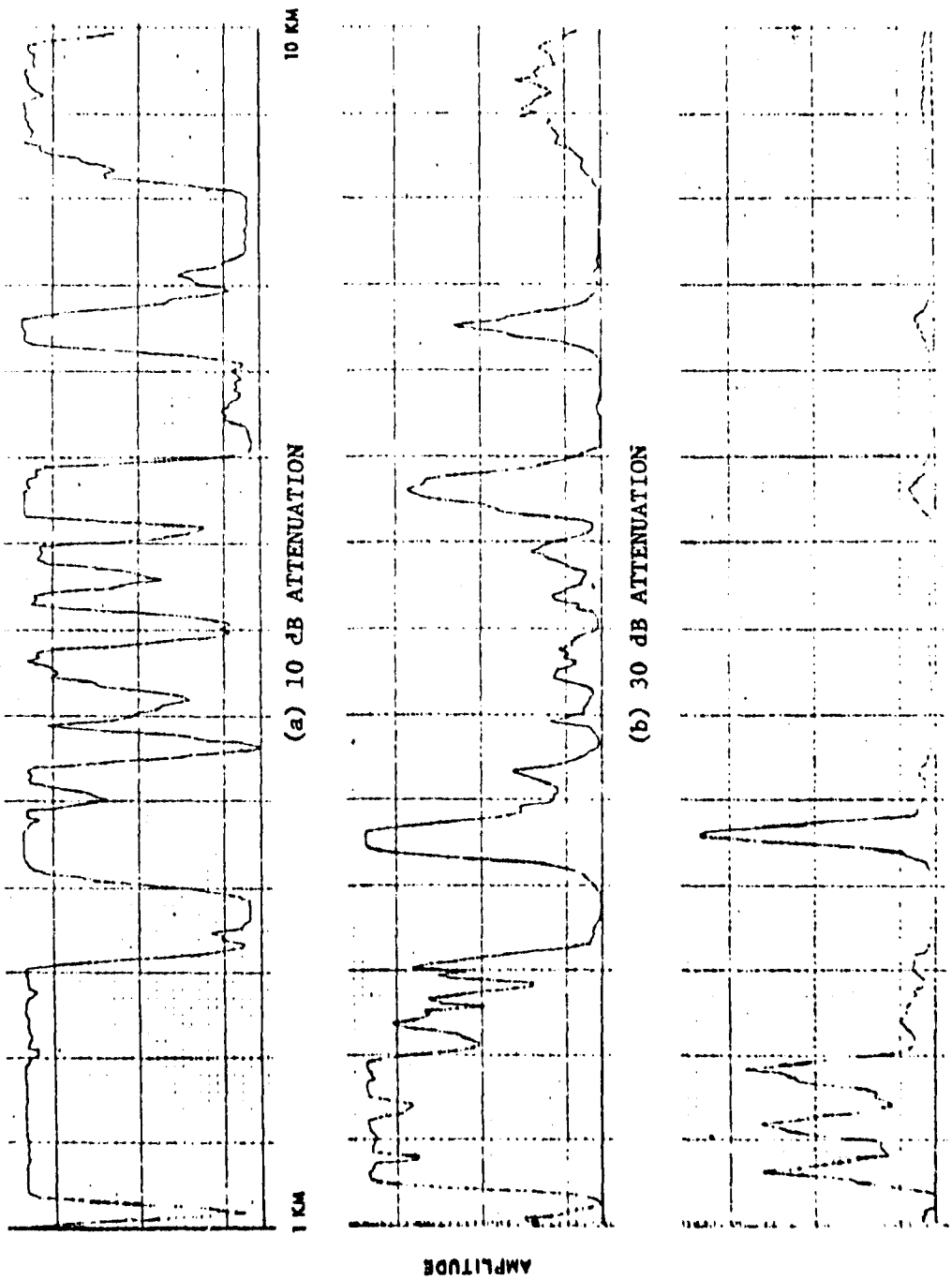

Figure 3-29

Land Clutter Profiles - 0.8 Microsecond Pulse - Effect of Clutter Attenuation [3-3]

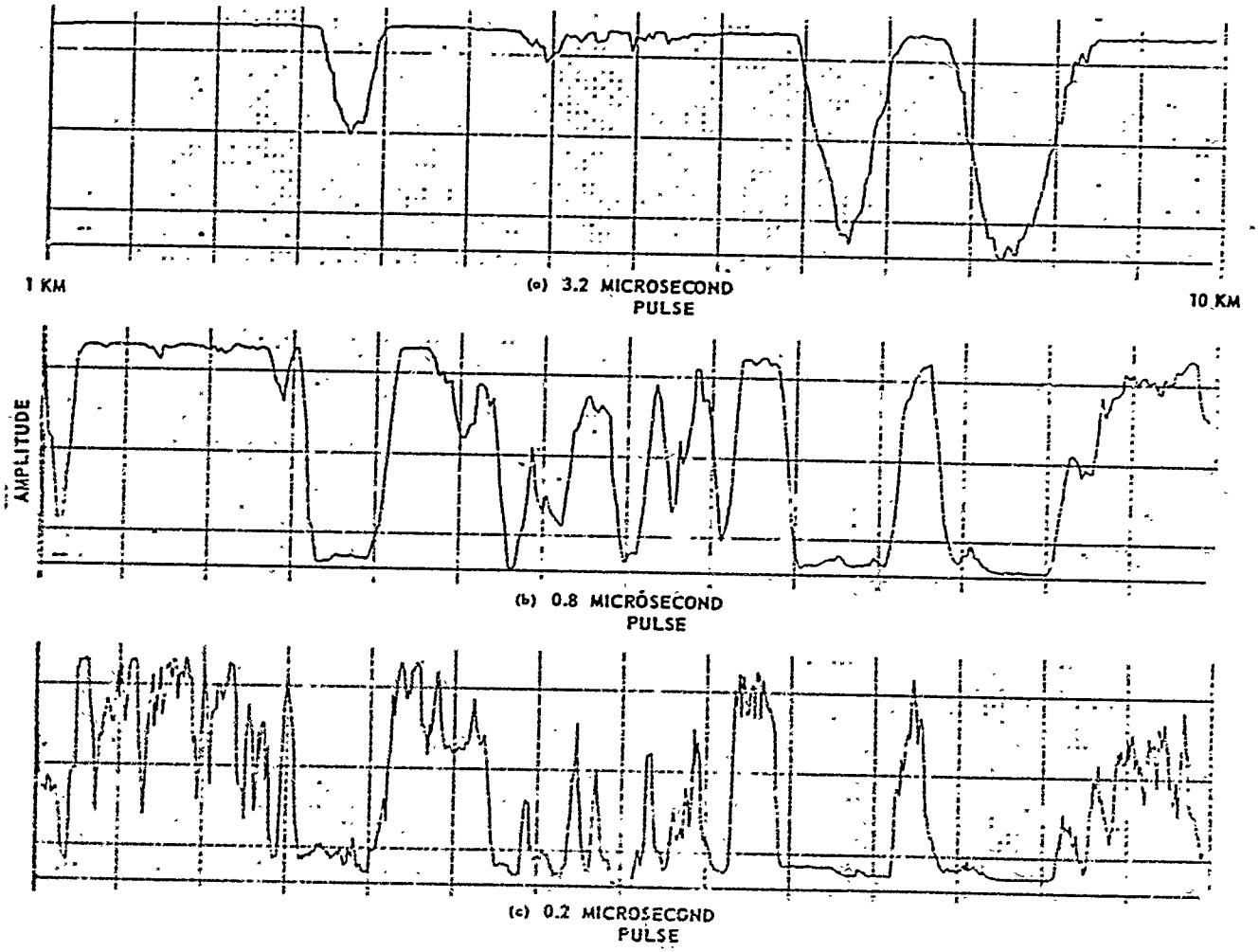

Figure 3-30

Land Clutter Profiles for Heavy Clutter Area - Effect of Pulse Length [3-3]

composite distributions. In figure 3-31 it is seen that: the cross section (distinct from cross section per unit area) of the larger scatterers is about constant; the shape of the distribution across the upper part (associated with the visible set of cells) is conserved with changes in pulse length; and the fraction of cells not containing appreciable clutter (the shadowed set) increases with decreasing pulse length.

A combined analysis of the data of references 3-3, 3-25 and 3-29 results in the model for the "visible" fraction of land clutter cells as a function of both pulse length and incidence angle shown in table 3-12. For that table, a beam width of the order of 1.5 degrees applies.

The large discrete scatterers, although statistically low in number compared to the number of cells containing distributed clutter, have rather large cross sections, and they do not necessarily decrease in average value with decreased cell size. The model of reference 3-23 gives cross section values in the range of +20 to +60 dB m^2, those of figure 3-21 are of the order of +30 dB m^2, and those of figure 3-31 are of the order of +40 to +50 dB m^2, for example. Cross section data on a variety of discretes are shown in figure 3-32 and they are described in table 3-13. These data were acquired at 3 GHz using horizontal polarization and a cell of dimensions 0.4 μs x 2° [3-30].

3.2.3 Spectrum of Land Clutter

The fluctuation spectrum of echoes from vegetated terrain arises from the relative motion of the scatterers (foliage) as they move about in the wind. As the wind speed increases, the motion increases and the spectrum width is almost directly proportional to the transmitted frequency, at least in the 3 to 30 GHz range of frequencies; figure 3-33 displays the spectrum width under the assumption of a Gaussian shape as a function of wind speed as determined from the data of many different sources - the transmitted frequency varied from 3.3 to 24 GHz. An estimated fit to the data is shown by the broken line. The polarizations used are unknown except for APL/Johns Hopkins experiments (vertical polarization)[3-3], and those of Fishbein, et al., (horizontal)[3-31]. The standard deviation of the clutter spectra (σ_v) in velocity units was determined by estimating the best fit to the Gaussian shape noting its standard deviation, and converting it to velocity units through the Doppler equation (each point of the APL data is an average of several measurements).

The thorough measurements by Kapitanov [3-32] revealed a spectrum composed of two parts. The region about the peak was Gaussian in shape down to 10 - 15 dB below the peak level. Below that level

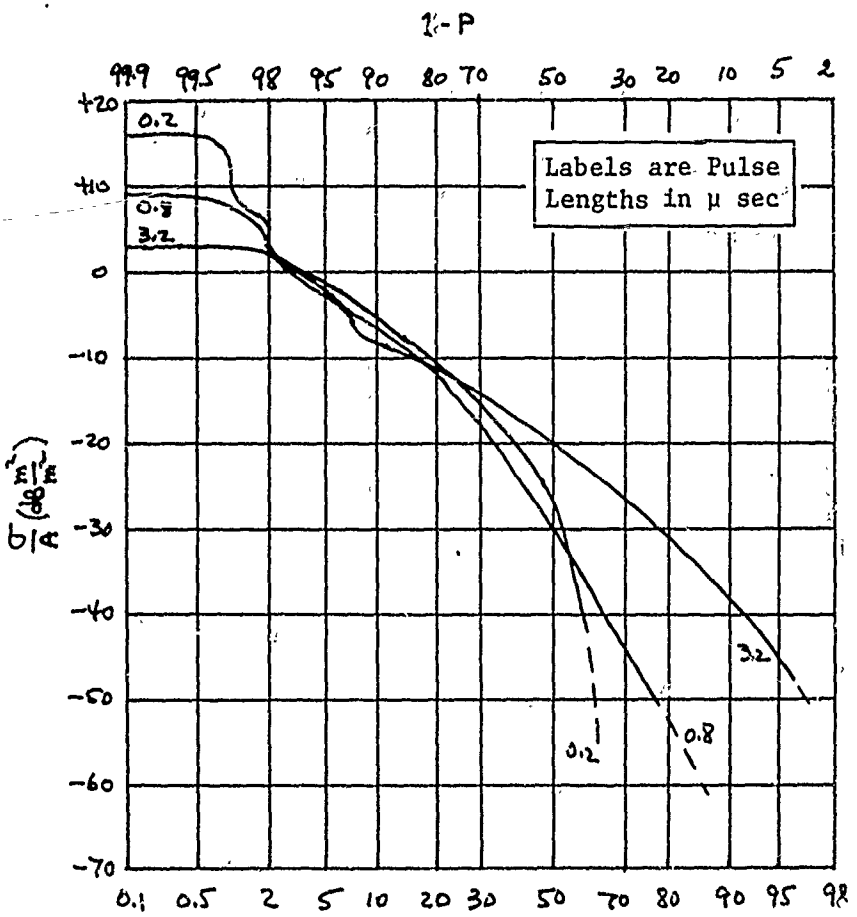

Figure 3-31

Nathanson's Figure 7-21 with the 3.2 μ sec Curve Calibrated Upward 5 dB [3-3]

Table 3-12

Fraction of Radar Cells Containing Clutter (Remainder is Considered Shadowed) Nominal Beamwidth is 1.5°

GRAZING ANGLE (deg)	PULSE LENGTH (μsec)		
	0.2	0.8	3.2
0.1	< 0.1	0.2	0.4
0.2	0.2	0.4	0.7
0.5	0.5	0.8	0.9
1	0.8	1.0	1.0
2	0.9	1.0	1.0

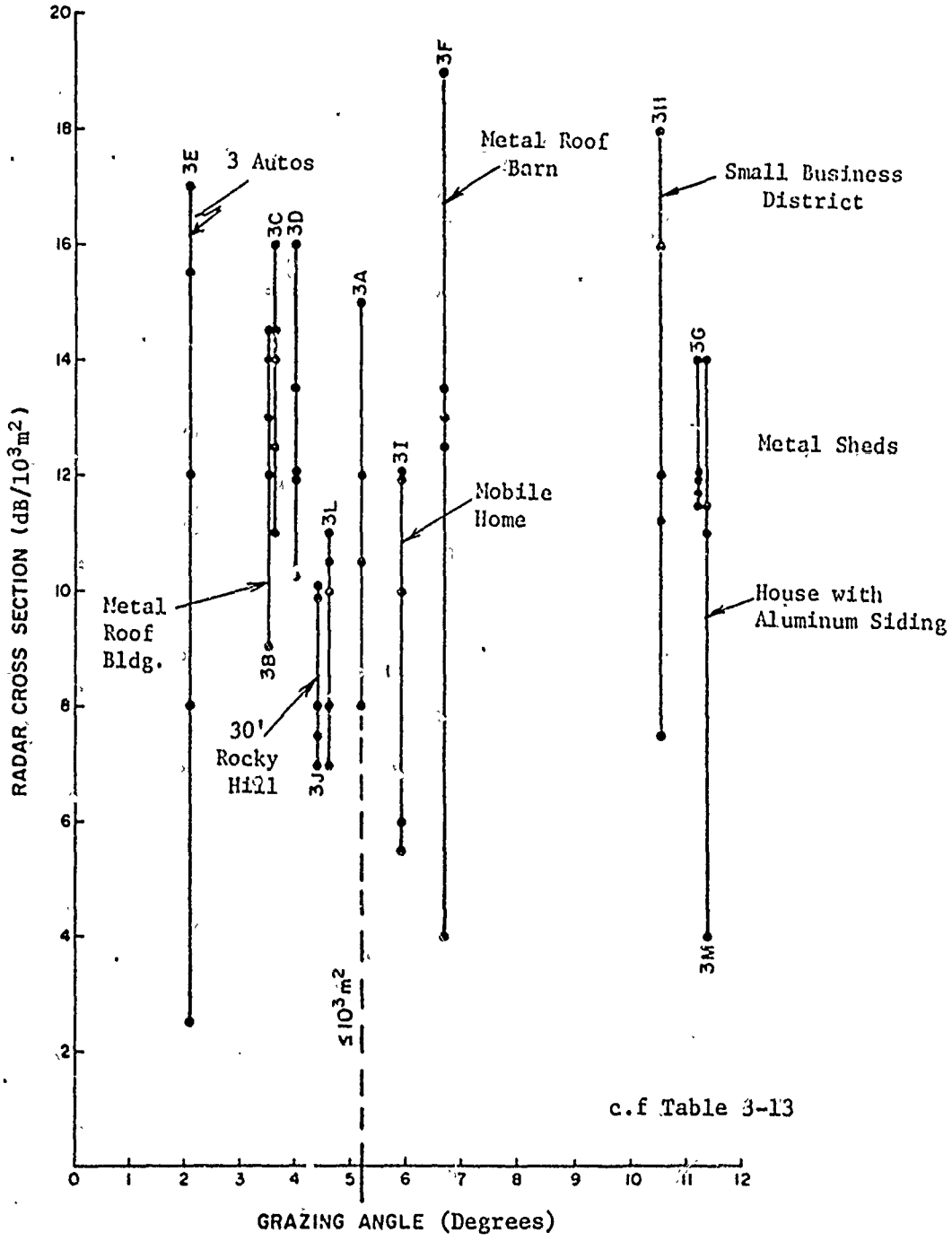

Figure 3-32

Radar Cross Section vs Grazing Angle for Targets 3A Through 3M [3-30]

Table 3-13

Characteristics of Discretes Observed from Site #3 [3-30]

Target, Figure Showing RCS	Range (nm)	Bearing Angle(°)	Grazing Angle(°)	Description	Comment
3A Figure 23	4.86	29.75	3.15	Hospital(?) N. Adams	Residential area at edge of business district; only large structure with metallic superstructure.
3B Figure 23	6.27	30.75	3.53	Farm Bldg's w/metal roof shed(?) N. Adams	Outside business district approximately 200 feet from target 1A.
3C Figure 23	6.23	31.5	3.57	Rural House N. Adams	Outside business district; in center of homes; aluminum sided house(?).
3D Figure 23	5.20	48.5	4.03	Mobile Home Park, N. Adams	Outside business district; approximately 30 units in two columns of parallel units with long axis approximately normal to line of sight.
3E Figure 24	7.93	84	2.13	Abandoned automobiles	Mountain meadow; three passenger vehicles parallel parked approximately six feet apart and one parallel to front bumpers of the other three offset about six ft.
3F Figure 24	3.22	101	6.70	Metal Roof barn, Adams	Outside business district. Long shed-like (≈40') structure w/roof line approximately normal to line of sight.
3G Figure 24	2.36	103	11.25	Metal Sheds, Adams	Business district; three all-metal sheds w/room lines parallel to line of sight. No separation between long walls.
3H Figure 24	2.39	106.5	10.55	Building, Adams	Business district; no obvious single building among a group of industrial buildings.
3I Figure 25	4.27	168.5	5.87	Mobile Home Park, Chesire	Rural area southeast of Adams; units occupy an area approximately 1000 ft. by 1000 ft; orientation of long axis of units appox. parallel to line of sight.
3J Figure 25	3.86	84.25	4.40	Side of Hill	Bare rock face approximately 30 feet high.
3K Figure 25	8.11	325.5	-	Side of Hill	Return from a steep face of mountain with vegetation; approximately normal to line of sight. Grazing angle definition not appropriate.
3L Figure 25	4.32	141	4.58	Rural Building	Rural area southeast of Adams.
3M Figure 25	2.28	104	11.43	Dual Family Dwelling	2-1/2 Story structure with aluminum siding.

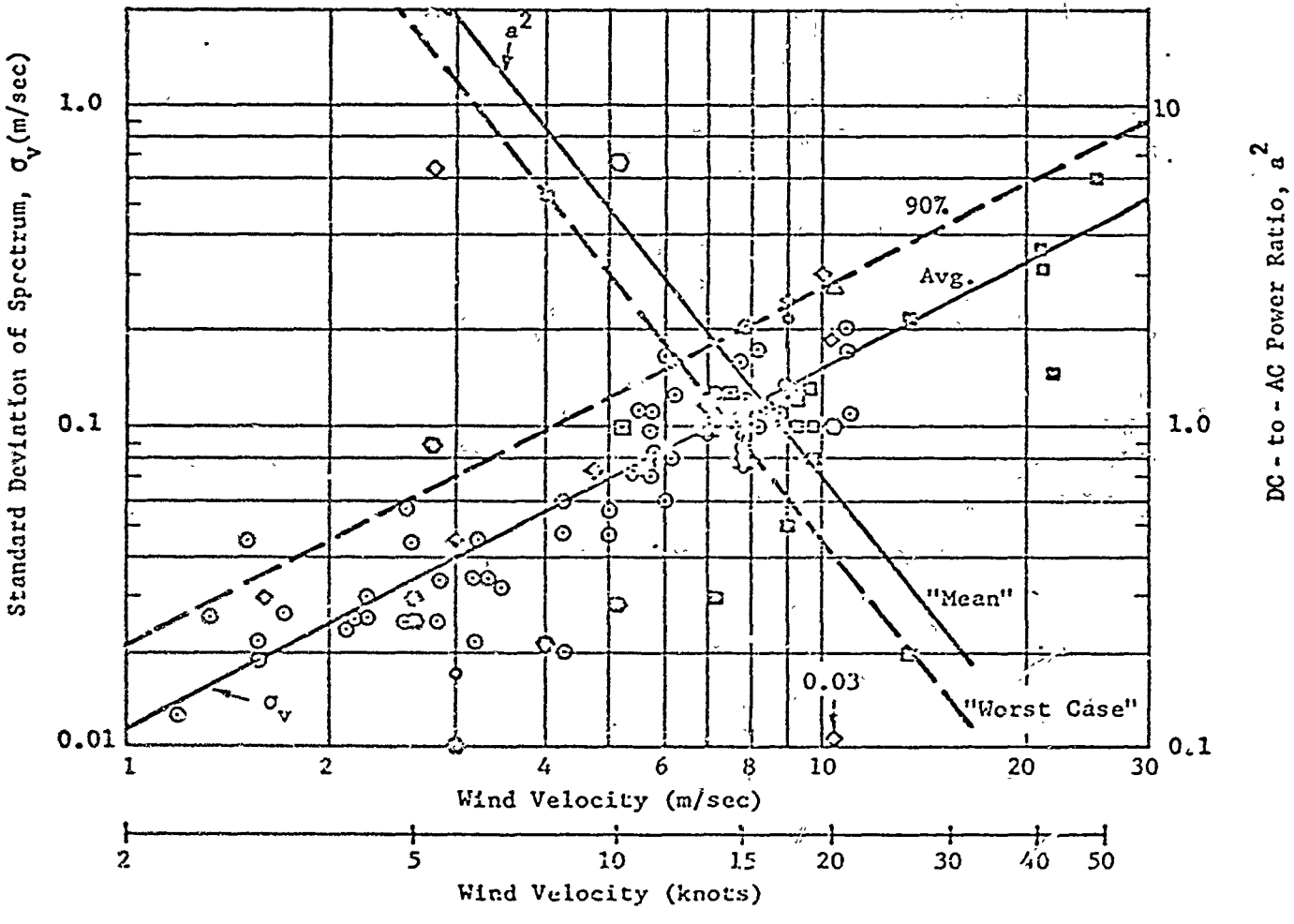

Figure 3-33

Spectrum Width for Land Clutter, Wooded Terrain (Fixed Antenna) [3-3]

down to at least -40 dB the spectrum fell off slower with frequency difference, like Δf^{-4}. Careful comparison of the cross-spectra and co-spectra with foliage velocity distributions resulted in a strong relationship of the Gaussian shape with the Doppler motion modulation and the f^{-4} part with amplitude modulation created by scatterer aspect angle changes. The Gaussian widths of the USSR data, taken at X-band and shown in figure 3-34, agree with the composite data of figure 3-33, and parameters of the f^{-4} tail portion are summarized in table 3-14.

It is believed that the DC component is composed of tree trunks, large branches and the surrounding terrain itself, while the AC component results from the leaves and smaller branches. As the wind increases, a greater proportion of the branches and trunks are set into motion. Even the relatively simple single MTI canceller will eliminate most of the DC component as long as the transmitter is stable and the dynamic range is not exceeded. The longer tails are more difficult to eliminate and there may be little improvement from additional stages of MTI. If cancellations of greater than 30 dB are desired, the details of the spectral shape should be included in the analysis.

Polar ice-covered terrain and sea ice resemble land return. Some points have larger returns than others, presumably because of ridges or tilted slabs of ice. The average cross section per unit area of artic ice is summarized in figure 3-35 from many data sets, including some taken from aircraft and some from ships, all at X-band [3-33]. When the sea state is low, there is a sharp demarcation between water and ice, as one would expect at a shore line, although at higher sea states, σ_0 values may become approximately equal. In figure 3-35, returns on horizontal polarization tended to lie nearer the upper boundary and on vertical polarization nearer the lower boundary shown.

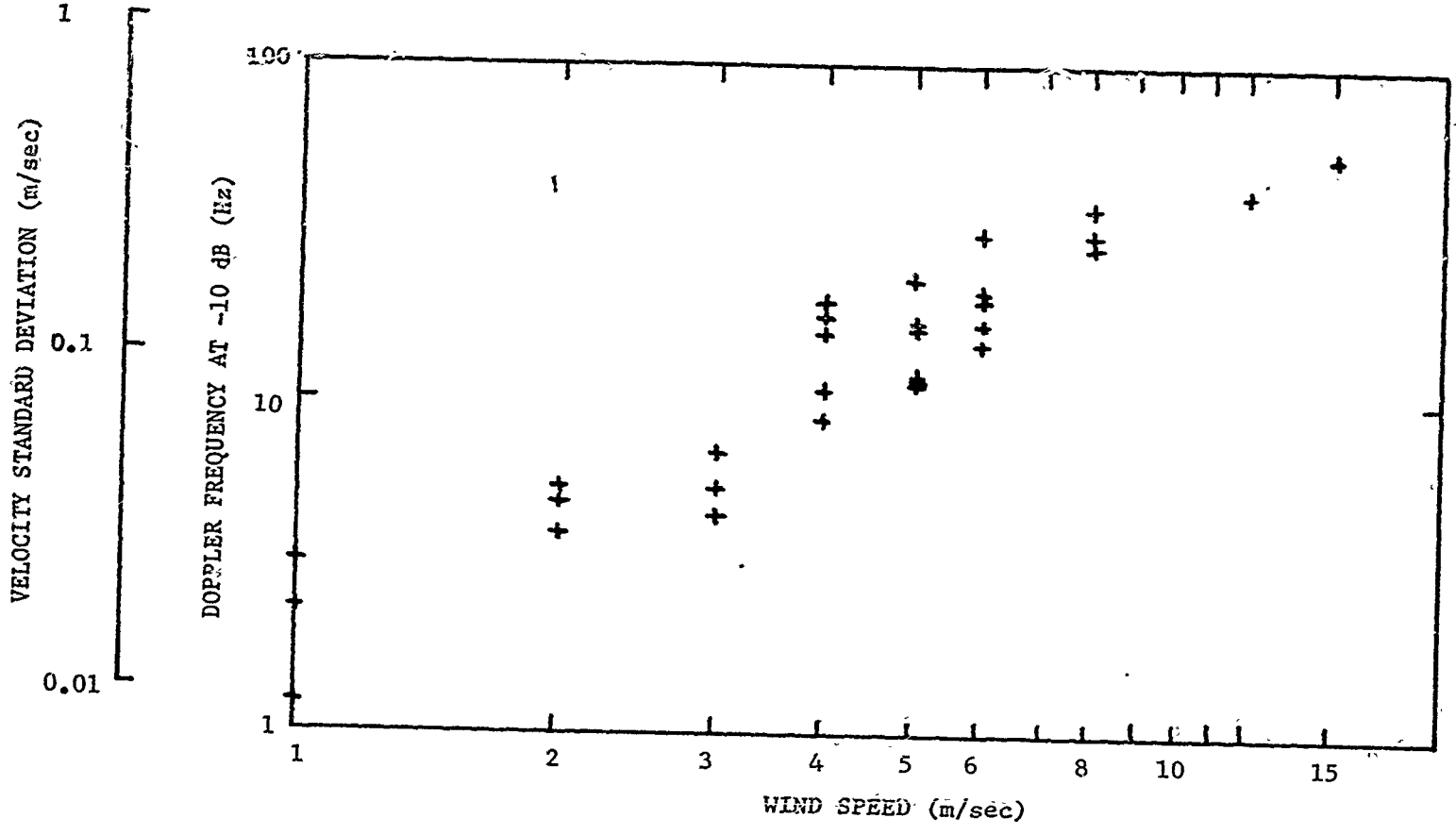

Figure 3-34

Half-width of Doppler Spectrum at -10 dB Level and Scatterer Motion Velocities as Functions of Wind Speed.
X-Band Coherent Spectra
Kapitanov, et al. [3-32]

Table [illegible]

Results of Measurements of Spectrum of Radar Signals from Forest

No.	Wind speed v, m/sec	Width of Spectrum at 0.5 Power Level	Width of Spectrum at 0.1 Power Level	Power exponent
1	4	5.6	9	-4
2	4	6.6	11	-3.9
3	2	2.7	4	-3.5
4	4	7.6	16	-3.8
5	3	3.3	4.5	-3.6
6	1	1.6	2.4	-3.2
7	1	2.1	3.2	-3.9
8	5	8.3	11.5	-3.8
9	5	11 5	17	-3.5
10	5	8	11	-4.2
11	2	3.4	5.6	-3.6
12	2	3.3	5	-4
13	1	0.8	1.2	-3.2
14	0-1	0.5	0.9	-3.5
15	15	32	56	-3.9
16	8	18	32	-3.7
17	8	20	38	-4
18	12	23	42	-3.9
19	6	9.5	15	-3.4
20	6	17	32	-3.6
21	4	10.5	20	- .3
22	5	13	23	-1.8
23	5	10	16	-4
24	3	4	5.6	-3.7
25	3	4.6	7	-3.4
26	6	11	17	-3.8
27	6	13	21	-4
28	4	11.5	18	-4
29	8	16	30	-3.7
30	6	12	19	-4.2

λ = 3.2 cm, vertical polarization, Kapitanov et. al. 1973 [3-32]

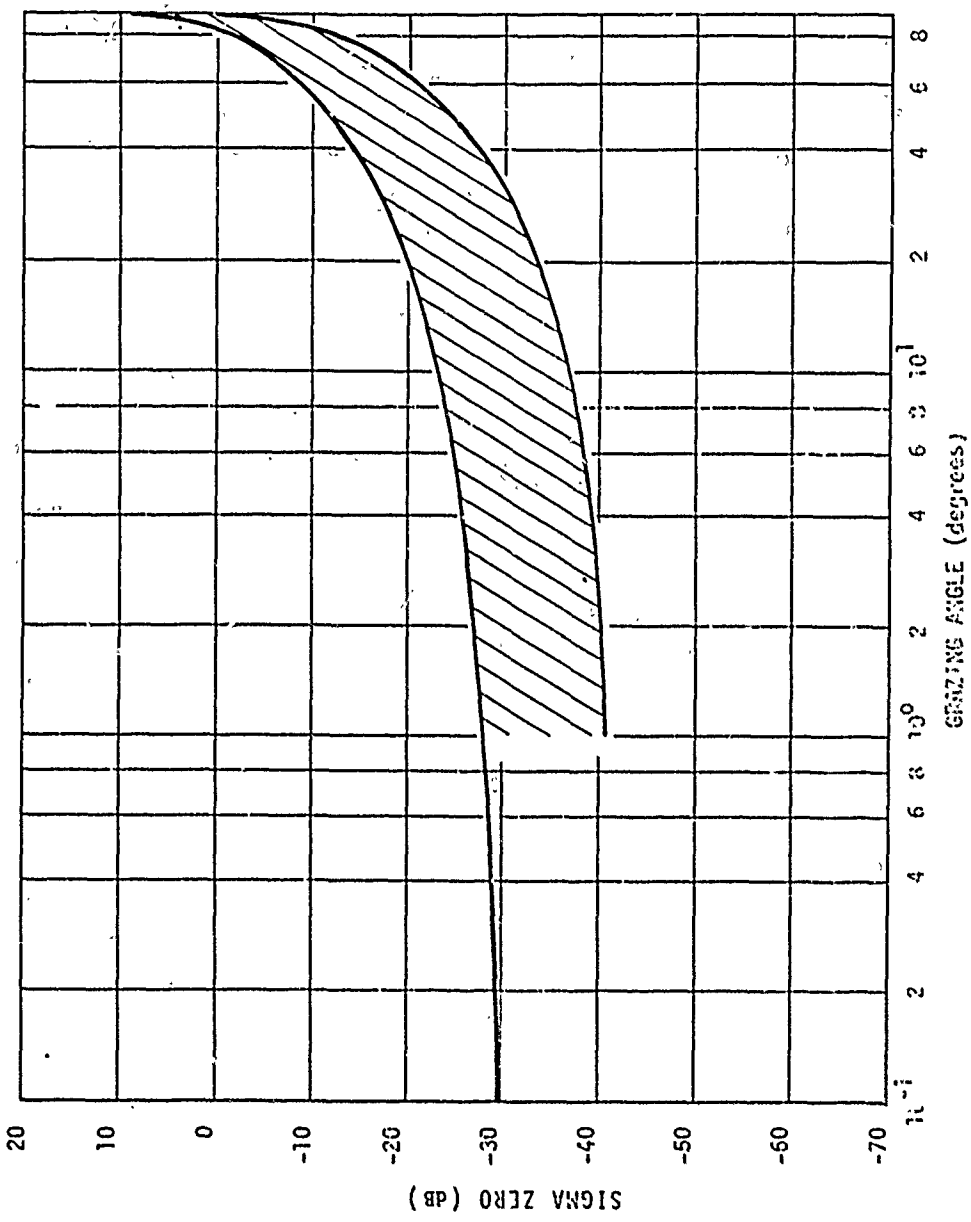

Figure 3-35
Composite Plot of Radar Scattering Coefficient of Artic Terrain [3-33]

3.3 References, Chapter 3

3-1 V. W. Pidgeon, "Time Frequency and Spatial Correlation of Radar Sea Return," American Astronautical Society, Use of Space Systems for Planetary Geology and Geophysics, 1967.

3-2 V. W. Pidgeon, "Doppler Dependence of Radar Sea Return," J. of Geophysical Research, 15 February 1968.

3-3 F. E. Nathanson, Radar Design Principles. McGraw-Hill Book Co., 1969.

3-4 D. E. Kerr, Propagation of Short Radio Waves, McGraw-Hill Book Co., 1951.

3-5 Blair Kinsman, Wind Waves, Prentice-Hall, Incorporated, 1965.

3-6 W. J. Pierson, G. Neuman and R. W. James, Practical Methods for Observing and Forecasting Ocean Waves by Means of Wave Spectra and Statistics, U.S. Hydrographic Office, 1960.

3-7 W. Bascom, Waves and Beaches, Doubleday and Co., Incorporated, 1964.

3-8 O. M. Phillips, Dynamics of the Upper Ocean, Cambridge University Press, 1966.

3-9 L. J. Cote, et al., "The Directional Spectrum of a Wind Generated Sea as Determined from Data Obtained by the Stereo Wave Observation Project." Meterological Papers 2, New York University, June 1960.

3-10 V. W. Pidgeon, JHU Applied Physics Laboratory; see Section 7.7 of reference 3-3.

3-11 G. Bishop, "Amplitude Distribution Characteristics of X-Band Radar Sea Clutter and Small Surface Targets," R.R.E. Memorandum No. 2348.

3-12 W. Rivers, S. P. Zehner and F. B. Dyer, "Modeling for Radar Detection," (U) Final Report on Contract N00024-69-C-5430, Georgia Institute of Technology, December 1969, AD 507 375L.

3-13 G. F. Myers and I. W. Fuller, Jr., "Nanosecond Radar Observations of Sea Clutter Cross-Section vs. Grazing Angle," NRL Report 6933, October 1969.

3-14 W. Rivers, "Low-Angle Radar Sea Return at 3 mm Wavelength," Final Report on Contract N62269-70-C-0489, Georgia Institute of Technology, November 1970.

3-15 F. B. Dyer, et al., "A Frequency-Agile Radar and Observations on Sea Return and Complex Targets," (U) 14th Tri-Service Radar Symposium Record, June 1968, AD-394-083L.

3-16 D. C. Schleher, "Radar Detection in Log-Normal Clutter," IEEE International Radar Conference Record, IEEE Publication 75 CHO 938-1 AES, April 1975.

3-17 V. W. Pidgeon, "Doppler Dependence of Radar Sea Return," J. of Geophysical Research, 15 February 1968.

3-18 R. L. Mitchell, "Radar Cross-Section Statistics of Randomly Oriented Disks and Rods," Transactions of the IEEE, AP-17, May 1969.

3-19 G. E. Pollon, "Course Lecture Notes, Topics in Radar Clutter Modeling," Technology Service Corporation, Santa Monica, CA, March 1973.

3-20 H. M. Finn, "Aperture Detection with Regulated Error Probabilities," RCA Review, 29, December 1967.

3-21 H. M. Finn and R. S. Johnson, "Adaptive Detection Mode with Threshold Control as a Function of Spatially Sampled Clutter-Level Estimates," RCA Review, 29, September 1968.

3-22 L. J. Greenstein, R. F. Pipkin and L. C. Calhoun, "ORT Clutter Model - March 1968," Technical Report on Contract F33615-67-C-1387, ITT Research Institute, March 1968.

3-23 L. J. Greenstein, A. E. Brindley and R. D. Carlson, "A Comprehensive Ground Clutter Model for Airborne Radars," Final Report on Contract F33615-69-C-1387, ITT Research Institute, September 1969.

3-24 S Kazel, et al., "Extensions to the ORT Clutter Model," Technical Report on Contract F33615-69-C-1387, ITT Research Institute, June 1971.

3-25 V. W. Pidgeon, "Radar Land Clutter for Small Grazing Angles at X- and L-Band," Use of Space Systems for Planetary Geology and Geophysics, The American Ascronautical Society, May 1967.

3-26 "Bistatic Clutter Experiment Report," Raytheon Co. Missile Systems Division, Report BR-6629, October 1971.

3-27 H. J. Evenson, et al., "An Experimental Investigation of Radar Ground Clutter," Boeing Aircraft Corporation, Report AD-11738, 15 January 1952.

3-28 R. R. Boothe, "The Weibull Distribution Applied to the Ground Clutter Backscatter Coefficient," U.S. Army Missile Command Report No. RE-TR-69-15, June 1969.

3-29 Unpublished Data, Raytheon Co., Missile Systems Division, Bedford, Massachusetts.

3-30 W. J. McEvoy, "Discrete Clutter Measurements Program: Operations in Western Massachusetts," Technical Report on Contract F19(628)-71-C-0002, The Mitre Corporation, March 1972, AD 742 297.

3-31 W. Fishbein, S. W. Graveline and O. E. Rittenbach, "Clutter Attenuation Analysis," U.S. Army Electronics Command Technical Report ECOM-2808, March 1967.

3-32 V. A. Kapitanov, Yu V. Melanichuk and A. A. Chernikov, "Spectra of Radar Signals Reflected from Forests at Centimeter Waves," Radio Engineering and Electronic Physics, 18, September 1973.

3-33 P. Hoekstra, "The Dielectric Properties and Reflection Coefficients of Ice and Snow at UHF and Microwave Frequencies," U.S. Army Cold Regions Research and Engineering Laboratory, Memorandum Report, August 1970.

4.0 PROPAGATION FACTORS

4.1 Sea-Reflection Multipath Effects

4.1.1 Pattern-Propagation Factor

The multipath effect is accounted for by a factor F such that the radar detection range R is related to the free-space range R_o by:

$$R = R_o F / L^{1/4} \tag{4-1}$$

The factor L is the atmospheric absorption loss factor, such that if the total absorption in decibels for the two-way path is L_{dB}, then

$$L = 10^{0.1 L_{dB}} \tag{4-2}$$

(Note: L_{dB} is here assumed positive, so that $L > 1$.) A suitable model for absorption loss in the normal atmosphere is given by curves in references [4-1] and [4-2]. Then the only non-free-space effect to be accounted for by F is the multipath effect, which can produce either a gain or a loss.

The following material outlines the treatment of the subject in reference [4-3]. For modeling purposes, reference should be made to the report and to reference [4-4].

A general expression for F is:

$$F = f(\theta_1) \left| \sqrt{1 + \chi^2 + 2\chi \cos \alpha} \right| \tag{4-3}$$

$$\chi = \frac{\rho_o \rho_s D f(\theta_2)}{f(\theta_1)} \tag{4-4}$$

$$\alpha = \frac{2\pi\delta}{\lambda} + \phi \tag{4-5}$$

where the quantities are defined as follows:

θ_1 -- elevation angle (at antenna) of the ray that goes direct from antenna to target,

θ_2 -- elevation angle at the antenna of the reflected ray,

(Definitions continued):

δ -- path length difference of the direct and reflected rays.

λ -- radar wavelength (in same units as δ).

ϕ -- phase angle of the reflection coefficient, i.e., the phase change of the wave that occurs in the reflection process.

α -- total phase difference of the direct and reflected rays at the radar target.

(Note 4: The path difference and phase difference are here defined on the basis of one-way propagation, i.e., antenna to target. The pattern propagation factor as thus calculated is assumed to be the same for the return path, target to antenna. If the transmitting antenna and receiving antenna are separate, the pattern factors will be different and two separate pattern propagation factors must then be calculated, F_t for the transmit path and F_r for the receive path, and then eq. (4-1) becomes:

$$R = R_o \sqrt{F_t F_r} \tag{4-7}$$

4.1.2 Pattern-Factor Calculation

If the actual antenna pattern is known in either tabular or functional form, $f(\theta_1)$ and $f(\theta_2)$ are obtainable directly. More commonly, the beamwidth and the tilt angle of the beam above the horizontal are known and it can be assumed (as a reasonable approximation) that the beam shape is

$$f(\theta) = (\sin u)/u \tag{4-8}$$

where

$$u = k \sin (\theta - \theta_t) \text{ radians}$$

and

$$k = 1.39.57/\sin (\theta_b/2)$$

where θ_b is the half-power beamwidth, θ is the elevation angle, and θ_t is the tilt angle.

If the beam is, in addition, "cosecanted" above the upper half-power-beamwidth point, eq. (8) is used below that point, and above that point the following formula is used:

$$f(\theta) = (.7071) \sin (\theta_b/2 + \theta_t)/\sin \theta \qquad (4\text{-}9)$$

(Note 5: In the "main beam:, $f(\theta)$ is a positive number, but in "sidelobes" it may be positive or negative, according to equation (4-8). This behavior represents the reversal of the phase angle of the radiation in alternate sidelobes.)

4.1.3 Intrinsic Reflection Coefficient and Phase Angle

The magnitude ρ_o and phase angle ϕ of the reflection coefficient are obtained from the complex reflection coefficient Γ given by

$$\Gamma = \rho_o e^{-j\phi} = \frac{a \sin\psi - \sqrt{\varepsilon_c - \cos^2 \psi}}{a \sin\psi + \sqrt{\varepsilon_c - \cos^2 \psi}} \qquad (4\text{-}10)$$

where ψ is the grazing angle of the ray, ε_c is the complex dielectric constant of the reflecting surface, and $a = \varepsilon_c$ for vertical polarization and $a = 1$ for horizontal polarization. The complex dielectric constant for sea water is:

$$\varepsilon_c = \varepsilon_1 - j60\,\lambda\sigma \qquad (4\text{-}11)$$

where ε_1 is the ordinary dielectric constant, λ is the wavelength in meters and σ is the total conductivity in mhos/meter. Let $\varepsilon_2 = 60\,\lambda\sigma$. Saxton and Lane [4-7] give frequency-dependent representations of ε_1 and ε_2 as follows, in terms of parameters which are only temperature and salinity dependent:

$$\varepsilon_1 = \frac{\varepsilon_s - \varepsilon_p}{1+x^2} + \varepsilon_p \qquad (4\text{-}12)$$

$$\varepsilon_2 = (\varepsilon_1 - \varepsilon_p)\, x + \frac{2\sigma_i}{f} \qquad (4\text{-}13)$$

where $x = 2\pi f\tau$
f = wave frequency (here units of Hertz are appropriate),
τ = a relaxation time,
ε_s = static (low-frequency) dielectric constant,
ε_p = dielectric constant due to electronic and nuclear polarization, and
σ_i = ionic conductivity

The value for ε_p suggested is 4.9. Values for the parameters ε_s, τ and σ_i are given in table 4-1 as functions of temperature. These values

Table 4-1

Dielectric Parameters of NaCl-Water Solutions
Concentration of 35 g/l [4-7]

TEMPERATURE (deg C)	ε_s	$\tau(10^{-12}$ sec)	$\sigma_i(10^{10}$ esu)
0	75.1	17.0	2.6
10	72.2	12.1	3.6
20	69.1	9.2	4.7
30	66.3	7.2	5.5
40	63.3	5.7	6.6

apply to salt water with a nominal concentration of 35 g/l salt solution (0.6 N for sodium-chloride equivalent).

4.1.4 Grazing Angle of Reflection

Subject to the conditions $h \ll a_e$, $R \ll a_e$, ψ small, where ψ is the grazing angle of incidence at the sea reflection point, the following algorithm applies [4-4]:

$$d \cong R \cos\theta_1 \cong R \tag{4-14}$$

$$p = \frac{2}{\sqrt{3}} \left[a_e (h + h_t) + \left(\frac{d^2}{2}\right)\right]^{1/2} \tag{4-15}$$

$$\phi = \sin^{-1} \left[\frac{2a_e d (h_t - h)}{p^3}\right] \tag{4-16}$$

$$d_1 \cong \frac{d}{2} - p \sin\frac{\phi}{3} \tag{4-17}$$

$$\psi = \tan^{-1} \left[\frac{h}{d_1} - \frac{d_1}{2a_e}\right] \tag{4-18}$$

4.1.5 Roughness Factor

The following formula is a good approximation:

$$\rho_s = \exp\left[-2\left(\frac{2\pi H \sin\psi}{\lambda}\right)^2\right] \tag{4-19}$$

where H is the standard deviation of the surface roughness, ψ is (as in Section 4.1.4) the grazing angle of the ray, and λ is the wavelength. If H' is the "significant" crest-to-trough height (average of highest 1/3) of sea waves,

$$H = 0.25\, H' \tag{4-20}$$

(Note 6: Eq. (19) assumes that the surface height variation is Gaussianly random rather than sinusoidal, and the actual sea is neither one; but the combination of eqs. (19) and (20) is a reasonable model.)

(Note 7: Experimental work by Beard and Katz has indicated that eq. (19) gives values of ρ_s that are too small at the large values of $H(\sin\psi/\lambda$ [4-5], but for present purposes eq. (19) is reasonable.)

4.1.6 Divergence Factor

The divergence factor is given by [4-4]:

$$D = \left(1 + \frac{2d_1\ (d-d_1)}{a_e d \sin \psi}\right)^{-1/2} \qquad (4\text{-}21)$$

4.1.7 Path Difference

The one-way path difference between direct and reflected rays between radar and target is

$$\delta = \frac{2h\ h_t}{d}\ \left(1 - \frac{d_1^2}{2a_e h}\right)\left(1 - \frac{(d-d_1)^2}{2a_e\ h_t}\right) \qquad (4\text{-}22)$$

4.1.8 Diffuse Reflection

Propagation paths exist via reflection from the rough sea surface over a substantial area, because of the random local tilt of the surface. The phases of wave components via the various incremental paths are random, so that the component is characterized as diffuse. As the surface roughness increases, the total effective reflection coefficient increases and saturates for projected roughness in wavelengths ($H \sin \psi/\lambda$) greater than about 0.1 (see figure 4-1). At its highest average level the total diffuse power is about 13 dB below that over a smooth-sea transmission path of the same distance.

The size of the region on the rough surface which contributes to the diffuse component is much greater than the coherent Fresnel spot. A part of the diffuse energy is reflected from very near the Fresnel spot and the rest from a very much larger region. Figure 4-2 shows contours of constant diffuse signal intensity for a path with terminal heights of 38 feet and length 5425 feet derived from the data of reference [4-5]. Normalization is to the peak level coming from the specular spot, and the data were acquired with a 0.3° beamwidth antenna at x-band. Note the difference in axis scales. Interpretation of these data in terms of reflection from sloped sea surface parcels is consistent with the slope distribution under the conditions the data were acquired (standard deviation of slope about 4.5°). Thus, the fall-off transverse to the beam direction will be very rapid and a diffuse region only a few tens of feet wide can be expected (standard deviation of wave slopes $\approx \tan^{-1}$ {lateral displacement standard deviation/antenna heights}); however, in the longitudinal direction, diffuse reflection will be seen over an angular region at the antenna

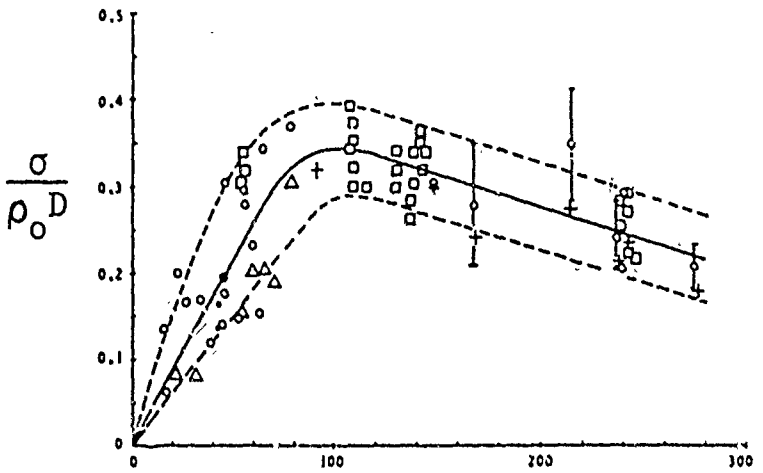

Figure 4-1

Diffusely Scattered Field Magnitude vs Projected Surface Roughness
Incoherent Power = $2\sigma^2$; Direct-Path Power D^2;
ρ_o = Fresnel Reflection Coefficient of Water [4-5]

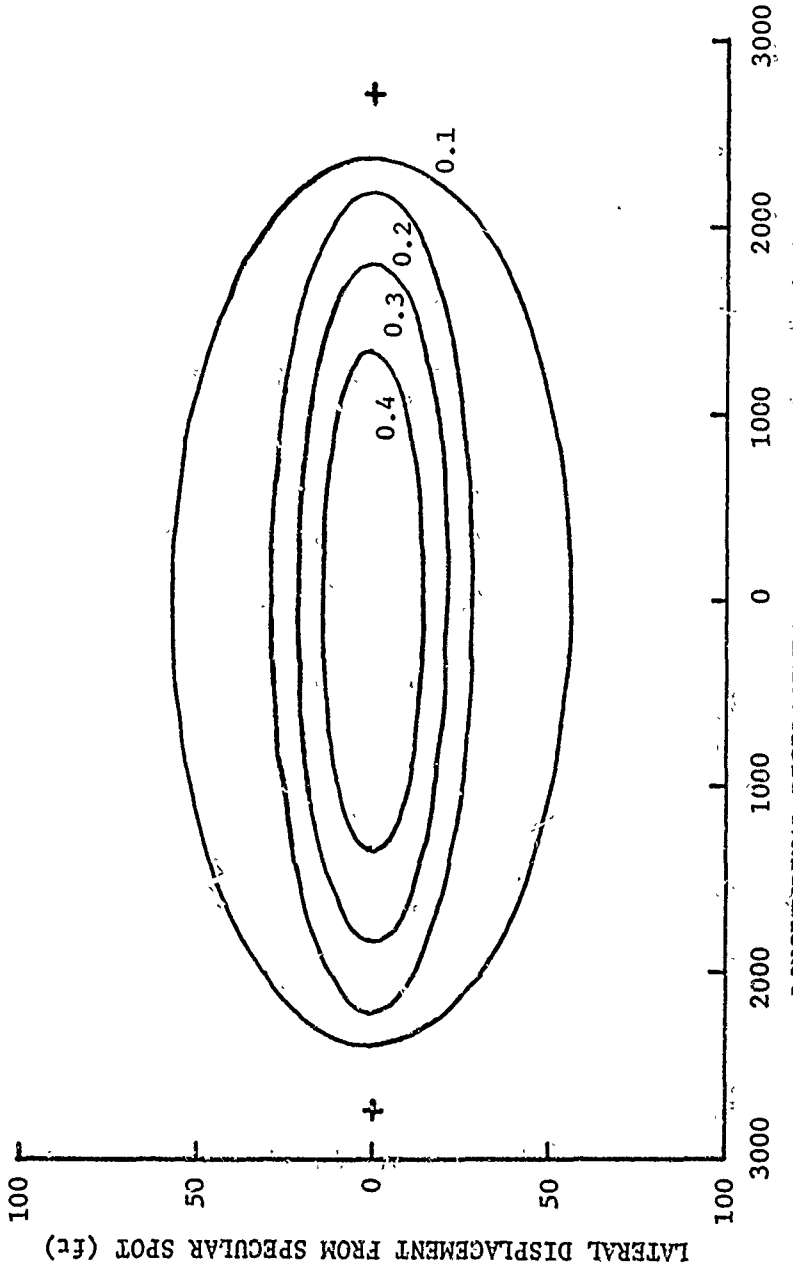

Figure 4-2
Contours of Constant Diffuse Signal [4-5]

of the order of the wave slope distribution. Figures 4-3a and 4-3b illustrate the geometries in the lateral and longitudinal directions, respectively.

4.2 Atmospheric Absorption

Atmospheric absorption refers to the component of propagation loss caused by molecular absorption, primarily atmospheric oxygen and water vapor, under clear air conditions. The absorption rate is a function of radar frequency and of altitude, which includes effects of atmospheric constituent densities, temperature and pressure. Loss in the atmosphere produces two radar system effects: target signals are attenuated, and the apparent temperature of the sky background against which air targets are viewed is increased at near-grazing angles of incidence. Figure 4-4 displays the apparent sky temperature as a function of frequency and for selected viewing angles. These calculations [4-1] are based on Van Vleck's molecular absorption theory applied to the ICAO dry atmosphere with added water vapor. The combined absorption loss rate due to oxygen and water vapor as a function of altitude and for selected frequencies is shown in figure 4-5 for this model. The surface values of the atmosphere model assume temperature of 15°C, total pressure of 1023 mb and absolute water vapor density of 7.5 g/m^3. This condition corresponds to relative humidity of 60% at low altitudes and a partial pressure of water vapor at the surface of 10 mb. The height model for water vapor was patterned after Sissenwine's data [4-27].

When radar and target are at different altitudes, variation of attenuation rate along the path must be considered. Reference [4-1] plots attenuation between radar and target as functions of range at selected frequencies and elevation angles. (The applicable target altitudes at positions along those curves must be inferred from the range and angle.) Reference [4-1] also provides the equations, algorithms, constants, and a computer program for calculating attenuation for arbitrary target elevation angles and ranges below the ionosphere, and for other humidity conditions.

4.3 Lens-Effect Loss

This term refers to weakening of the radar transmitted wave due to the "defocusing" effect of atmospheric refraction, as described by T. A. Weil [4-6]. Weil has made calculations of this loss for the normal atmosphere.

The lens-effect loss and the absorption loss are directly additive, in decibels, or as power-loss factors they are multiplicative.

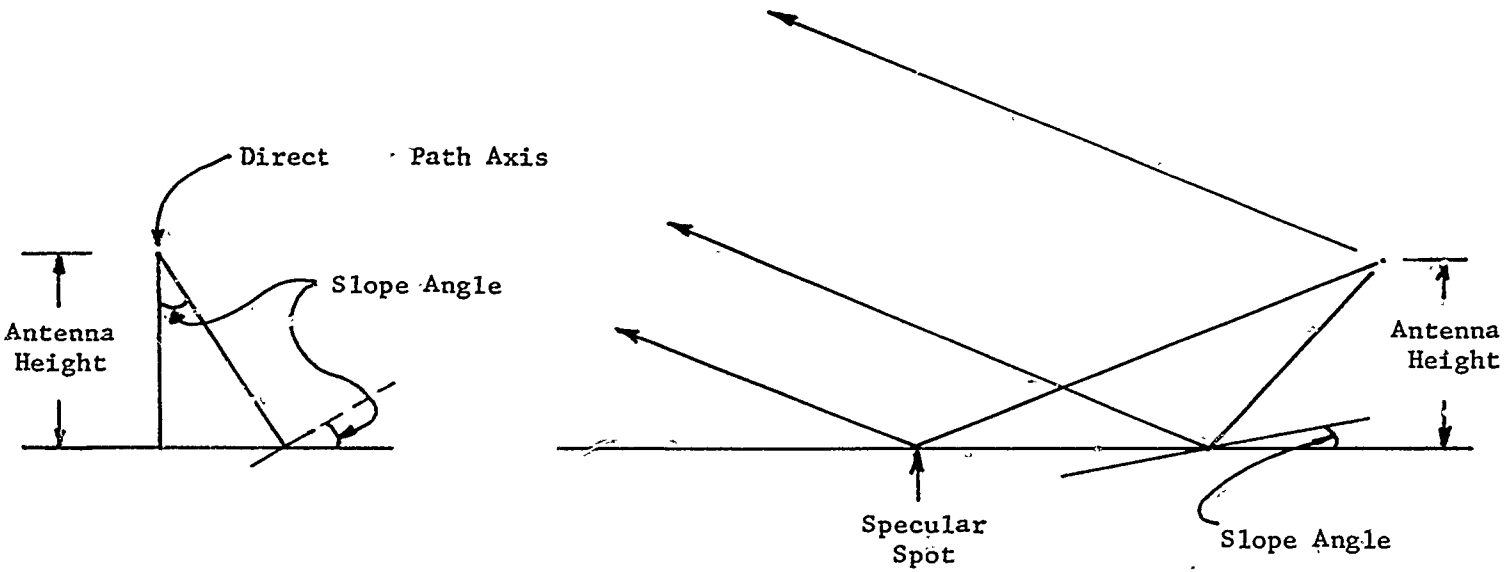

(a) Lateral Displacement of a Diffuse Scattering Spot; Along-Path View

(b) Longitudinal Displacement of Diffuse Scattering Spot; Cross-Path View

Figure 4-3

Geometry for Diffuse Scattering

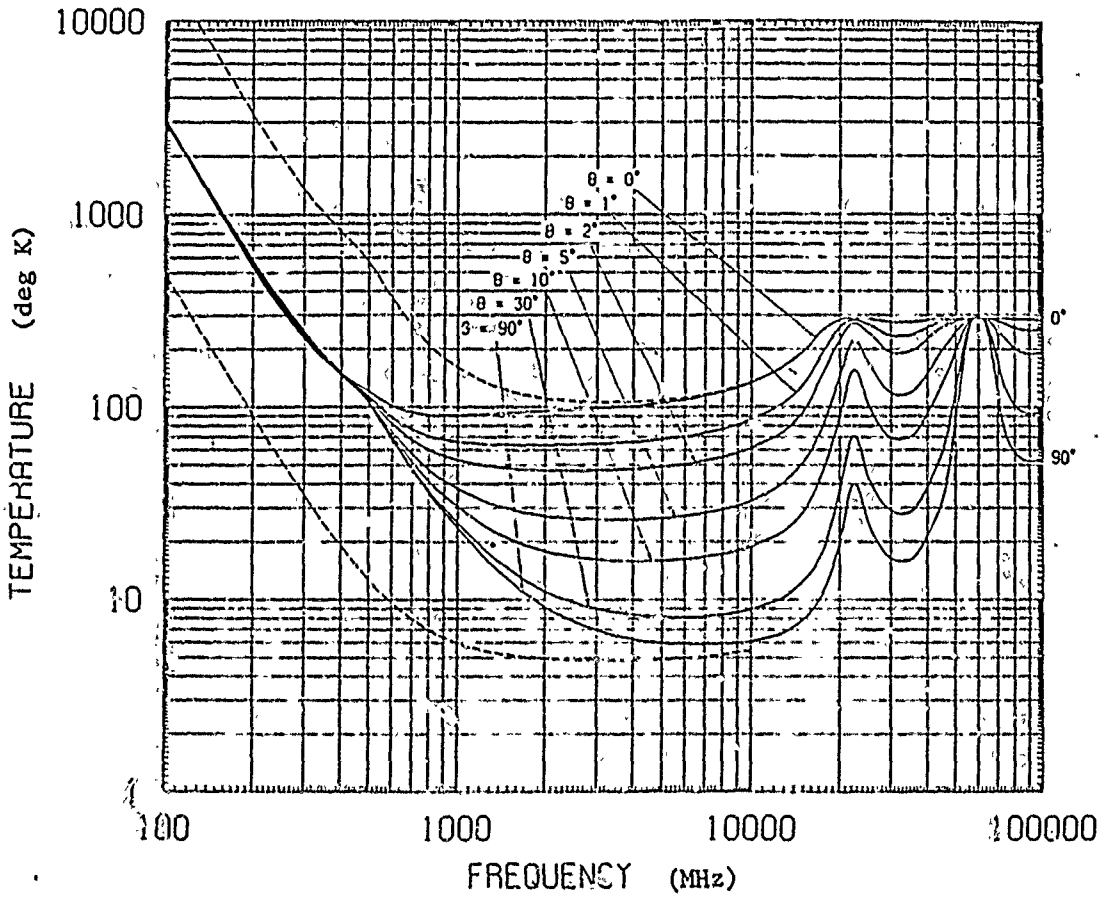

Figure 4-4

Apparent Sky Temperature as Functions of Frequency at Selected Elevation Angles

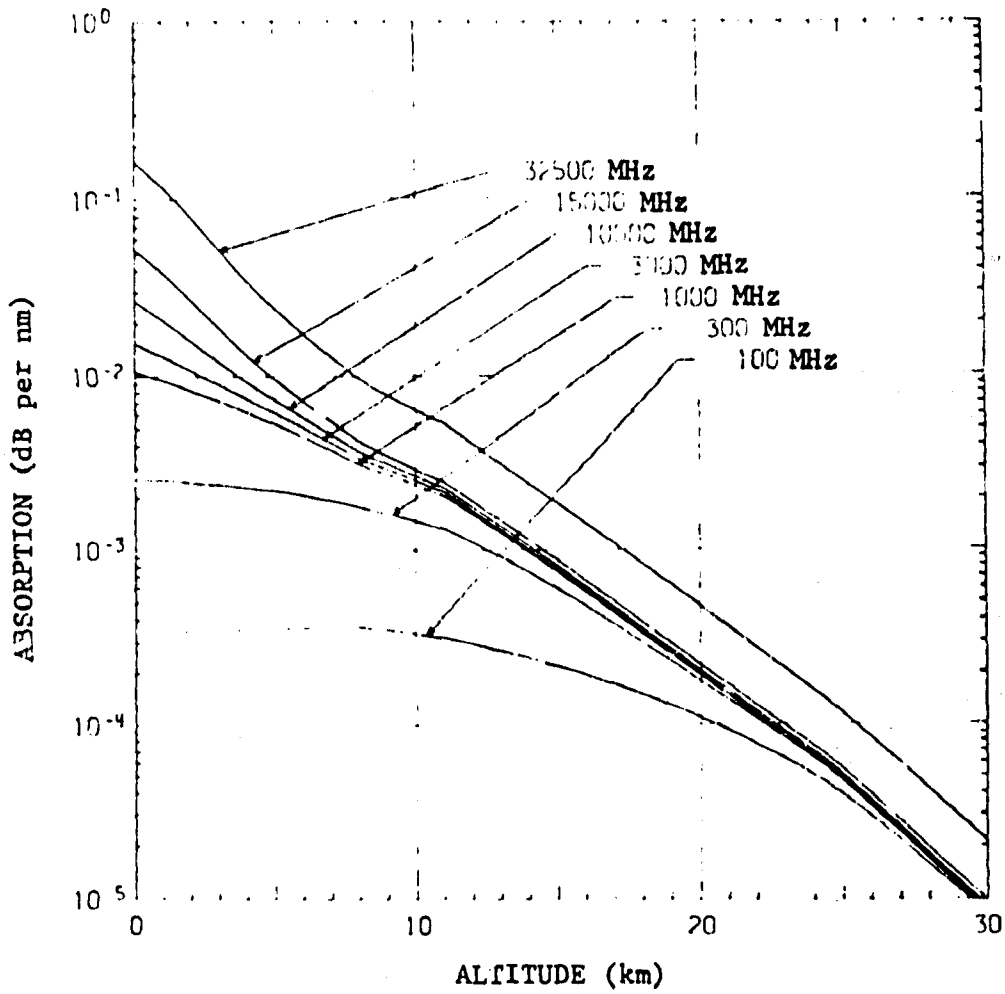

(Oxygen Plus Water Vapor)

Figure 4-5

Absorption Rate in Standard Atmosphere as Functions of Altitude for Selected Frequencies (One-Way) [4-1]

Thus, if the absorptions power-loss factor is L_a and the lens-effect loss is L_ℓ, then the total loss factor L in equation 1 is:

$$L = L_a L_\ell$$

4.4 Attenuation in Rain

Microwave propagation path loss expressed as a ratio $L(\Delta Z)$ of the power density at $Z + \Delta Z$ to that at Z produced by attenuation by rain (and excluding any other loss or spreading effects) is given by

$$L(\Delta Z) = e^{-A^*\Delta Z} \qquad (4\text{-}23)$$

in which A* is the rain attenuation rate in nepers per unit distance. More commonly, the rate is expressed in dB, and distance units of miles or nm or km are used. Let the symbol A denote hereafter a loss rate in units of dB/km one-way.

Microwave attenuation rate in rain is a function of frequency, rain rate, polarization and temperature (at least), in decreasing order of dependence. The wavelength dependence is a result primarily of the coupling to drops which are small compared to a wavelength. The rain rate associates not only with the number of drops per unit volume but also with the size and distribution of sizes. The drops in their fall through the air are distorted from spherical shape (are oblate with the short axis vertical), so that coupling to horizontally polarized electric fields is stronger than to vertical components. Temperature dependence arises because of its effect on the dielectric properties of water.

Modelers of rain attenuation universally use the relation

$$A = \alpha\, r^{\beta}, \qquad (4\text{-}24)$$

in which A is the attenuation rate, one-way, in dB/km, and r is the nominal rainfall rate, in mm/hr, to represent the results of both computations and measurements. The parameter β is generally treated as a weak function of frequency, and sometimes of temperature and polarization as well. The coefficient α is a strong function of frequency, but its dependences on temperature and polarization are also weak.

Recently Crane [4-8] and Lin [4-9] provided recommended values of α and β at selected wave frequencies, and Lin also included polarization effects. Earlier estimates by Gunn and East [4-10] and Medhurst [4-11] were at different frequencies. All of these reports based their estimates on computations of attenuation rates using a scattering theory [e.g., 4-10, 11 & 12] and measured drop-size distributions observed to occur at various rain rates. This method has been carefully validated

[4-13] in a controlled experiment which found good agreement between measured attenuation and the attenuation calculated using the theory and the measured drop-size distributions under the same conditions. Close agreement is obtainable only under controlled uniform rain conditions and is not generally seen for natural rain. The values of α and β given by the above references are listed in table 4-2 and plotted in figures 4-6, 4-7 and 4-8.

Root [4-14] has modeled attenuation caused by atmospheric water over the frequency range of 1 to 300 GHz. His formulas for α and β fit to the results of his scattering theory as functions of wavelength in cm are:

$$\alpha = \frac{0.024}{(2-\lambda)^2 + 16} + 0.25\,\lambda^{-2\lambda^{0.4}} \qquad (4\text{-}25)$$

$$\beta = 0.5 + \frac{0.12}{(\lambda - 1)^2 + 0.4} + \frac{3}{(\lambda - 3.9)^2 + 12} + \frac{0.046}{(0.24 - \frac{1}{\lambda})^2 + 0.08} \qquad (4\text{-}26)$$

To this droplet absorption Root recommends adding an attenuation component to account for the high humidity that can occur during rain, as high as 300% at the surface and dropping to 100% at 3 km altitude and above. Values of α and β for these formulas without the additional humidity effect are plotted in figures 4-6, 4-7 and 4-8.

A model resulting from CCIR activity representing values of α and β as functions of wave frequency [e.g., 4-16] is:

$$\alpha = [3\,(f - 2)^2 - 2\,(f - 2)] \times 10^{-4} \qquad (4\text{-}27)$$

$$\beta = [1.14 - 0.07\,(f - 2)^{1/3}][1 + 0.085\,(f - 3.5)\exp(-0.006f^2)] \qquad (4\text{-}28)$$

where f is the wave frequency in GHz. These formulas reportedly resulted from a fit to a measurement by Hathaway and Evans [4-16] at 11 GHz and to the older computations of Ryde and Ryde [4-17]. The latter were redone by Gunn and East [4-10] using refined values for the permittivity of water. The CCIR model is also plotted in figures 4-4 through 4-6. Note that it appears to have poor asymptotic behavior at both low and high frequencies.

Table 4-2

Rain Attenuation Model Parameters, A Summary

A = Attenuation rate, one-way, in dB/km

r = Rain rate, in mm/hr

$A = \alpha r^{\beta}$ is the model.

Source	Crane [4-8]		Lin [4-9]		Medhurst [4-11]		Gunn & East [4-10]	
Drop Distribution	Mueller & Sims		Composite		Laws & Parsons		Laws & Parsons	
Frequency (GHz)	α	β	α	β	α	β	α	β
2.0					.00013	.906		
2.8	.000459	.954						
3.0					.000282	.974	.00030	1.00
5.5					.00124	1.150	.0022	1.17
7.5	.00459	1.06			.00323	1.294		
9.4	.0087	1.19					.0074	1.31
10					.00865	1.216		
11.4			.013V .015H	1.22V 1.23H				
15					.0322	1.224		
16	.0374	1.10					.045	1.14
18			.030V .054H	1.11V 1.14H				
20					.0683	1.128		
24							.12	1.05
30			.15V .17H	1.04V 1.04H	.166	1.063		
33							.22	1.00
35	.225	1.05						
60					.63	.854		
67	.729	.893						
100					1.094	.739		

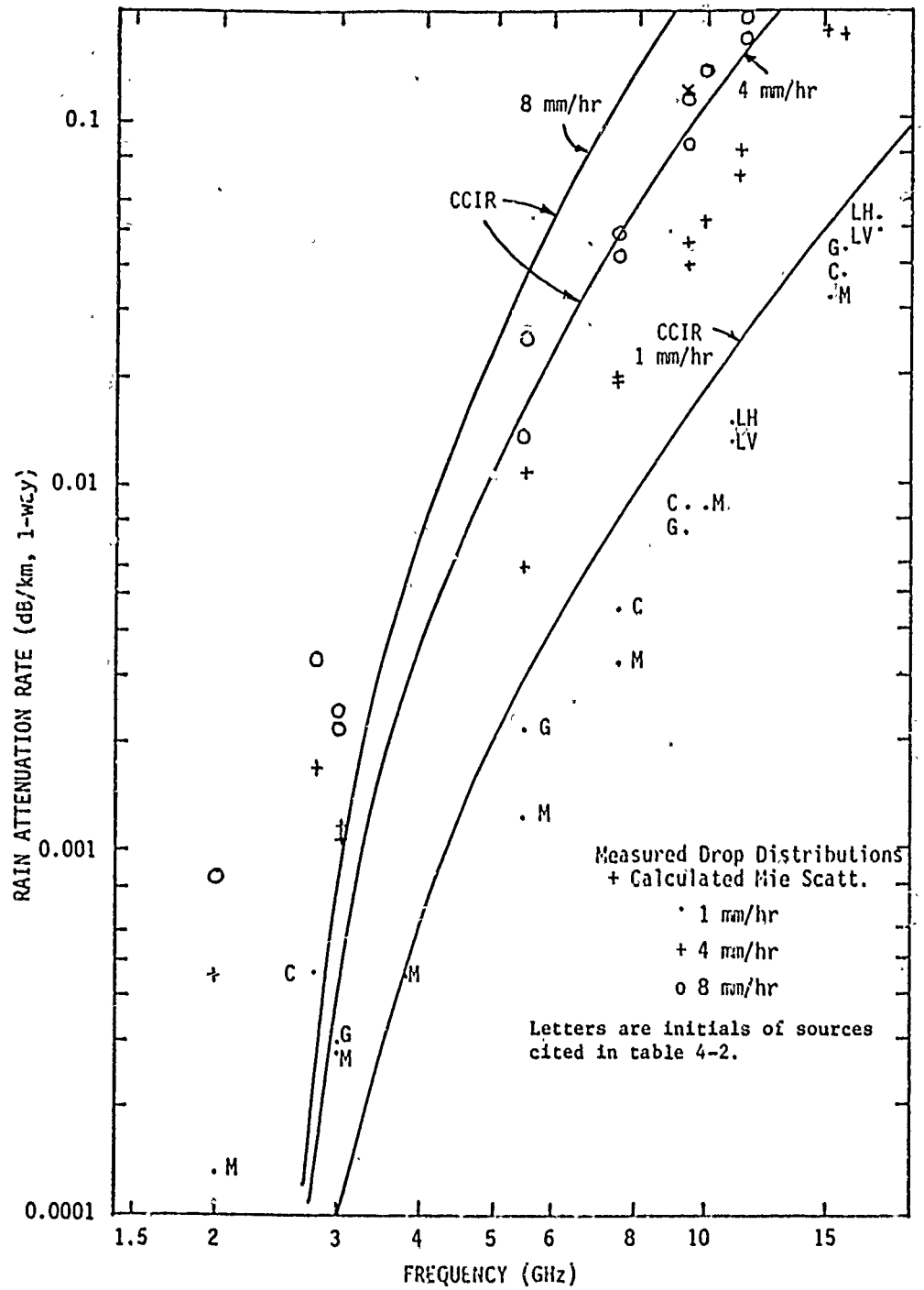

Figure 4-6

Rain Attenuation Rate Model Parameters

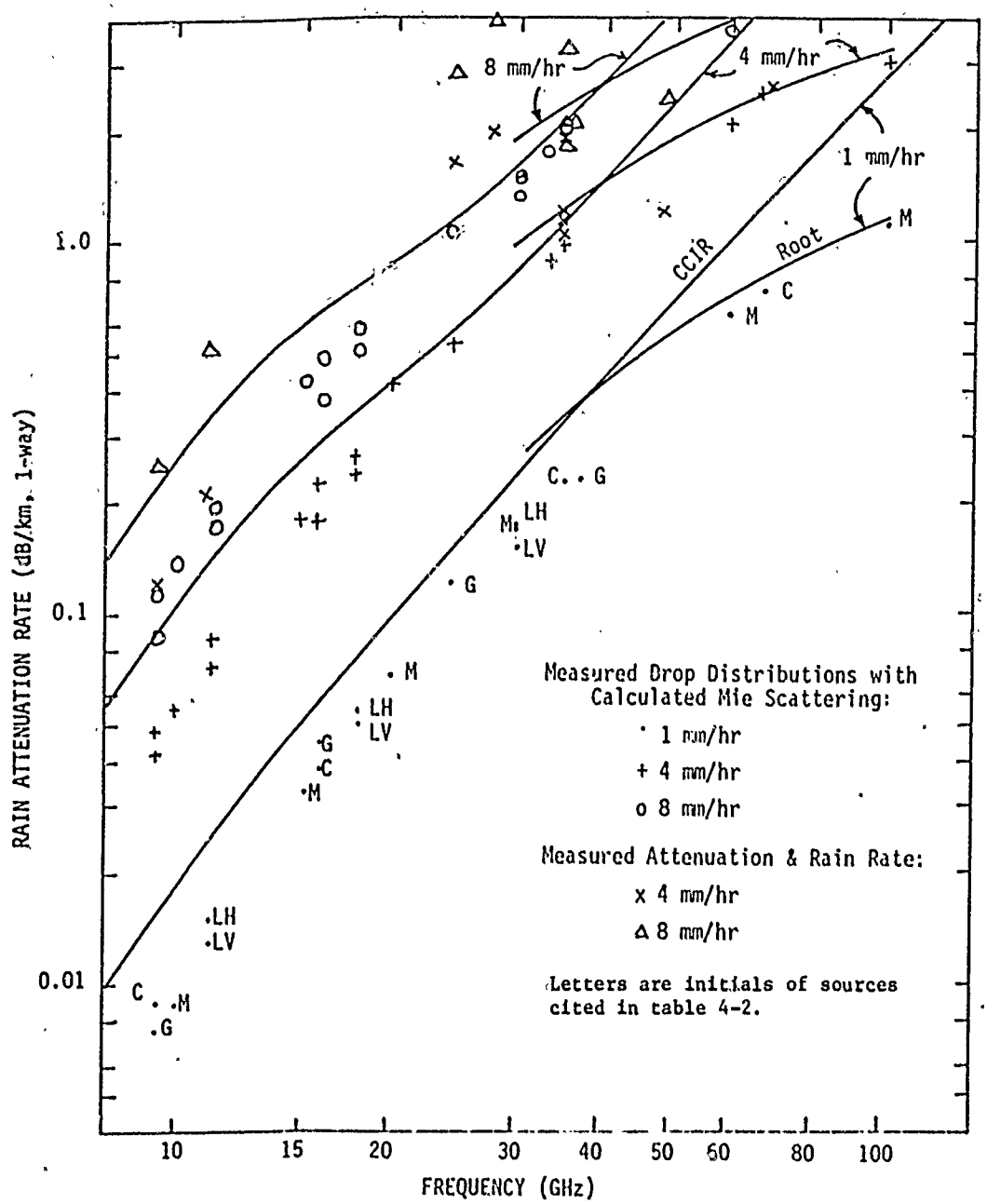

Figure 4-7

Rain Attenuation Rate Model Parameters

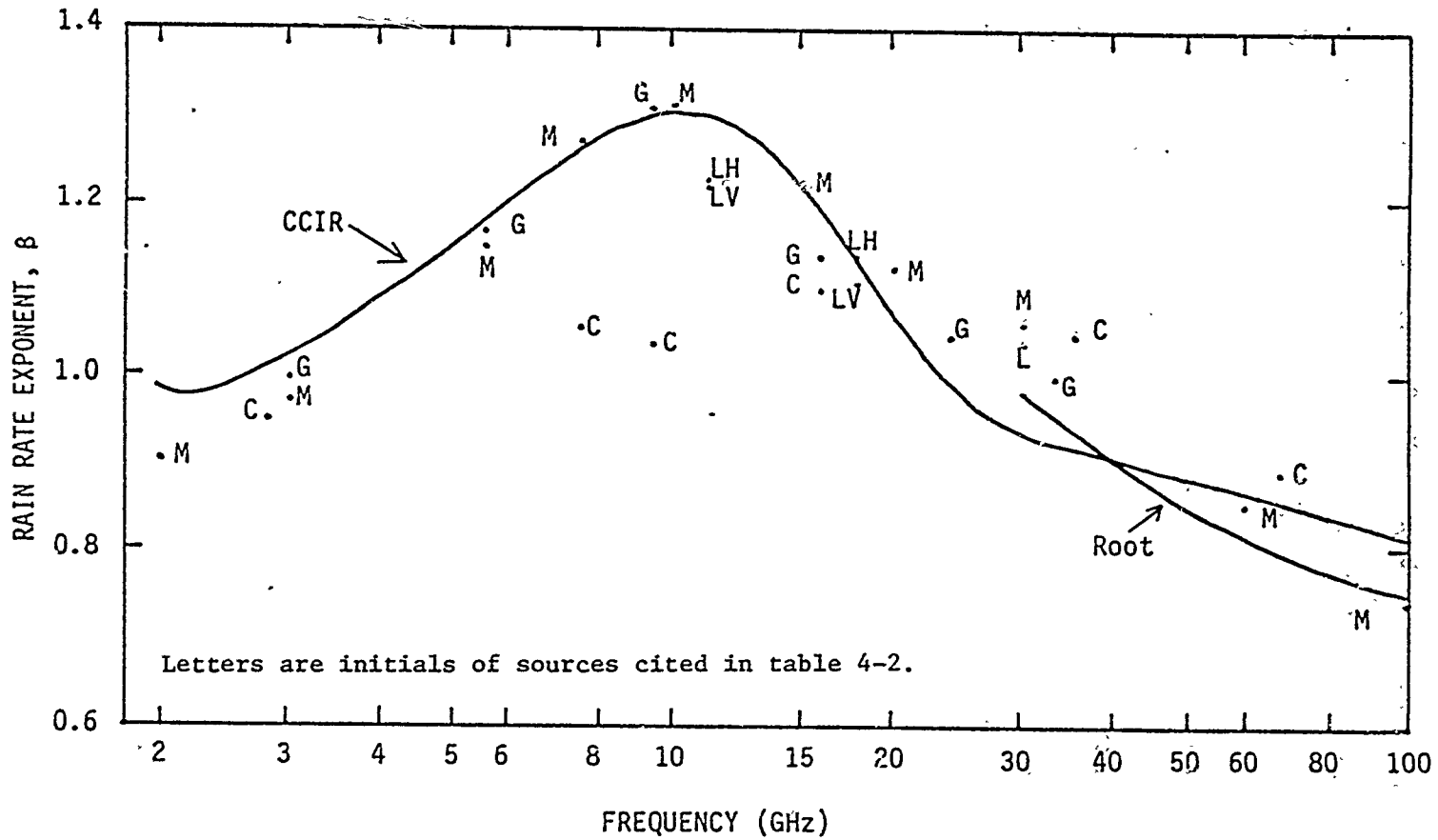

Figure 4-8

Rain Attenuation Rate Model - Parameter β

The disagreement referred to above between attenuation measurements and computed values using scattering theory plus measured drop-size distributions was examined thoroughly by Medhurst [4-11]. He explored the effect of extreme forms of drop-size distributions (for the same nominal rain rate) on the computed attenuation rates and compared the results with measurements of attenuation. He concluded that attenuation rates had been reported which were higher than theory predicts is possible, under the assumption of uniform rain at the nominal rate and free of any constraint on drop-size distribution. Crane's general assessment [4-18] of the disagreement attributes it largely to a combination of inadequate sampling of rain rate over propagation paths and a restrictive interpretation of the rain-rate measurements that are made. His controlled experiment [4-13] demonstrates that measurements can be made with adequate care to assure agreement. Root's contention that the air is super-saturated during rain could explain additional error in the predictions on the low side.

The measurements displayed by Medhurst [4-11] have been replotted to allow extraction of values of α and β, and these parameter values are listed in table 4-3. Also included there are values from newer experiments. Attenuation rate values from each of these measured data sets are plotted in figure 4-7 for nominal rain rates of 4 and 8 mm/hr. It is seen that mostly they lie well above the values computed under assumed uniform rain using the scattering theory.

Even with understanding of the factors contributing to the difference between measurement and computations for the same nominal conditions, a dilemma still exists, represented by these two extreme alternatives. Should one:

(a) Attribute the difference to non-uniform rain under conditions of measurement such that the effective rain rate is higher than the nominal value assigned based on use of only a few rain gauges, and use model parameters based on the validated theory; or

(b) Alter the model parameter values generally upward from the theory to conform with the measurements?

Neither of these is wholly satisfactory. Alternative (a) could result in confusion for systems people who specify rain rates as conditions for some levels of system performance. Alternative (b) could confuse the use of results of those specializing in the physics of attenuation of microwaves by rain.

Table 4-3

Parameters from Selected Measurements of Rain Attenuation

$A = \alpha r^{\beta}$, A in dB/km one-way

Experimeter	Frequency (GHz)	Polarization	Rate r (mm/hr)	α dB/km	β -
Robertson & King [4-19]	9.4	Hor.	3-100	0.031	1.00
Hathaway & Evans [4-16]	11.4	Unk.	1-7	0.034	1.30
Anderson Et al. [4-20]	24.	Unk.	4-80	0.54	0.81
Robertson & King [4-19]	27.5	Vert.	2-100	0.50	1.00
Funakawa & Kato [4-26]	34.9	Unk.	0.2-3	0.44	0.72
N. P. Robinson [4-21]	34.9	Cir.	1-10	0.26	1.00
S. Godard [4-22]	34.9	Hor. & Vert.	0.1-4	0.46	0.667
Emerson Electric [4-23]	35.0	Unk.	2-12	0.66	0.78
Usikov, German & Vakser [4-24]	36.8	Unk.	~70	0.26	1.00
G.E. Mueller [4-25]	48.4	Hor.	3-100	0.30	1.00

Some help in selecting a model strategy is found by considering the amount and kind of differences, as in table 4-4. The average of attenuation measurements tends to lie above the average of scattering theory results for the same nominal rain rate. Both of these major contributing factors would cause bias in that direction, the rate distribution (because of its skewness) and the molecular effects (because of the truncation of drop-size distributions, or neglect altogether of vapor). The difference is about a factor of two increase in effective rain rate over the nominal, which is equivalent to an increase in attenuation rate of 2.5 near 10 GHz but only 2 near 35 GHz.

Variability of the measured attenuations for the same reported rain rates is easily attributed to the rain rate sampling procedures, to natural drop-size distribution variation, and to differing rain dielectric constant and absolute humidity (at different temperatures). Drop-size distribution variation ought to contribute 22% variation (rms) in attenuation rate at a given rain rate [4-8] to an overall estimated 30% rms variation.

In consideration of the comments above it appears satisfactory to define a model based on a concensus of the scattering theory computations with the understanding that its use must be qualified by the bias and variability factors. Formulas which fit the trend of the points plotted in figures 4-4 through 4-6 for scattering theory computations are given in equations 4-29 and 4-30 for α and β, respectively, for use in equation 4-24.

$$\alpha = \frac{k\, f^2 (1+f^2/f_1^2)^{1/2}}{(1+f^2/f_2^2)^{1/2}(1+f^2/f_3^2)^{1/2}(1+f^2/f_4^2)^{1/2}} \qquad (4\text{-}29)$$

in which $k = 3.1 \times 10^{-5}$
f = frequency in GHz, $2 \leq f \leq 100$
$f_1 = 3$
$f_2 = 35$
$f_3 = 50$
$f_4 = 110.$

$$\beta = 1.30 + 0.0372\,(1 - (1 + x^2)^{1/2}), \qquad (4\text{-}30)$$

in which $$x = \frac{\log_{10}(f/10)}{0.06}$$

Table 4-5 lists values of attenuation rate and the exponent β computed from these formulas.

Table 4-4

Summary of Error Sources

	Bias	Variability
Sources:	o Rain Rate Sampling - resulting in a nominal rain rate lower than effective. o Molecular Effects - Presence of water vapor not accounted for in scattering calculations	o Rain Rate Sampling - o Drop Size Distribution - can be different for same nominal rain rate. o Absolute humidity - will vary with temperature at a given rain rate.
Amount:	o About a factor of 2 in effective rain rate over the nominal value.	o About ± 30% rms, with rate uncertainty dominating.

Table 4-5

Model Values of Rain Attenuation Rate (dB/km)

FREQ(GHz)	RAIN (mm/hr) 1	4	8	EXPONENT
1.99526	.000147834	.000515936	.000963844	.901608
2.51189	.000254065	.000965909	.00188335	.963344
3.16228	.000447512	.00185311	.00377094	1.02498
3.98107	.000808063	.00364366	.00773721	1.08643
5.01187	.00149179	.00732118	.0162188	1.14752
6.30957	.00280161	.0149465	.0345228	1.20774
7.94327	.0053179	.0307106	.0738006	1.2649
9.99999	.01013	.0614167	.151226	1.3
12.5893	.019215	.110964	.266658	1.2649
15.8489	.0359855	.191982	.443431	1.20774
19.9526	.0658978	.323403	.716543	1.14752
25.1188	.116733	.526363	1.11772	1.08643
31.6227	.197825	.819176	1.66696	1.02498
39.8107	.317573	1.20735	2.35413	.963345
50.1186	.479554	1.67363	3.1266	.901609
63.0956	.679084	2.1754	3.89355	.839808
79.4326	.902507	2.65357	4.55069	.777962
99.9998	1.13011	3.04964	5.00969	.716086

Equations 4-29 and 4-30

4.5 References, Chapter 4

4-1 L. V. Blake, "Radar/Radio Tropospheric Absorption and Noise Temperature," NRL Report 7461, October 1972.

4-2 M. Skolnik, Radar Handbook, McGraw-Hill Book Company, 1970.

4-3 L. V. Blake, "Machine Plotting of Radio/Radar Vertical-Plane Coverage Diagrams," NRL Report 7098, June 1970.

4-4 N. E. Durlach, "Influence of the Earth's Surface on Radar," MIT/Lincoln Laboratory, Technical Report 373, January 1965, AD 627 635.

4-5 C. I. Beard, "Coherent and Incoherent Scattering of Microwaves from the Ocean," IRE Transactions, AP-9, September, 1961.

4-6 T. A. Weil, "Atmospheric Lens Effect; Another Loss for the Radar Range Equation," IEEE Transactions, AES-9, January 1973.

4-7 J. A. Saxton and J. A. Lane, "Electrical Properties of Sea Water," Wireless Engineer, Vol. 29, p. 269-275, October 1952.

4-8 R. K. Crane, "Propagation Phenomena Affecting Satellite Communication Systems Operating in the Centimeter and Millimeter Wavelength Bands," Proc. IEEE, Vol. 59, p. 173-188, February 1971.

4-9 S. H. Lin, "A Method for Calculating Rain Attenuation Distributions on Microwave Paths," Bell Sys. Tech. J., Vol. 54, p. 1051-1086, July-August 1975.

4-10 K. L. S. Gunn and T. W. R. East, "The Microwave Properties of Precipitation Particles," Quart. J. of the Royal Met. Soc., Vol. 80, p. 522-545, October 1954.

4-11 R. G. Medhurst, "Rainfall Attenuation of Centimeter Waves: Comparison of Theory and Measurements," IEEE Trans. on Antennas and Propagation, Vol. AP-13, p. 550-564, July 1965.

4-12 J. W. Ryde, "The Attenuation and Radar Echoes Produced at Centimeter Wavelengths by Various Meteorological Phenomena," Meteorological Factors in Radio Wave Propagation, Physical Society, London (1946); p. 169-189.

4-13 R. K. Crane, "The Rain Range Experiment - Propagation Through a Simulated Rain Environment," IEEE Trans. on Antennas and Propagation, Vol. AP-22, p. 321-328, March 1974.

4-14 L. Root, U.S. Army Missile Research and Development Command, Code DRDMI-TEG, Redstone Arsenal, Huntsville, Alabama 35809.

4-15 P. L. Rice, et al., "Transmission Loss Predictions for Tropospheric Communication Circuits," NBS Technical Note 101, January 1967.

4-16 S. D. Hathaway and H. W. Evans, "Radio Attenuation at 11 kmc and Some Implications Affecting Relay System Engineering," Bell Sys. Tech. J., Vol. 38, p. 73-97, January 1959.

4-17 J. W. Ryde and D. Ryde, "Attenuation of Centimetre and Millimetre Waves by Rain, Hail, Fog and Clouds," General Electric Co., Research Lab., Wembley, Report 8670, May 1945.

4-18 R. K. Crane, "Attenuation Due to Rain - A Mini Review," IEEE Trans. on Antennas and Propagation, Vol. AP-23, p. 750-752, September 1975.

4-19 S. D. Robertson and A. P. King, "The Effect of Rain Upon the Propagation of Waves in the 1- and 3-Centimeter Regions," Proc. IRE, Vol. 34, p. 178P-180P, April 1946.

4-20 L. J. Anderson, et al., "Attenuation of 1.25 Centimeter Radiation Through Rain," Proc. IRE, Vol. 35, p. 351-354, April 1947.

4-21 N. P. Robinson, "Measurements of the Effect of Rain, Snow, and Fogs on 8.6 mm Radar Echoes," Proc. IEE, Vol. 102B, p. 709-714, September 1955.

4-22 S. Godard, "Properties of the Attenuation of Radio Waves in the 0.86 cm Band by Rain," J. de Rech. Atmospheriques, Vol. 2, p. 121-167, 1965.

4-23 Emerson Electric Co., "K_a Radar Weather Performance Data and Analysis," Report No. 1840, 9 December 1964.

4-24 O. Ya Usikov, V. L. German and I. Kh. Vasker, "Investigation of the Absorption and Scatter of Millimeter Waves in Precipitations," Ukr. Fiz. Zh., Vol. 6, p. 618-640, 1961.

4-25 G. E. Mueller, "Propagation of 6-Millimeter Waves," Proc. IRE, Vol. 34, p. 181P-183P, April 1946.

4-26 K. Kunakawa and J. Kato, "Experimental Studies of Propagation Characteristics of 8.6 mm Waves on the 24-km Path," J. Radio Research Labs. (Tokyo), Vol. 9, p. 351-367, September 1962.

4-27 N. Sissenwine, D. D. Grantham and H. A. Salmeda, "Humidity up to the Mesopause," Air Force Cambridge Research Laboratories, Report AFCRL-68-0550, (Air Force Surveys in Geophysics No. 206), October 1968.